Weak integrability breaking and full counting statistics

Stefan Michael Groha

Magdalen College

University of Oxford

A thesis submitted for the degree of

Doctor of Philosophy in Theoretical Physics

Trinity Term 2018

Weak integrability breaking and full counting statistics

Stefan Michael Groha
Magdalen College, University of Oxford
A thesis submitted for the degree of *Doctor of Philosophy in Theoretical Physics*
Trinity Term 2018

Abstract

In this thesis two questions of equilibrium and non-equilibrium properties in many-body quantum mechanical systems are investigated.

The first part is focused on probability distributions of quantum observables in many-body quantum systems. After an introduction to probability distributions, full counting statistics and the transverse field Ising model we give a brief overview over related experiments and then derive an expression for the probability distribution of the transverse field magnetization of a finite subsystem in any Gaussian state. We study the probability distribution in ground and thermal states as well as in a non-equilibrium setting after a quantum quench. We find an analytic expression for the time evolution after the quench and compare to numerics.

The second part of the thesis is concerned with the stability of exact quasi-particle excitations of an integrable model after weak integrability breaking perturbations are introduced. For this we first discuss the stability of excitations in integrable systems and then give an introduction to the Heisenberg XXX-model in a magnetic field. After constructing exact excitations we calculate the decay rate in leading order perturbation theory using methods of integrability.

Acknowledgements

First and foremost I want to thank my advisor Prof Fabian Essler for guidance and mentorship during my PhD. I am extremely grateful for all the time and patience he has dedicated to making me a better physicist and I have undoubtedly benefited and learned a great amount. I could not have asked for a better advisor. I also want to thank him for carefully reading the manuscript.

I am sincerely grateful to my collaborators Bruno Bertini, Pasquale Calabrese, Mario Collura and Neil Robinson.

I furthermore want to thank the other faculty members at the Rudolf Peierls Center for Theoretical Physics for providing a very vibrant and interesting atmosphere, especially Profs John Chalker and Steve Simon, who I had the privilege to learn from in lectures, journal clubs, and discussions.

I have been very fortunate to meet and interact with a number of exceptionally talented and friendly people during my time in Oxford, which I am very grateful for. Whilst there are too many to enumerate, I especially want to thank Thomas Veness, Yuri van Nieuwkerk and Richard Fern for very helpful discussions. I am furthermore extremely grateful to Dima Kovrizhin and Adam Nahum for fruitful discussions and helpful advice. Thank you to the people I shared an office with during my time in Oxford; thank you to Richard Fern and Dillon Liu for always lightening up the atmosphere.

I am eternally grateful to my parents, sister and to Rebeca, who are always there for me, to offer support and encouragement.

The work presented in this thesis is based on two papers [1, 2]. My work in Oxford has been supported by the Clarendon Scholarship Fund and the Santander Graduate Award.

Contents

1 Introduction

A defining property of condensed matter systems is that they are made up of an enormous number of constituents with complicated interplay between them. While for most systems the building blocks are the same, the interplay, interactions and environment can produce vastly different "macroscopic" outcomes, distinguishing metals from insulators, superconductors, magnets or even more exotic quantum hall liquids or topological insulators. To get an understanding of these systems it is therefore not important to probe ever more fundamental laws of nature, but to understand emergent phenomena appearing from the interplay of very simple ingredients.

Despite the vast number of components and the interactions between those, much more simple theoretical models can capture the essence of the emergent property of many systems and understanding these models can help us to elucidate condensed matter systems. This at first baffling possibility to learn about complicated models from toy examples can often be understood by one of the most important ideas in theoretical physics: the renormalisation group (RG). Schematically the RG reduces the number of degrees of freedom of the model, filtering out the important ingredients at the energy scales of interest. Coincidentally, by the RG procedure many real life physical systems turn out to be described by the same "effective" degrees of freedom and interactions at the energies we observe them. This is known as universality and is one of the cornerstones of theoretical physics, enabling us to understand classes of systems without having to know all their microscopic characteristics.

In particular low dimensional many body quantum systems present a playground for understanding strongly interacting quantum systems and many-particle

systems in general. In 1D, strong correlations and collective phenomena are known to have a particularly strong influence [3]. However despite this, there exist a number of one dimensional models where analytic progress can be made and exact solutions are possible, for example by non-local mapping to free systems [4, 5] or due to an infinite number of symmetries [6, 7]. These exact solutions of physically important models can help form an understanding of interacting many-body quantum systems and quantum mechanics in general.

This thesis is divided into two parts. The first part is focused on the probabilistic nature of quantum mechanics and its measurement [8], calculating the full counting statistics of certain operators in a one dimensional model of interacting spins in a magnetic field.

The second part is concerned with weak integrability breaking, defined as perturbing an integrable model with a parametrically small interaction, which takes the model away from the integrable point. Weak integrability breaking has attracted much interest in recent years in non-equilibrium dynamics, where there is a dichotomy between the relaxation of integrable and non-integrable theories after a sudden change of a global parameter (quantum quench) [9–12]. It is an interesting questions what the influence of an integrability breaking perturbation is on the time evolution (cf. [13] and references therein) and a relation to the decay of quasi-particles has been proposed [14]. In the first part of the thesis we will be interested in a related question, however in equilibrium. We will be interested in the stability of exact quasi-particles of a lattice integrable model when a weak integrability breaking perturbation is introduced.

The outline of the thesis is as follows: The first part introduces the notion of the probabilistic nature of measurement in quantum mechanics in Section 2.1 and gives a general strategy to calculate it in a generic system in Section 2.2. We then motivate the theoretical discussion by briefly outlining some important experiments of full probability distributions in many-body quantum systems in Section 2.3. After introducing the transverse field Ising model as a paradigm to

calculate full probability distributions in Section 2.4, Section 3.1 gives a detailed discussion of how to calculate full counting statistics for a general Gaussian density matrix and certain observables. We then examine probability distributions in equilibrium in Section 3.2, focus on the time evolution after a quantum quench in Section 3.3 and derive an analytic formula in Section 3.4 which asymptotically describes the time evolution of the full probability distribution of a specific observable.

In the second part we first briefly talk about the stability of integrable excitations in Section 4.2 before introducing a paradigmatic model of integrability: the Heisenberg XXX-model in Section 4.3. We discuss its solution by means of the Bethe Ansatz and how to calculate matrix elements using Algebraic Bethe Ansatz and Inverse Scattering Theory. In Section 5.1 we then motivate why we are interested in the stability of excitations under a weak integrability breaking perturbation and introduce the framework we are calculating the leading order decay rate with. We then explicitly construct exact excitations, important for the decay process in Section 5.2, find an efficient formula for the decay rate in Section 5.3 and solve it numerically in Section 5.4.

In Section 6 we give a brief conclusion and outlook for both problems considered in this thesis.

This thesis is based on the following publications:

- Stefan Groha, Fabian H. L. Essler, Spinon decay in the spin-1/2 Heisenberg chain with weak next nearest neighbour exchange, J. Phys. A: Math. Theor. 50 334002 (2017)

- Stefan Groha, Fabian H. L. Essler, Pasquale Calabrese, Full Counting Statistics in the Transverse Field Ising Chain, arXiv:1803.09755 (2018)

Other publications, which are not part of the thesis due to restrictions on the length thereof:

- Bruno Bertini, Fabian H. L. Essler, Stefan Groha, Neil J. Robinson, Prethermal-

ization and thermalization in models with weak integrability breaking, Phys. Rev. Lett. 115, 180601 (2015)

- Bruno Bertini, Fabian H. L. Essler, Stefan Groha, Neil J. Robinson, Thermalization and light cones in a model with weak integrability breaking, Phys. Rev. B 94, 245117 (2016)

- Mario Collura, Fabian H. L. Essler, Stefan Groha, Full counting statistics in the spin-1/2 Heisenberg XXZ chain, J. Phys. A: Math. Theor. 50 414002 (2017)

Full counting statistics

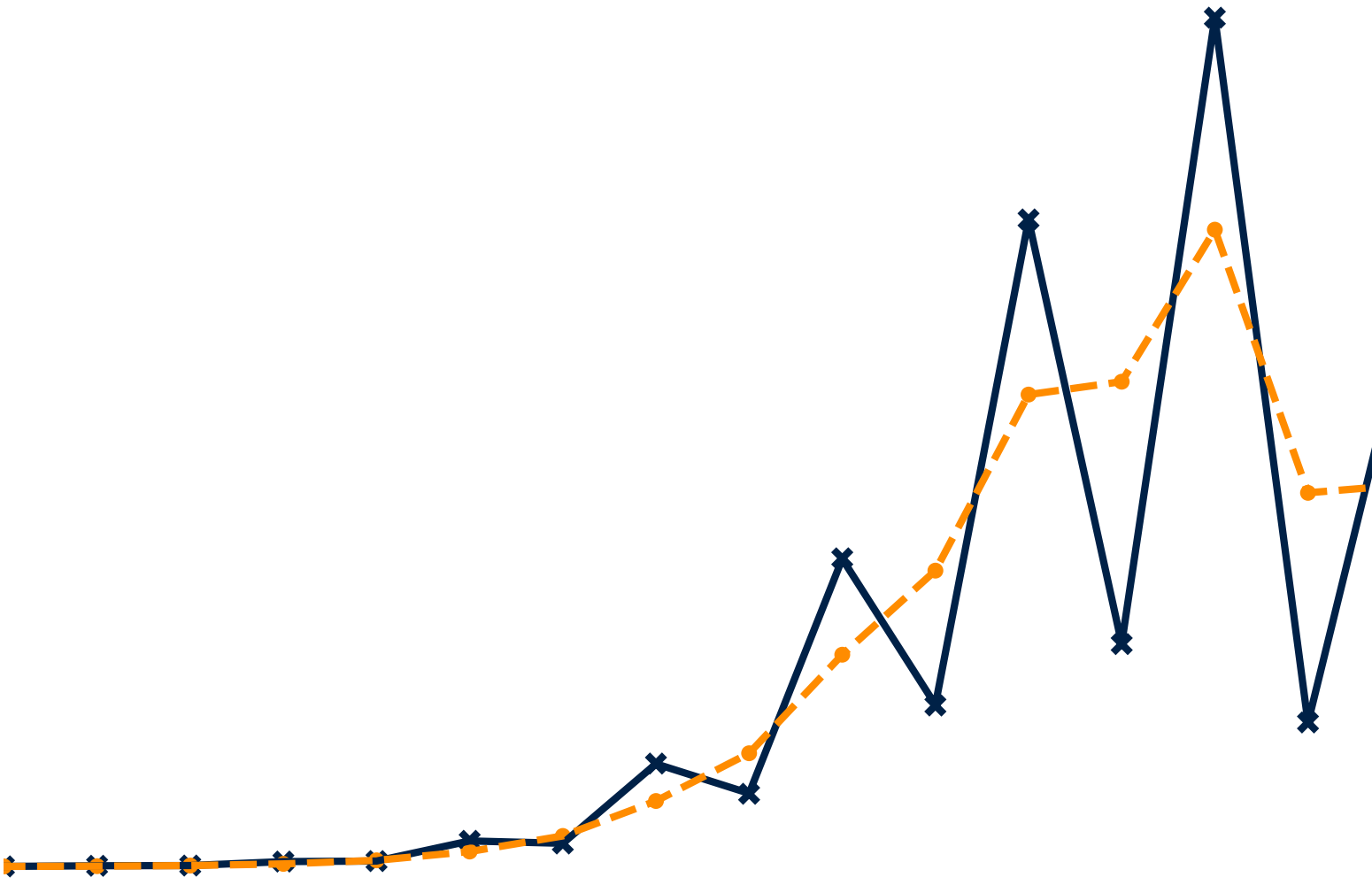

2

Full counting statistics, probability distributions and the transverse field Ising model

Contents

2.1 Description of quantum mechanical systems and probabilistic nature of measurement

A quantum mechanical many-body system of N particles or spins is fully described by its quantum mechanical wave function $\psi(n_1, \ldots, n_N; t)$, which is the projection of the quantum mechanical state $|\psi(t)\rangle$ onto a preferred basis

$$\psi(n_1, \ldots, n_N; t) = \langle n_1, \ldots, n_N \mid \psi(t)\rangle \tag{2.1}$$

where the n_i can e.g. be position or spin in the z-direction for particles and spins respectively. However in the case of interacting many-body systems this full information is generally not accessible theoretically and as the information needed to fully specify the wave function grows exponentially with the system size, it is practically not possible to numerically obtain for a generic state. There are exceptions, for example states with low entanglement, e.g. ground states of gapped 1D systems (cf. [15–17]) or eigenstates of 1D quantum integrable systems (cf. [6, 18,

19]). Also experimentally, accessing the wave function is very hard for single particle quantum mechanical objects [20–22], however so far impossible for interacting many-particle systems. We therefore generically have to resort to measurement and calculation of quantum mechanical expectation values of observables of interest or correlation functions thereof. Examples include neutron and light scattering experiments measuring spin and charge response functions or conductivity measurements giving access to current-current correlation functions [23].

A fundamental principle of quantum mechanics is the statistical nature of measurements of observables. Measuring the same observable in identically prepared systems leads to different measurement outcomes that are described by a probability distribution that depends on both the state $|\Psi\rangle$ and on the observable $\mathcal{O}$ considered. While expectation values and correlation functions average over all the fluctuations and give information about the first few moments, the full probability distribution $\mathrm{Pr}_{\mathcal{O},|\psi\rangle}(O)$ encodes detailed information about quantum fluctuations in the system. It is of particular interest in situations where the first few moments do not provide a good description of the distribution (cf. Figure. 2.1). This happens for example for the probability distribution of the order parameter

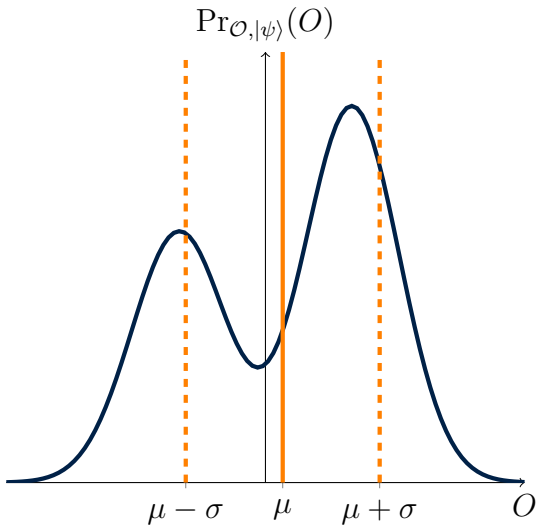

Figure 2.1: Example of a probability distribution that is not well described by mean μ and standard deviation σ. Generally every multimodal or flat distribution can not be characterized just by its first few moments.

in the XXZ-model at criticality [24].

Quantum mechanical probability distributions in the guise of *Full Counting Statistics* (FCS) have been studied for some time in mesoscopic devices [25, 26]. More recently it has become possible to analyse them in systems of ultra-cold atomic gases [27–32]. This has broken new ground in the sense that one is dealing with (strongly) interacting many-particle systems and a variety of observables, typically defined on subsystems, can be accessed. This has motivated a number of theoretical works of FCS in equilibrium states [24, 33–42], and after quantum quenches [29, 42–46]. A second motivation for studying FCS has been the observation that in non-interacting fermionic systems with particle number conservation the FCS of particle number within a subsystem is directly related to the entanglement entropy [47–56] and provides indirect information about the latter.

2.2 Probability distribution and full counting statistics

In the following we want to look at the FCS and probability distribution of certain observables $\mathcal{O}$ within a state $|\psi\rangle$. Let us further simplify the following discussion by only considering operators $\mathcal{O}$ with discrete spectra, so for example spin operators acting on a finite subsystem (cf. Fig. 2.2). The outcome of any measurement of this

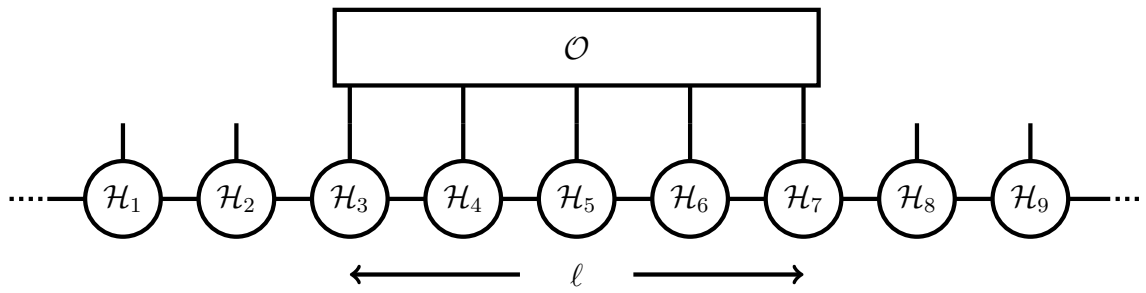

Figure 2.2: Pictorial representation of the kind of setup we want to look at. We are interested in a system with sites, which can be finite or infinite. Each site has a finite local Hilbert space dimension. The operator is acting on a finite subset of the system, a subsystem of size ℓ, giving a number of eigenvalues, which is finite, however generically exponential in the length of the subsystem ℓ. Specifically we will be interested in spin-$1/2$ at each site, with some spin operator having support on ℓ sites.

observable in any state according to the Born rule [8] is any of the eigenvalues $O_1, O_2, \ldots$ of the operator $\mathcal{O}$ with associated probability:

$$\mathrm{Pr}_{\mathcal{O},|\psi\rangle}(O_n) = |\langle o_n \mid \psi\rangle|^2 \tag{2.2}$$

where $|o_n\rangle$ is the associated eigenvector to the eigenvalue O_n and therefore

$$\mathrm{Pr}_{\mathcal{O},|\psi\rangle}(O_n) = \langle\psi| \hat{P}_{O_n} |\psi\rangle \tag{2.3}$$

where $\hat{P}_{O_n}$ is the projection operator on the subspace corresponding to the eigenvalue O_n, such that we can write

$$\mathcal{O} = \sum_m O_m \hat{P}_{O_m}. \tag{2.4}$$

Let us now define the quantity

$$\mathrm{P}_{\mathcal{O},|\psi\rangle}(O) = \langle\psi| \delta(\mathcal{O} - O) |\psi\rangle . \tag{2.5}$$

where $\delta(x)$ is the Dirac distribution. Using the plane wave integral representation of the delta function, we can write this quantity as

$$\begin{aligned} \mathrm{P}_{\mathcal{O},|\psi\rangle}(O) &= \langle\psi| \int_{-\infty}^{\infty} \frac{\mathrm{d}\lambda}{2\pi} e^{i\lambda(O-\mathcal{O})} |\psi\rangle \\ &= \langle\psi| \int_{-\infty}^{\infty} \frac{\mathrm{d}\lambda}{2\pi} e^{i\lambda(O-\sum_{O_m} O_m \hat{P}_{O_m})} |\psi\rangle . \end{aligned} \tag{2.6}$$

We can now use the properties of the projection operators $\hat{P}_{O_m}$

$$\hat{P}_{O_m}\hat{P}_{O_n} = \hat{P}_{O_m}\delta_{mn} \tag{2.7}$$

$$\sum_m \hat{P}_{O_m} = \mathbb{1}. \tag{2.8}$$

These properties imply that any power of the operator $(O_n - \mathcal{O})$ can be rewritten as

$$\begin{aligned} \left(O - \sum_m \hat{P}_{O_m} O_m\right)^l &= \left(\sum_m \hat{P}_{O_m}(O - O_m)\right)^l \\ &= \sum_{m_1,\ldots,m_l} \hat{P}_{O_{m_1}} \ldots \hat{P}_{O_{m_l}} (O - O_{m_1}) \ldots (O - O_{m_l}) \\ &= \sum_m \hat{P}_{O_m} (O - O_m)^l \end{aligned} \tag{2.9}$$

and therefore we can rewrite the quantity $\mathrm{P}_{\mathcal{O},|\psi\rangle}$ as

$$\begin{aligned}\mathrm{P}_{\mathcal{O},|\psi\rangle}(O) &\equiv \langle\psi|\,\delta(\mathcal{O}-O)\,|\psi\rangle \\ &= \sum_m \delta(O-O_m)\,\langle\psi|\,\hat{P}_{O_m}\,|\psi\rangle \\ &= \sum_m \delta(O-O_m)\,\mathrm{Pr}_{\mathcal{O},|\psi\rangle}(O_m)\end{aligned} \tag{2.10}$$

This relation, as well as the Fourier transform of the first line, will be very helpful in calculating probability distributions for observables later. To compute the first line of (2.10) it will again be useful to look at the Fourier transform of the probability distribution. Using the plane wave integral representation of the Dirac delta distribution we can write

$$\mathrm{P}_{\mathcal{O},|\psi\rangle}(O) = \int_{-\infty}^{\infty} \frac{\mathrm{d}\lambda}{2\pi} e^{-i\lambda O} \chi_{\mathcal{O},|\psi\rangle}(\lambda) \tag{2.11}$$

where $\chi_{\mathcal{O},|\psi\rangle}(\lambda)$ is defined as

$$\chi_{\mathcal{O},|\psi\rangle}(\lambda) = \langle\psi|\,e^{i\lambda\mathcal{O}}\,|\psi\rangle \tag{2.12}$$

and is called the *full counting function* of the operator $\mathcal{O}$ in the state $|\psi\rangle$. For a hermitian operator $\mathcal{O}$ it is easy to see from this definition that

$$\chi_{\mathcal{O},|\psi\rangle}(\lambda) = \big(\chi_{\mathcal{O},|\psi\rangle}(-\lambda)\big)^* \tag{2.13}$$

$$\chi_{\mathcal{O},|\psi\rangle}(0) = 1. \tag{2.14}$$

For a generic operator and wave function, where the operator has finite support on a finite number of sites with finite Hilbert space dimension on each site (cf. Figure 2.2), the number of eigenvalues of the operator grows exponentially with the length of the subsystem. Therefore obtaining the probabilities from (2.10) becomes exponentially hard. For large enough subsystems one can however recover the probability density of the operator $\mathcal{O}$ in the state $|\psi\rangle$ by mollifying the delta-distribution. Using a mollifier $\phi_\varepsilon(x)$, we get

$$\int_{-\infty}^{\infty} \mathrm{d}x\ \phi_\varepsilon(x-O)\mathrm{P}_{\mathcal{O},|\psi\rangle}(x) = \sum_m \phi_\varepsilon(O-O_m)\,\mathrm{Pr}_{\mathcal{O},|\psi\rangle}(O_m) \tag{2.15}$$

$$\equiv \mathrm{Pr}^{\varepsilon}_{\mathcal{O},|\psi\rangle}(O), \tag{2.16}$$

where for ε small the mollified probabilities $\mathrm{Pr}^{\varepsilon}_{\mathcal{O},|\psi\rangle}(O)$ are a good approximation of the probabilities in an interval of order ε around O. To obtain $\mathrm{P}_{\mathcal{O},|\psi\rangle}(O)$ from the generating function the mollification implies

$$\mathrm{Pr}^{\varepsilon}_{\mathcal{O},|\psi\rangle}(O) = \int_{-\infty}^{\infty} \mathrm{d}x\ \phi_{\varepsilon}(x-O)\mathrm{P}_{\mathcal{O},|\psi\rangle}(x) = \int_{-\infty}^{\infty} \mathrm{d}\lambda\ \tilde{\phi}_{\varepsilon}(O-\lambda)\chi_{\mathcal{O},|\psi\rangle}(\lambda) \tag{2.17}$$

where

$$\tilde{\phi}_{\varepsilon}(O-\lambda) = \int_{-\infty}^{\infty} \mathrm{d}x\ e^{-i\lambda x}\phi_{\varepsilon}(O-x). \tag{2.18}$$

Mollifying the delta distribution also effectively reduces the support of the integral in (2.17) by suppressing large λ, making the integral numerically tractable. As a possible mollifier $\phi_{\varepsilon}(x)$ we can use e.g. the Gaussian approximation for a delta function

$$\phi_{\varepsilon}(x) = \frac{1}{\sqrt{2\pi\varepsilon}} e^{-\frac{x^2}{2\varepsilon}}. \tag{2.19}$$

We will now specify the discussion to spin-$1/2$ systems and specific operators. We will be interested in operators defined on a subsystem $1,\ldots,\ell$ of the form

$$\mathcal{O}_{\ell} = \sum_{i=1}^{\ell} f(i)\sigma_i^{\alpha}. \tag{2.20}$$

where σ_i^{α} is a Pauli matrix in $\alpha = x,y,z$ direction on site i and $f(i) = 1$ or $f(i) = (-1)^i$, which corresponds to subsystem magnetisation and staggered subsystem magnetisation respectively. As the Pauli matrices have eigenvalues ± 1 the eigenvalues of $\mathcal{O}_{\ell}$ are integers. There are $\ell+1$ eigenvalues, which are highly degenerate. Unlike the generic case discussed above, this poses a very special case that cannot be solved by regularising the delta functions. However we have a periodicity constraint on $\chi_{\mathcal{O}_{\ell},|\psi\rangle}(\lambda)$ of the form

$$\chi_{\mathcal{O}_{\ell},|\psi\rangle}(\lambda+\pi) = (-1)^{\ell}\chi_{\mathcal{O}_{\ell},|\psi\rangle}(\lambda) \tag{2.21}$$

With this we can show that

$$\begin{aligned}
\mathrm{P}_{\mathcal{O}_\ell,|\psi\rangle}(m) &= \int_{-\infty}^{\infty} \frac{\mathrm{d}\lambda}{2\pi} e^{-i\lambda m} \chi_{\mathcal{O}_\ell,|\psi\rangle}(\lambda) \\
&= \sum_{n\in\mathbb{Z}} \int_{-\pi/2+n\pi}^{\pi/2+n\pi} \frac{\mathrm{d}\lambda}{2\pi} e^{-i\lambda m} \chi_{\mathcal{O}_\ell,|\psi\rangle}(\lambda) \\
&= \sum_{n\in\mathbb{Z}} \int_{-\pi/2}^{\pi/2} \frac{\mathrm{d}\lambda}{2\pi} e^{-i(\lambda-n\pi)m} (-1)^{n\ell} \chi_{\mathcal{O}_\ell,|\psi\rangle}(\lambda) \\
&= \sum_{n\in\mathbb{Z}} e^{inm\pi+i\pi\ell n} \int_{-\pi/2}^{\pi/2} \frac{\mathrm{d}\lambda}{2\pi} e^{-i\lambda m} \chi_{\mathcal{O}_\ell,|\psi\rangle}(\lambda) \\
&= \begin{cases} \sum_{r\in\mathbb{Z}} \delta(m-2r+\ell) \times 2 \int_{-\pi/2}^{\pi/2} \frac{\mathrm{d}\lambda}{2\pi} e^{-i\lambda(2r-\ell)} \chi_{\mathcal{O}_\ell,|\psi\rangle}(\lambda) & \text{for } \ell \text{ odd} \\ \sum_{r\in\mathbb{Z}} \delta(m-2r) \times 2 \int_{-\pi/2}^{\pi/2} \frac{\mathrm{d}\lambda}{2\pi} e^{-2i\lambda r} \chi_{\mathcal{O}_\ell,|\psi\rangle}(\lambda) & \text{for } \ell \text{ even} \end{cases}
\end{aligned} \tag{2.22}$$

and therefore comparing with (2.10) we obtain for the probability distribution:

$$\mathrm{Pr}_{\mathcal{O}_\ell,|\psi\rangle}(m) = \int_{-\pi/2}^{\pi/2} \frac{\mathrm{d}\lambda}{\pi} e^{-i\lambda m} \chi_{\mathcal{O}_\ell,|\psi\rangle}(\lambda) \tag{2.23}$$

It is furthermore useful to note that the FCS is the generating function for the moments of $\mathcal{O}$:

$$\langle \mathcal{O}^n \rangle = \frac{1}{i^n} \frac{d^n}{d\lambda^n} \left\langle e^{i\lambda\mathcal{O}} \right\rangle \big|_{\lambda=0} \tag{2.24}$$

whereas the logarithm of the generating function is the generating function for the cumulants C_n:

$$C_n = \frac{1}{i^n} \frac{d^n}{d\lambda^n} \ln \left\langle e^{i\lambda\mathcal{O}} \right\rangle \big|_{\lambda=0}. \tag{2.25}$$

2.3 Experimental measurement of full counting statistics

As mentioned, quantum mechanical probability distributions have been studied in mesoscopic systems and quantum optics. Examples include the measurement of fractional charge in fractional quantum Hall systems and quantum noise in photon counting experiments [57–59]. In recent years new interest has been generated by experiments analysing probability distributions for quantum observables in

cold atomic gases. These experiments allow for the measurement of the FCS of a number of observables acting on a large subsystem in (strongly) interacting many-particle systems in and out of equilibrium in one and two dimensions.

While most experimental works in the early days of cold atom experiments were focused on weakly interacting bosons, including the creation of Bose Einstein condensation (BEC) [60–62], interference of BECs [63] and atom lasers [64], the main interest in recent years has been on engineering theoretical strongly correlated quantum systems with ultra-cold atom setups. While the former often can be successfully described by mean field like Gross-Pitaevski equations, the latter typically probe strongly interacting many-body physics, which is of great interest to understand quantum aspects of many-body systems. This progress has been mainly fuelled by major advances in experimental techniques. First and foremost the possibility to control scattering lengths to be comparable to inter-particle distances by means of magnetically tuned Feshbach resonances [65, 66] has made it possible to influence the effective interaction between particles. Furthermore confinement in optical lattices is a powerful ingredient for engineering quantum systems. Hereby atoms are placed in a periodic potential created by a standing laser beam. Changing the intensity of the laser beam can be used to tune the relative strength between kinetic and interaction energy [67]. Another useful tool is the ability to reduce the dimensionality of the system by applying strong confinement potentials in the "unwanted dimensions". Having engineered a certain quantum mechanical system, cold atomic experiments do not only offer certain experimental techniques mimicking many solid state analogues, e.g. Bragg spectroscopy [68] being similar to light and neutron scattering, but there are additional techniques not available in solid state systems. Some of them prove themselves useful for the measurement of FCS, e.g. site resolved measurement [69, 70].

In the following we will briefly discuss two experiments motivating the theoretical discussion in Section 3.

2.3.1 Staggered subsystem magnetisation in the Hubbard model

While site resolved measurement is not possible in solid-state systems, ultracold atom experiments have length scales accessible with high-resolution optical microscopy [69, 70]. This opens up the possibility of measuring certain observables on each site of an optical lattice, which is created as described above. In Ref. [71] this technique is used to extract the probability distribution of the staggered magnetisation, which is defined below. The experimental system is well described by a two-dimensional Hubbard model with the Hamiltonian:

$$H = -t \sum_{\sigma,\langle i,j\rangle} \left(c^\dagger_{i\sigma} c_{j,\sigma} + h.c. \right) + U \sum_i n_{i\downarrow} n_{i\uparrow} \tag{2.26}$$

where the sum $\langle i,j\rangle$ goes over nearest neighbours, $c^\dagger_{i\sigma}$, $c_{i\sigma}$ are fermionic creation and annihilation operators, $n_{i\sigma} = c^\dagger_{i\sigma} c_{i\sigma}$ and the ratio of interaction to hopping given by $\frac{U}{t} \sim 7.2$. At half filling and $\frac{U}{t} \gg 1$ the low energy degrees of freedom are well described just in terms of the spins $S^\alpha_i = \frac{1}{2} c^\dagger_{i\beta} \sigma^\alpha_{\beta\gamma} c_{i\gamma}$, with σ^α the Pauli spin matrices, with an effective Hamiltonian given by:

$$H = J \sum_{\langle i,j\rangle} \vec{S}_i \cdot \vec{S}_j, \tag{2.27}$$

which is known as the antiferromagnetic Heisenberg model. To set up the experiment a mixture of the two lowest hyperfine states of ^{6}Li, corresponding to up-spin $|\uparrow\rangle$ and down-spin $|\downarrow\rangle$, are loaded into a trap with a 2d optical square lattice. After cooling the atoms down to appropriate temperatures, Feshbach resonances are used to tune the interaction of the atoms to simulate the 2d Hubbard model. The charge occupation of the system is measured by rapidly increasing the lattice depths to pin the atoms at the sites and capturing the fluorescence of the atoms by high-resolution microscopy, being able to resolve every lattice site (cf. Fig. 2.3a). The measurement technique does however not distinguish between empty and doubly occupied sites. As the ratio of interaction to hopping is large and the experiment is done at half-filling, these sites are however very rare as

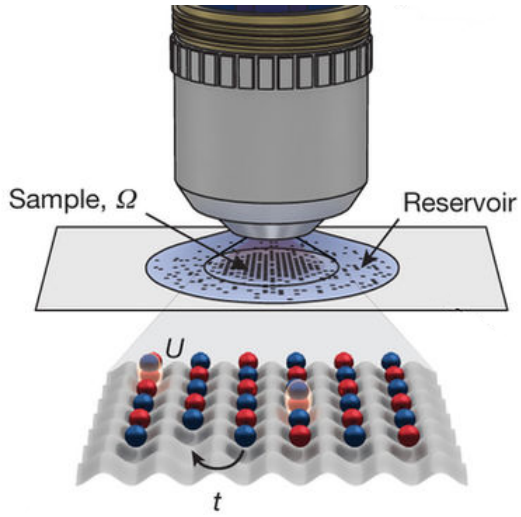

(a) Experimental setup for measuring the charge occupation of the lattice. A subsystem of the cold atomic cloud, where the density is approximately constant, is measured with an optical microscope. (Illustration from [71], slightly modified)

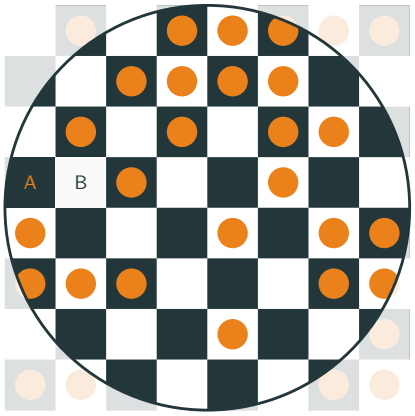

(b) Example realisation of measured occupied or unoccupied sites of the up-spin orientation. The other spin orientation has been removed. As the interaction is quite large ($\frac{U}{t} \sim 7.2$) and the experiment is done at half filling the staggered magnetisation can be calculated by looking at neighbouring sites: ■□ corresponds to $S_i^z = +1$ and ■● corresponds to $S_i^z = -1$.

long as the temperature is of the order of hopping and not interaction. Furthermore the charge occupation is measured, not the spin of the particles. Therefore an extra step has to be taken, which removes one spin orientation from the trap, leaving the other spin orientation untouched. This is realised by using resonant pulses driving transitions for atoms in one of the hyperfine states, ejecting the respective spin direction. Now from the measured charge occupation the staggered magnetisation on N^2 sites can be calculated:

$$S^s(N) = \frac{1}{N^2}\left(\sum_{j\in A} S_j^z - \sum_{j\in B} S_j^z\right) \tag{2.28}$$

with the sites A and B defined as in Fig. 2.3b. Fig. 2.3b shows a typical measurement of the charge occupation after removal of one of the spin directions. This measurement is done multiple times for fixed temperatures and the resulting total magnetisations of each measurements are plotted in a histogram. By the law of large numbers this histogram approaches the probability distribution of the staggered magnetisation of the Hubbard model at half filling for $\frac{U}{t} \gg 1$. This is compared to Monte Carlo calculations of the Heisenberg model, which shows a

good agreement (see Fig. 2.4) [71].

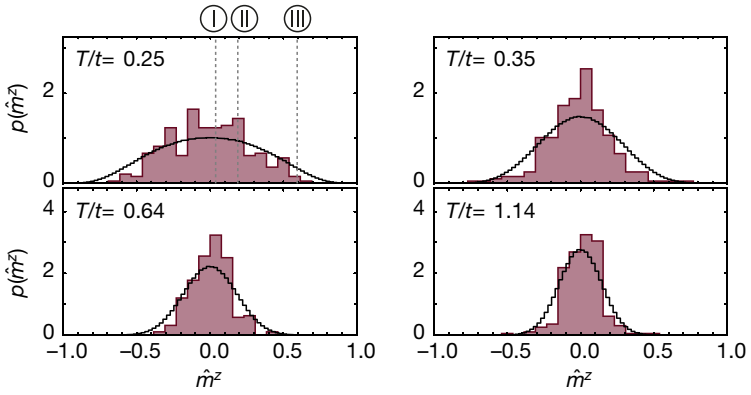

Figure 2.4: Histogram of the staggered subsystem magnetisation at different temperatures. The histograms approach the probability distributions calculated by Monte Carlo simulations in the Heisenberg model at the respective temperature. (from [71].)

2.3.2 Non-equilibrium FCS in time of flight experiments

Measurement of probability distributions in cold atom systems is not only possible in equilibrium, but insights into non-equilibrium evolution of FCS and probability distributions are possible. The time dependence of probability distributions of certain quantities was used to reveal prethermalisation of closed weakly perturbed integrable quantum systems (cf. Ref. [30, 72]).

For this a trapped 1D gas of ^{87}Rb bosons is prepared in the quasi-condensate regime, which means density fluctuations are suppressed, whereas strong phase fluctuations, determined by the temperature T and the density of the system, are present. By quickly changing the trap potential in one of the dimensions orthogonal to the 1D system from a single well to a double well potential, the single condensate is quickly and coherently split into two uncoupled 1D gases with identical wave function phase profiles. Thereafter the gases are allowed to evolve in the double well potential for some time t and then the two condensates are released from the traps and expand until the clouds overlap. After this, absorption imaging is used to determine the interference pattern of the densities of the system. When

the two condensates are coherent, the relative phase between the two clouds determines the interference fringes. The low energy degrees of freedom are described by Luttinger Liquid theory [3], where the wave function of the condensates $\alpha = 1, 2$ in both wells are described by wave functions $\psi_{B,\alpha}(x) \sim \sqrt{\rho}e^{i\phi_\alpha(x)}$with densities ρ and phases $\phi_\alpha(x)$. Schematically the density after the interference can then be described as [44, 73]

$$\rho(x) \sim e^{i(\phi_1(x)-\phi_2(x))}. \tag{2.29}$$

The measurement is along the length of the system (see Fig. 2.5), optically integrating over the density. One can show [44] that the modulation of the integrated fringe contrast along the system is related to the integrated phase density, which is intuitively clear by looking at the integrated density, again schematically (exact description: [44, 73]):

$$\int_{-L/2}^{L/2} dx\rho(x) = C(L)e^{i\Phi(L)}, \tag{2.30}$$

where $C(L)$ is the quantity of interest. Doing multiple measurements after the same time t and plotting the resulting fringe contrast squared and normalized in a histogram, one obtains the probability distribution of interest. The probability distributions for different times are shown in Fig. 2.6. With these it was shown that at late times, although the system is not integrable, it does not thermalise. This shows that non-equilibrium probability distributions of meaningful quantities are experimentally obtainable and physically interesting.

2.4 The Transverse field Ising model

In the following we consider the spin-$1/2$ transverse field Ising model on an infinite $1D$ chain with Hamiltonian

$$H(h) = -\sum_{j=-\infty}^{\infty} \left[\sigma_j^x \sigma_{j+1}^x + h\sigma_j^z\right]. \tag{2.31}$$

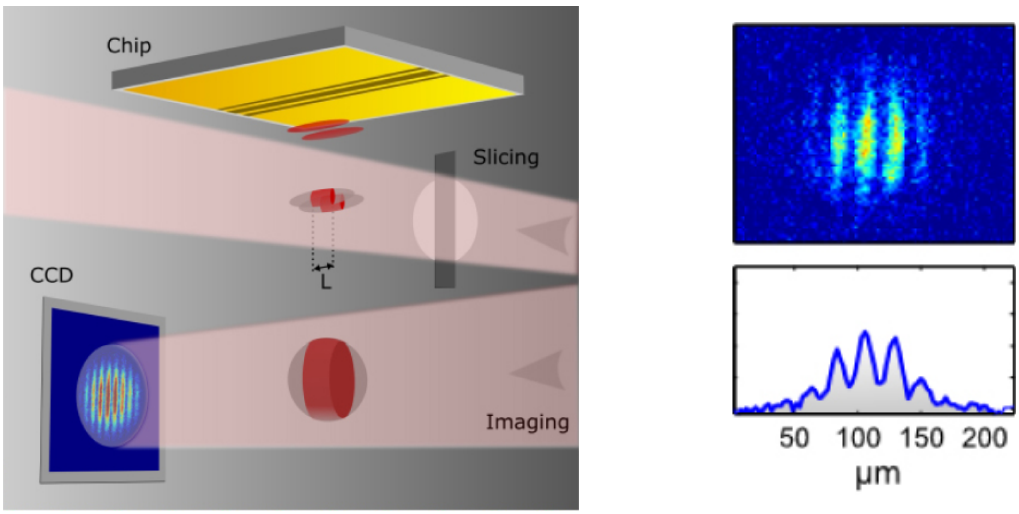

Figure 2.5: In (a) the experimental setup is shown. The two condensates are released after time t and are freely expanding until they overlap and interfere. This is called time-of-flight experiment. The resulting interference pattern is measured along the system direction using absorption measurement, revealing the interference pattern. An example pattern is shown in (b) with the fringe contrast, which clearly shows the modulation. The amplitude of the modulation is the quantity of interest. (Illustration and plots from [30, 72].)

The ground state phase diagram features ferromagnetic ($h < 1$) and paramagnetic ($h > 1$) phases separated by a quantum critical point in the universality class of the two-dimensional Ising model [74].

$$T = 0: \quad \underset{0}{\bullet} \xrightarrow[\text{FM}]{\langle \sigma_j^x \rangle \neq 0} \underset{1}{\bullet} \xrightarrow[\text{PM}]{\langle \sigma_j^x \rangle = 0} h$$

The order parameter that characterizes the transition is the longitudinal magnetisation $\langle \mathrm{GS}|\sigma_j^x|\mathrm{GS}\rangle$. At finite temperature spontaneous breaking of the $\mathbb{Z}_2$ symmetry in $1D$ is forbidden and hence the order present in the ground state at $h < 1$ melts.

In the following we will summarize the relevant steps for diagonalizing the Hamiltonian (2.31). We will start out discussing finite systems, closely following the appendix in [75], then introduce the quantities of interest in this chapter and in the end take the system size L to infinity, utilizing properties of the operators and expectation values in the TFIM to simplify the discussion.

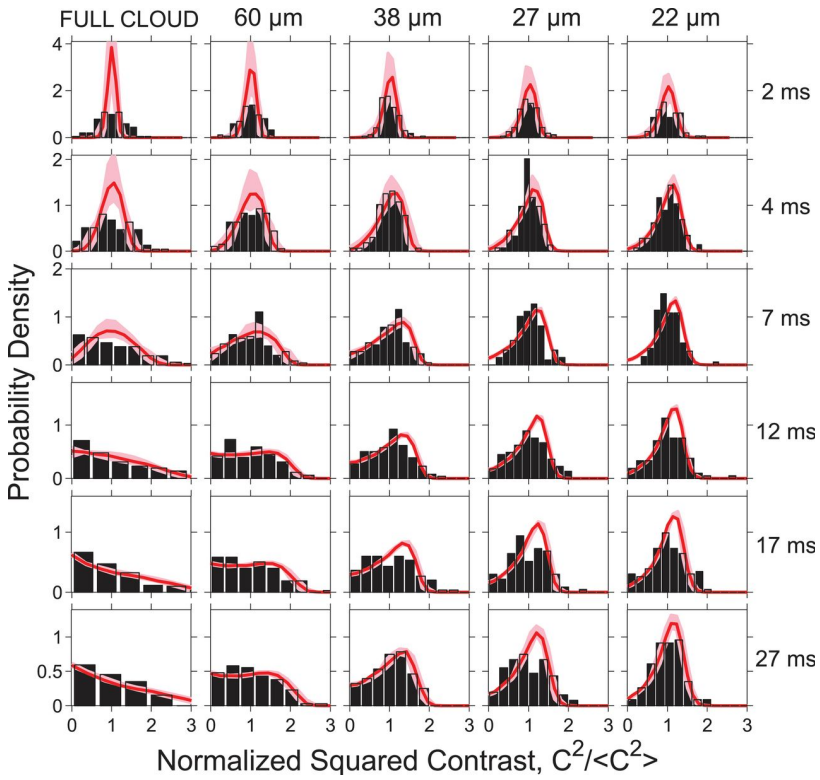

Figure 2.6: Probability distributions of the squared fringe contrast at different times and integration lengths over the system. Different integration lengths are realised by slicing away parts of the system before measurement (cf. Fig. 2.5). The plots are extracted from [30].

2.4.1 Diagonalisation of the Transverse Field Ising chain

We consider the Hamiltonian (2.31) on a finite system $1, \ldots, L$

$$H = -\sum_{j=1}^{L} \left[\sigma_j^x \sigma_{j+1}^x + h\sigma_j^z\right] \tag{2.32}$$

with even L and periodic boundary conditions for the spins $\sigma_{L+1}^\alpha = \sigma_1^\alpha$. The TFIC is mapped to a model of spinless fermions by a Jordan-Wigner transformation

$$\sigma_j^z = 1 - 2c_j^\dagger c_j \ , \qquad \sigma_j^x = \prod_{l=1}^{j-1}(1 - 2c_l^\dagger c_l)(c_j + c_j^\dagger) \ , \tag{2.33}$$

where c_j are spinless fermion operators obeying canonical anticommutation relations $\{c_j^\dagger, c_k\} = \delta_{j,k}$. Substituting into the Hamiltonian we obtain

$$\begin{aligned} H(h) = &- \sum_{j=1}^{L-1} (c_j^\dagger - c_j)(c_{j+1} + c_{j+1}^\dagger) - h(c_j c_j^\dagger - c_j^\dagger c_j) \\ &- e^{i\pi\hat{N}} \left(c_L - c_L^\dagger\right)\left(c_1 + c_1^\dagger\right). \end{aligned} \tag{2.34}$$

where the fermion number $\hat{N}$ is defined as $\hat{N} = \sum_{j=1}^{N} c_j^\dagger c_j$. As $[H, \hat{N}] = 0$ the Hamiltonian is block-diagonal in terms of the fermions with the two blocks being characterised by even and odd fermion number. Imposing anti-periodic and periodic boundary conditions for even and odd fermion number respectively we can write the Hamiltonian in both sectors as

$$H(h) = - \sum_{j=1}^{L-1} (c_j^\dagger - c_j)(c_{j+1} + c_{j+1}^\dagger) - h(c_j c_j^\dagger - c_j^\dagger c_j) \tag{2.35}$$

where for even fermion number $c_{L+1} = -c_1$ and $c_{L+1} = c_1$ for odd fermion number. In the following we will refer to the sector with even fermion number and anti-periodic boundary conditions on the fermions as *Neveu-Schwarz* (NS) sector, whereas the sector with odd fermion number and periodic boundary conditions will be called *Ramond* (R) sector.

The next step towards diagonalizing the transverse field Hamiltonian is a Fourier transform:

$$c_k = \frac{1}{\sqrt{L}} \sum_{j=1}^{L} c_j e^{ikj} \tag{2.36}$$

Depending on the sector and the associated boundary conditions the momenta are quantized differently

$$k_n^{NS/R} = \begin{cases} \frac{2\pi(n+1/2)}{L} \\ \frac{2\pi n}{L} \end{cases}, \qquad n = -\frac{L}{2}, \ldots, \frac{L}{2} - 1. \tag{2.37}$$

To diagonalise the Hamiltonian we introduce Bogoliubov fermions $\alpha_{k^{NS/R}}$

$$c_{k_n^{NS/R}} = \cos\left(\frac{\theta_{k_n^{NS/R}}}{2}\right) \alpha_{k_n^{NS/R}} + i \sin\left(\frac{\theta_{k_n^{NS/R}}}{2}\right) \alpha^\dagger_{-k_n^{NS/R}} \tag{2.38}$$

$$c^\dagger_{-k_n^{NS/R}} = i \sin\left(\frac{\theta_{k_n^{NS/R}}}{2}\right) \alpha_{k_n^{NS/R}} + \cos\left(\frac{\theta_{k_n^{NS/R}}}{2}\right) \alpha^\dagger_{-k_n^{NS/R}}, \tag{2.39}$$

where $\{\alpha_k, \alpha_p^\dagger\} = \delta_{p,k}$ for momenta in the same sector and the Bogoliubov angle is

$$e^{i\theta_k} = \frac{h - e^{ik}}{\sqrt{1 + h^2 - 2h\cos k}} \,. \tag{2.40}$$

We can express the Hamiltonian as

$$H_{NS} = \sum_{n=-L/2}^{L/2-1} \varepsilon(k_n^{NS}) \left[\alpha_{k_n^{NS}}^\dagger \alpha_{k_n^{NS}} - \frac{1}{2}\right] \tag{2.41}$$

$$H_R = \sum_{\substack{n=-L/2 \\ n\neq 0}}^{L/2-1} \varepsilon(k_n^R) \left[\alpha_{k_n^R}^\dagger \alpha_{k_n^R} - \frac{1}{2}\right] - 2(1-h)\left[\alpha_0^\dagger \alpha_0 - \frac{1}{2}\right] \tag{2.42}$$

in the even and odd fermion sector respectively, where the dispersion relation is given by

$$\varepsilon(k) = 2\sqrt{1 + h^2 - 2h\cos(k)}. \tag{2.43}$$

We see from (2.42) that depending on $h > 1$ or $h < 1$ we can obtain different ground states. This manifests itself in the different phases depending on $h > 1$ or $h < 1$ respectively. For $h > 1$ the extra term in the Ramond sector is positive and the lowest state in this sector with odd fermion number is the state where the $k = 0$ mode is occupied. Therefore the ground state of the full Hamiltonian is given by the vacuum state in the NS sector:

$$|GS\rangle_{h>1} = |0\rangle_{NS} \tag{2.44}$$

where the vacuum is defined as the state which is annihilated by application of any annihilation operator. This is the paramagnetic phase of the TFIM. A complete set of states is given by

$$\left|k_1^{NS}, \ldots, k_{2m}^{NS}\right\rangle_{NS} = \prod_{j=1}^{2m} \alpha_{k_j^{NS}}^\dagger \left|0\right\rangle_{NS} \tag{2.45}$$

$$\left|k_1^{R}, \ldots, k_{2m+1}^{R}\right\rangle_{R} = \prod_{j=1}^{2m+1} \alpha_{k_j^{R}}^\dagger \left|0\right\rangle_{R} \tag{2.46}$$

for m integer and with momenta $k_j^{NS/R}$ satisfying (2.37) for states in the NS/R sector respectively. For $h < 1$ to get a positive energy we perform a particle-hole transformation $\alpha_0^\dagger \leftrightarrow \alpha_0$ and again define the vacuum in the Ramond sector to be the state which is annihilated by any annihilation operator. Due to the nature of the particle-hole transformation the new vacuum has odd fermion number and therefore both NS and R vacuua $|0\rangle_{NS}$ and $|0\rangle_R$ are physical states. A complete set of states is given by

$$\left|k_1^{NS}, \ldots, k_{2m}^{NS}\right\rangle = \prod_{j=1}^{2m} \alpha_{k_j^{NS}}^\dagger |0\rangle_{NS} \tag{2.47}$$

$$\left|k_1^{R}, \ldots, k_{2m}^{R}\right\rangle = \prod_{j=1}^{2m} \alpha_{k_j^{R}}^\dagger |0\rangle_{R} \,. \tag{2.48}$$

The lowest energy states are the two vacuua with the energies of these states are given by

$$E(|0\rangle_{NS}) = -\frac{1}{2} \sum_{n=-\frac{L}{2}}^{\frac{L}{2}-1} \varepsilon(k_n^{NS}) \tag{2.49}$$

$$E(|0\rangle_{R}) = -\frac{1}{2} \sum_{n=-\frac{L}{2}}^{\frac{L}{2}-1} \varepsilon(k_n^{R}) \tag{2.50}$$

which can be shown to be equal up to corrections, which are exponentially small in system size and vanish in the large L limit. Therefore for $L \to \infty$, which is the case of interest for us, we have a ground state degeneracy with the two ground states given by

$$|GS\rangle_{h<1}^{(1,2)} = \frac{1}{\sqrt{2}}(|0\rangle_R \pm |0\rangle_{NS}) \tag{2.51}$$

Spontaneous symmetry breaking selects one of the ground states characterising the ferromagnetic phase of the TFIM.

2.4.2 Full Counting Statistics and Generating Function

We are interested in the properties of the smooth and staggered components of the transverse magnetization of a chain segment of length $\ell < L$. These are de-

fined as

$$S_u^z(\ell) = \sum_{j=1}^{\ell} \sigma_j^z \ , \qquad S_s^z(\ell) = \sum_{j=1}^{\ell} (-1)^j \sigma_j^z \ . \tag{2.52}$$

Given a density matrix ρ that specifies the quantum mechanical state of our system, the probability distributions for the transverse subsystem magnetizations are given in the same way as in Chapter 2.2 by

$$P^{(\mathrm{u,s})}(m) = \mathrm{Tr}\big(\rho\, \delta\big(m - S_{u,s}^z(\ell)\big)\big) \ . \tag{2.53}$$

In the following we will focus on the characteristic functions of these probability distributions, which are defined as

$$\begin{aligned} P^{(\mathrm{u,s})}(m) &= \int_{-\infty}^{\infty} \frac{d\lambda}{2\pi}\, e^{-i\lambda m}\, \chi^{(\mathrm{u,s})}(\lambda, \ell) \ , \\ \chi^{(\mathrm{u,s})}(\lambda, \ell) &= \mathrm{Tr}\left[\rho\, e^{i\lambda S_{u,s}^z}\right] . \end{aligned} \tag{2.54}$$

By construction, the expansion of $\chi^{(\mathrm{u,s})}(\lambda, \ell)$ around $\lambda = 0$ generates the moments of the associated probability distribution. Analogous to the discussion in 2.2 the following relations are readily inferred from the definition of $\chi^{(\mathrm{u,s})}(\lambda, \ell)$

$$\begin{aligned} \chi^{(\mathrm{u,s})}(\lambda, \ell) &= \left[\chi^{(\mathrm{u,s})}(-\lambda, \ell)\right]^* , \\ \chi^{(\mathrm{u,s})}(0, \ell) &= 1 \ , \\ \chi^{(\mathrm{u,s})}(\lambda + \pi, \ell) &= (-1)^{\ell} \chi^{(\mathrm{u,s})}(\lambda, \ell) \ . \end{aligned} \tag{2.55}$$

These properties imply

$$P^{(\mathrm{u,s})}(m) = \begin{cases} 2 \sum_{r \in \mathbb{Z}} \delta(m - 2r + \ell) P_w^{(\mathrm{u,s})}(r - \frac{\ell}{2}) & \text{if } \ell \text{ is odd} \\ 2 \sum_{r \in \mathbb{Z}} \delta(m - 2r) P_w^{(\mathrm{u,s})}(r) & \text{if } \ell \text{ is even} \end{cases} \tag{2.56}$$

where we have defined the weights

$$P_w^{(\mathrm{u,s})}(r) = \int_{-\pi/2}^{\pi/2} \frac{d\lambda}{2\pi} e^{-2i\lambda r} \chi^{(\mathrm{u,s})}(\lambda, \ell) \ . \tag{2.57}$$

These weights are closely related to the probability distribution of the transverse smooth and staggered subsystem magnetization as shown in 2.2.

2.4.3 Expectation values of even operators and $L \to \infty$

We are interested in expectation values of the form

$$\mathrm{Tr}\big(\rho\, e^{i\lambda S^{u,s}(\ell)}\big)\,. \tag{2.58}$$

The complete set of states both for $h > 1$ and $h < 1$ split into states in the NS sector and the R sector, distinguished by the total fermion number $\hat{N}$. Therefore the density matrix ρ, similarly to the Hamiltonian, can be written in block-form

$$\begin{aligned}\rho = &\sum_{i,j} \rho_{ij}^{NS} \left|i, NS\right\rangle \left\langle j, NS\right| + \sum_{i,j} \rho_{ij}^{R} \left|i, R\right\rangle \left\langle j, R\right| \\ &+ \sum_{i,j} \rho_{ij}^{NS-R} (\left|i, R\right\rangle \left\langle j, NS\right| + \left|i, NS\right\rangle \left\langle j, R\right|)\end{aligned} \tag{2.59}$$

where ρ_{ij}^{NS} and ρ_{ij}^{R} are the amplitudes for states from only NS and R sector respectively and ρ_{ij}^{NS-R} amplitudes of states connecting both sectors. As an example we can consider the density matrix corresponding to the ground state in the ferromagnetic regime

$$\rho_{GS,h<1} = \frac{1}{2} \left|0\right\rangle_{NS\ NS} \left\langle 0\right| + \frac{1}{2} \left|0\right\rangle_{R\ R} \left\langle 0\right| \pm \frac{1}{2} (\left|0\right\rangle_{NS\ R} \left\langle 0\right| + \left|0\right\rangle_{R\ NS} \left\langle 0\right|) \tag{2.60}$$

The fermionic parity operator $\mathcal{F} = e^{i\pi\hat{N}}$ distinguishes both sectors, which differ by total fermion number where for a state $|NS\rangle$ from the NS sector $\mathcal{F}\left|NS\right\rangle = \left|NS\right\rangle$ and for a state $|R\rangle$ from the R sector we have $\mathcal{F}\left|R\right\rangle = -\left|R\right\rangle$. Importantly the operators we are interested in are even under the fermionic parity operator

$$\mathcal{F} e^{i\lambda S^{u,s}(\ell)} \mathcal{F}^{\dagger} = e^{i\lambda S^{u,s}(\ell)} \tag{2.61}$$

and therefore the expectation value can be written as

$$\begin{aligned}\mathrm{Tr}\big(\rho\, e^{i\lambda S^{u,s}(\ell)}\big) =& \mathrm{Tr}\Bigg[\Big(\sum_{i,j} \rho_{ij}^{NS} \left|i, NS\right\rangle \left\langle j, NS\right| + \sum_{i,j} \rho_{ij}^{R} \left|i, R\right\rangle \left\langle j, R\right| \\ &+ \sum_{i,j} \rho_{ij}^{NS-R} (\left|i, R\right\rangle \left\langle j, NS\right| + \left|i, NS\right\rangle \left\langle j, R\right|)\Big) e^{i\lambda S^{u,s}(\ell)}\Bigg] \qquad (2.62) \\ =& \sum_{a=NS,R} \sum_{ij} \rho_{ij}^{a} \left\langle j, a\right| e^{i\lambda S^{u,s}(\ell)} \left|i, a\right\rangle \\ &+ \sum_{ij} \rho_{ij}^{NS-R} (\left\langle j, R\right| e^{i\lambda S^{u,s}(\ell)} \left|i, NS\right\rangle + \left\langle j, NS\right| e^{i\lambda S^{u,s}(\ell)} \left|i, R\right\rangle). \qquad (2.63)\end{aligned}$$

Using that the operator is even under fermionic parity we see that

$$\mathrm{Tr}\left(\rho\, e^{i\lambda S^{u,s}(\ell)}\right) = \sum_{a=NS,R} \sum_{ij} \rho^a_{ij} \left\langle j,a\right| e^{i\lambda S^{u,s}(\ell)} \left|i,a\right\rangle . \tag{2.64}$$

In the $L \to \infty$ limit expectation values in the Ramond and Neveu-Schwarz sector are equal (cf. [76]) and with the correct normalization of the expectation value we obtain

$$\mathrm{Tr}\left(\rho e^{i\lambda S^{u,s}(\ell)}\right) = \mathrm{Tr}_{NS}\left(\rho_{NS} e^{i\lambda S^{u,s}(\ell)}\right) \tag{2.65}$$

where we only have to consider states in the NS sector for both trace and density matrix. In the example given above for the GS of the ferromagnetic phase we therefore obtain

$$\mathrm{Tr}\left(\rho_{GS,h<1} e^{i\lambda S^{u,s}(\ell)}\right) = {}_{NS}\left\langle 0\right| e^{i\lambda S^{u,s}(\ell)} \left|0\right\rangle_{NS} . \tag{2.66}$$

As the Hamiltonian is block-diagonal in the fermion number basis time evolution does not mix sectors and we only have to consider time evolution in the NS sector in the large L limit. Therefore we can from now on drop the subscript NS and go to $L \to \infty$. The transformation between fermions on sites and operators diagonalizing the Hamiltonian (2.31) is then given by

$$c_j = \int_{-\pi}^{\pi} \frac{dk}{2\pi} e^{-ikj} \left[\cos(\theta_k/2)\alpha_k + i\sin(\theta_k/2)\alpha^\dagger_{-k}\right], \tag{2.67}$$

and the Hamiltonian takes the form

$$H(h) = \int_{-\pi}^{\pi} \frac{dk}{2\pi} \varepsilon(k) \left[\alpha^\dagger_k \alpha_k - \frac{1}{2}\right], \tag{2.68}$$

where the dispersion relation is again given by

$$\varepsilon(k) = 2\sqrt{1 + h^2 - 2h\cos(k)}. \tag{2.69}$$

For the purpose of taking the expectation value of the operators of interest the ground state of $H(h)$ is equal to the Bogoliubov vacuum state defined by

$$\alpha_k \left|0\right\rangle = 0. \tag{2.70}$$

and is even under fermionic parity $\mathcal{F}$, which will be useful later.

3

Full counting statistics in the transverse field Ising chain

Contents

From a theoretical point of view calculating the FCS for a given observable on a sizeable subsystem poses a formidable problem and as a result only very few exact results are available even in simple equilibrium situations. Even less is known about FCS after quantum quenches. This motivates reconsidering FCS in the transverse field Ising chain (TFIC). The TFIC is a key paradigm for quantum phase transitions [74] and a simple, but non-trivial, many-body system without particle number conservation and therefore provides an ideal playground for studying FCS both in and out of equilibrium. Indeed, thanks to the mapping of the TFIC to a model of non-interacting spinless fermions with pairing term it is possible to analytically determine ground state and thermal properties, see e.g. [74, 77, 78], as well as describe the non-equilibrium dynamics of local observables [75, 79–84] and of the reduced density matrix of a block of adjacent sites [83, 85–87] after a global quantum quench. A summary of these developments is given in the recent reviews Refs [76, 88].

In this work we focus on the FCS of the simplest observable, the transverse

magnetization within a block of ℓ adjacent spins. In the ground state this problem has been previously analysed in Refs [33, 35] and generic Gaussian states have been considered as well [38]. We note that the ground state FCS of the longitudinal magnetization in the field theory limit at the critical point has been determined in Ref. [34] and the ground state FCS of the subsystem energy was considered in Ref. [40].

This chapter is organised as follows. In Section 3.1 we provide a novel derivation of an efficient determinant representation for the FCS in general $\mathbb{Z}_2$ invariant Gaussian states. The result is equivalent to that of Ref. [38]. This result is applied in Section 3.2 to the determination of the FCS in equilibrium states. In the ground state we recover the results of Ref. [33]. Our results for the FCS in finite temperature equilibrium states are to the best of our knowledge new. In Section 3.3 we turn to the main point of interest: the time evolution of the FCS after a global quantum quench. We consider the situation where the system is prepared in a pure state at finite energy density and then time evolved with a Hamiltonian that does not commute with the initial state density matrix, which leads to non-trivial dynamics. We present explicit results for general "transverse field" quenches as well as evolution starting from a classical Néel state. The main result of this work is presented in Section 3.4: an analytic expression for the time evolution of the FCS after a transverse field quench.

3.1 Generating Function for a general Gaussian state

In this section we show how to obtain the generating function (2.54) for the operators

$$S^z_u(\ell) = \sum_{j=1}^{\ell} \sigma^z_j \ , \qquad S^z_s(\ell) = \sum_{j=1}^{\ell} (-1)^j \sigma^z_j \tag{3.1}$$

in a general Gaussian state with a novel method that recovers the results of Ref [38].

Our starting point is the realization that (2.54) depends only on the reduced

density matrix of the block A of ℓ adjacent spins

$$\chi^{(u,s)}(\lambda,\ell) = \mathrm{Tr}\left[\rho\, e^{i\lambda S^z_{u,s}(\ell)}\right] = \mathrm{Tr}\left[\rho_A\, e^{i\lambda S^z_{u,s}(\ell)}\right] \ , \tag{3.2}$$

where the reduced density matrix ρ_A is defined as the result of tracing out the complement of A from the density matrix ρ

$$\rho_A = \mathrm{Tr}_{\bar{A}}\left(\rho\right) \ . \tag{3.3}$$

As the Pauli matrices together with the identity form an orthonormal basis in the space of operators over $\mathbb{C}^2$ the reduced density matrix of a subsystem A that consists of ℓ neighbouring spins at sites $i = 1, \ldots, \ell$ can be expressed in the form

$$\rho_A = \frac{1}{2^\ell} \sum_{\{\alpha_1 \ldots \alpha_\ell\}} \mathrm{Tr}(\rho\, \sigma_1^{\alpha_1} \ldots \sigma_\ell^{\alpha_\ell})\, \sigma_1^{\alpha_1} \ldots \sigma_\ell^{\alpha_\ell} \ , \tag{3.4}$$

where $\alpha_i = 0, x, y, z$. In order to proceed we need to specify a convenient basis of operators. This is provided by Majorana fermions related to the lattice spin operators by

$$a_{2l-1} = \left(\prod_{m<l} \sigma_m^z\right) \sigma_l^x \ , \qquad a_{2l} = \left(\prod_{m<l} \sigma_m^z\right) \sigma_l^y \ , \qquad \sigma_l^z = i a_{2j} a_{2j-1}. \tag{3.5}$$

The Majorana fermions satisfy the algebra

$$\{a_j, a_k\} = 2\delta_{j,k} \ . \tag{3.6}$$

We now restrict our discussion to density matrices that are invariant under the $\mathbb{Z}_2$ fermionic parity transformation $\mathcal{F}$, which is given in terms of Pauli operators as $\mathcal{F} = \prod_{i=-\infty}^{\infty} \sigma_i^z$ and therefore satisfying the relations

$$\mathcal{F}\sigma_l^z\mathcal{F} = \sigma_l^z \ , \qquad \mathcal{F}\sigma_l^{x,y}\mathcal{F} = -\sigma_l^{x,y} \ . \tag{3.7}$$

In this case the Jordan-Wigner strings cancel and the reduced density matrix (RDM) is mapped to an operator expressed in terms of Majorana fermions acting on the same spatial domain

$$\rho_A = \frac{1}{2^\ell} \sum_{\{\mu_1 \ldots \mu_{2\ell}=0,1\}} \mathrm{Tr}(\rho\, a_1^{\mu_1} \ldots a_{2\ell}^{\mu_{2\ell}})\, a_{2\ell}^{\mu_{2\ell}} \ldots a_1^{\mu_1} \ . \tag{3.8}$$

We note that the case where $\mathcal{F}\rho\mathcal{F} \neq \rho$ can be dealt with by the method set out in Ref. [87], however as seen in the discussion in 2.4.3 for the even operators we are interested in and in the infinite system size limit, we can always work in just one of the sectors and therefore with a density matrix even under the fermionic parity operation.

Following Refs. [89–91] we can now show that the reduced density matrix ρ_A is Gaussian if the density matrix itself has this property. As we require the density matrix to be Gaussian, we can use (3.8) and Wick's theorem to express ρ_A in terms of the subsystem *correlation matrix* Γ^A_{nm}

$$\Gamma^A_{nm} = \mathrm{Tr}\left[\rho\, a_m a_n\right] - \delta_{nm}\ , \qquad 1 \leq m, n \leq 2\ell. \tag{3.9}$$

The RDM (3.8) can be written in an explicit Gaussian form as

$$\rho_A = \frac{1}{Z}\exp\left(\frac{1}{4}\sum_{m,n} a_m W_{mn} a_n\right), \tag{3.10}$$

if all the correlation functions of Majoranas within $1, \ldots, \ell$ with respect to this Gaussian density matrix and with respect to the reduced density matrix (3.8) agree. The matrix W is a skew symmetric $2\ell \times 2\ell$ hermitian matrix. As we have a Wick's theorem for both cases, we simply have to show that the two-point functions and therefore the correlation matrices are the same. Let us therefore look at

$$\Gamma^A_{nm} + \delta_{mn} = \mathrm{Tr}\left[\frac{1}{Z}\exp\left(\frac{1}{4}\sum_{i,j} a_i W_{ij} a_j\right) a_m a_n\right]. \tag{3.11}$$

As W is skew-symmetric we can perform an orthogonal transformation that block -diagonalises W such that

$$O^T W O = B \tag{3.12}$$

where

$$B = \begin{pmatrix} 0 & \lambda_1 & & & \\ -\lambda_1 & 0 & & & \\ & & 0 & \lambda_2 & \\ & & -\lambda_2 & 0 & \\ & & & & \ddots \end{pmatrix}. \tag{3.13}$$

Defining $b_n \equiv \sum_m O^T_{nm} a_m$, we can rewrite Γ^A_{nm} as

$$\Gamma^A_{nm} + \delta_{mn} = \sum_{k,l} \mathrm{Tr}\left[\frac{1}{Z}\exp\left(\frac{1}{4}\sum_{i,j} b_i B_{ij} b_j\right) b_l b_k\right] O^T_{lm} O_{nk} \tag{3.14}$$

Due to the block-diagonal structure of B, the blocks in the trace decouple and we only need to look at a 2×2 block of the matrix B:

$$\exp\left(\frac{1}{2} b_1 B_{12} b_2\right) = \left(\cosh\frac{\hat{B}}{2}\right)_{11} + \left(\sinh\frac{\hat{B}}{2}\right)_{12} b_1 b_2 \tag{3.15}$$

with

$$\hat{B} = \begin{pmatrix} 0 & B_{12} \\ -B_{12} & 0 \end{pmatrix}. \tag{3.16}$$

Therefore it is easy to see that

$$\begin{aligned} \Gamma^A_{nm} + \delta_{mn} =& \sum_{k,l}\left[\left(\tanh\frac{B}{2}\right)_{kl} + \delta_{kl}\right] O^T_{lm} O_{nk} \\ =& \left(\tanh\frac{W}{2}\right)_{nm} + \delta_{mn} \end{aligned} \tag{3.17}$$

where we used the orthogonality property to arrive at the second line. Therefore the matrix W can be related to the correlation matrix (3.9)

$$\tanh\frac{W}{2} = \Gamma^A \tag{3.18}$$

and the reduced density matrix ρ^A is explicitly Gaussian. Furthermore introducing the auxiliary "density matrices"

$$\widetilde{\rho}^{(u,s)} \equiv \frac{1}{\widetilde{Z}^{(u,s)}}\, e^{i\lambda S^z_{u,s}(\ell)}, \qquad \widetilde{Z}^{(u,s)} = \mathrm{Tr}\left[e^{i\lambda S^z_{u,s}(\ell)}\right] = (2\cos(\lambda))^\ell. \tag{3.19}$$

where the "partition function" $\widetilde{Z}^{(a)}$ ensures the normalisation $\mathrm{Tr}\big(\widetilde{\rho}^{(a)}\big) = 1$, the generating function can be written as

$$\chi^{(u,s)}(\lambda,\ell) \equiv \widetilde{Z}\ \mathrm{Tr}\left[\rho_A\ \widetilde{\rho}^{(u,s)}\right]\ , \quad a = u,s. \tag{3.20}$$

It is easily seen that the auxiliary density matrix $\tilde{\rho}^{(u,s)}(a)$ is Gaussian by writing the operator $S^{(u,s)}(\ell)$ in terms of fermions following Section 2.4.1. The corresponding

$2\ell \times 2\ell$ correlation matrices $\widetilde{\Gamma}^{(u,s)}$ of Majorana fermions are given by

$$\begin{aligned}
\widetilde{\Gamma}^{(u)}_{ij} &= \mathrm{Tr}\left[\widetilde{\rho}^{(u)}\ a_j a_i\right] = \frac{1}{\widetilde{Z}^{(u)}}\mathrm{Tr}\left(\prod_{k=1}^{\ell}(\cos\lambda - \sin\lambda a_{2k}a_{2k-1})a_j a_i\right) - \delta_{ij}\ , \\
\widetilde{\Gamma}^{(s)}_{ij} &= \mathrm{Tr}\left[\widetilde{\rho}^{(s)}\ a_j a_i\right] \\
&= \frac{1}{\widetilde{Z}^{(s)}}\mathrm{Tr}\left[\prod_{k=1}^{\ell}\left(\cos(\lambda) - (-1)^k \sin(\lambda)\ a_{2k}a_{2k-1}\right) a_j a_i\right] - \delta_{ij}. \qquad (3.21)
\end{aligned}$$

The only non-vanishing matrix elements are

$$\begin{aligned}
\widetilde{\Gamma}^{(u)}_{2j,2j-1} &= -\widetilde{\Gamma}^{(u)}_{2j-1,2j} = \frac{1}{2\cos\lambda}\mathrm{Tr}\left[(\cos\lambda - \sin\lambda\, a_{2j}a_{2j-1})a_{2j-1}a_{2j}\right] = -\tan\lambda\ , \\
\widetilde{\Gamma}^{(s)}_{2j,2j-1} &= -\widetilde{\Gamma}^{(s)}_{2j-1,2j} \\
&= \frac{1}{2\cos\lambda}\mathrm{Tr}\left[(\cos\lambda - (-1)^j \sin\lambda\, a_{2j}a_{2j-1})a_{2j-1}a_{2j}\right] \\
&= -(-1)^j \tan\lambda\ . \qquad (3.22)
\end{aligned}$$

This implies that $\widetilde{\Gamma}^{(u,s)}$ are block-diagonal, e.g.

$$\widetilde{\Gamma}^{(u)} = i\tan\lambda \begin{bmatrix} \sigma_y & 0 & \dots \\ 0 & \sigma_y & \dots \\ & & \ddots \end{bmatrix} \equiv i\tan(\lambda)\Sigma_y, \qquad (3.23)$$

where σ_y is the 2×2 Pauli matrix.

We have seen that both ρ_A and $\widetilde{\rho}^{(a)}$ are Gaussian operators in the fermionic representation of our problem and are univocally determined by the correlation matrices of the fundamental fermionic operators [89–91]. Moreover, the trace of the product of Gaussian operators such as (3.2) can be expressed in terms of the associated correlation matrices [92]. This is a very useful property, see e.g. Ref. [87] for a related application, that forms the basis of our analysis. We are now in a position to write down a convenient determinant representation for the generating functions $\chi^{(u,s)}(\lambda,\ell)$. To do so we employ a relation derived in Ref. [92]: given two Gaussian density matrices $\rho_{1,2}$ with correlation matrices $\Gamma_{1,2}$ the trace of their product is given by

$$\mathrm{Tr}\left[\rho_1\ \rho_2\right] = \pm\sqrt{\det\left(\frac{1+\Gamma_1\Gamma_2}{2}\right)}\ , \qquad (3.24)$$

with a sign ambiguity that needs to be fixed manually from the symmetries of $\chi^{(a)}(\lambda,\ell)$. Applying this relation to our case we arrive at the following determinant representations

$$\chi^{(a)}(\lambda,\ell)=\pm\frac{1}{(2\cos\lambda)^{\ell}}\sqrt{\det\left(\frac{1+\Gamma^{A}\widetilde{\Gamma}^{(a)}}{2}\right)}\,,\quad a=u,s\,, \tag{3.25}$$

where Γ^{A} and $\Gamma^{(u,s)}$ are given in (3.9) and (3.22), (3.23) respectively.

3.1.1 Simplifications in special cases

Equation (3.25) has been derived for a general $\mathbb{Z}_2$-invariant Gaussian state with density matrix ρ. If the state is also invariant under translations and reflections with respect to a site the generating function $\chi^{(u)}(\lambda,\ell)$ can be simplified further. Just from translation invariance the correlation matrix assumes a block Toeplitz form [85, 90]

$$\Gamma^{A}=\begin{pmatrix}\Pi_0 & \Pi_{-1} & \cdots & \Pi_{1-\ell}\\ \Pi_1 & \Pi_0 & & \vdots\\ \vdots & & \ddots & \vdots\\ \Pi_{\ell-1} & \cdots & \cdots & \Pi_0\end{pmatrix},\qquad \Pi_l=\begin{pmatrix}f_l^{oo} & g_l^{eo}\\ g_l^{oe} & f_l^{ee}\end{pmatrix}, \tag{3.26}$$

Using translational invariance again we can relate g_l^{oe} and g_l^{eo}

$$g_l^{oe}=\langle a_1a_{2l+2}\rangle=\langle a_{-2l-1}a_0\rangle=-\langle a_0a_{-2l-1}\rangle=-g_{-l}^{eo} \tag{3.27}$$

where the expectation value is defined as $\langle A\rangle=\mathrm{Tr}(\rho A)$ and we used translational invariance as well as the fermionic commutation of the Majorana operators. To relate f_l^{oo} to f_l^{ee} we need the additional reflection symmetry with respect to a site.

Assuming $l > 0$ we can write

$$\begin{aligned} f_l^{oo} + \delta_{l0} = \langle a_1 a_{2l+1} \rangle &= \left\langle \sigma_1^x \prod_{m=1}^{l} \sigma_m^z \sigma_{l+1}^x \right\rangle \\ &= \left\langle \sigma_{-1}^x \prod_{m=-l}^{-1} \sigma_m^z \sigma_{-l-1}^x \right\rangle \\ &= \left\langle \sigma_l^x \prod_{m=1}^{l} \sigma_m^z \sigma_0^x \right\rangle \\ &= \left\langle \sigma_0^x \sigma_0^z \prod_{m=0}^{l-1} \sigma_m^z \sigma_l^x \sigma_l^z \right\rangle \\ &= -\left\langle \sigma_0^y \prod_{m=0}^{l-1} \sigma_m^z \sigma_l^y \right\rangle = -\langle a_0 a_{2l} \rangle = -f_l^{ee} + \delta_{l0}, \end{aligned} \tag{3.28}$$

where we used the Jordan-Wigner mapping and mapping between Majorana fermions and complex fermions in the first line and reflection symmetry in the second line. With this we can write the blocks of the Toeplitz matrix as

$$\Pi_l = \begin{pmatrix} -f_l & g_l \\ -g_{-l} & f_l \end{pmatrix}, \tag{3.29}$$

here

$$\begin{aligned} g_l &= \mathrm{Tr}\big(\rho a_{2n} a_{2n+2l-1}\big) = -\mathrm{Tr}\big(\rho a_{2n-1} a_{2n-2l}\big) \,, \\ f_l &= \mathrm{Tr}\big(\rho a_{2n} a_{2n+2l}\big) - \delta_{l0} \,. \end{aligned} \tag{3.30}$$

Taking advantage of the block diagonal form of the correlation matrix of the auxiliary density matrix in (3.23) we can cast the generating function in the form

$$\chi^{(u)}(\lambda, \ell) = (2\cos\lambda)^{\ell} \sqrt{\det\left(\frac{1 - \tan(\lambda)\Gamma'}{2}\right)} \,, \tag{3.31}$$

where Γ' is a block Toeplitz matrix

$$\Gamma' = \begin{pmatrix} \Pi'_0 & \Pi'_{-1} & \cdots & \Pi'_{1-\ell} \\ \Pi'_1 & \Pi'_0 & & \vdots \\ \vdots & & \ddots & \vdots \\ \Pi'_{\ell-1} & \cdots & \cdots & \Pi'_0 \end{pmatrix}, \qquad \Pi'_l = \begin{pmatrix} g_l & f_l \\ f_l & g_{-l} \end{pmatrix}. \tag{3.32}$$

3.1.2 Expressions for the first few cumulants

The determinant representation (3.25) of the generating function provides an efficient way for determining the cumulants of the probability distribution, which is the main purpose of the function itself. The cumulants are obtained in the usual way from the series expansions of $\ln \chi^{(u,s)}(\lambda,\ell)$

$$\ln \chi^{(u,s)}(\lambda,\ell) = \sum_{n=1}^{\infty} \frac{C_n^{(u,s)}}{n!}(i\lambda)^n. \tag{3.33}$$

The first few terms of the series expansion are

$$\begin{aligned} \ln \chi^{(u)}(\lambda,\ell) &= \ell \ln(\cos\lambda) - \frac{1}{2}\sum_{n=1}^{\infty} \frac{(\tan\lambda)^n}{n} \mathrm{Tr}\left[(\bar{\Gamma})^n\right] \\ &= -\ell\frac{\lambda^2}{2} - \frac{\lambda}{2}\mathrm{Tr}\big(\bar{\Gamma}\big) - \frac{\lambda^2}{4}\mathrm{Tr}\big(\bar{\Gamma}^2\big) \\ &\quad -\frac{\lambda^3}{6}(\mathrm{Tr}\big(\bar{\Gamma}^3\big) + \mathrm{Tr}\big(\bar{\Gamma}\big)) + O(\lambda^4)\,, \end{aligned} \tag{3.34}$$

where we have defined

$$\bar{\Gamma} = -i\Gamma_A \Sigma_y\,, \tag{3.35}$$

with Σ_y defined in (3.23). The first three cumulants are

$$C_1 = \frac{i}{2}\mathrm{Tr}\big(\bar{\Gamma}\big)\,, \quad C_2 = \ell + \frac{\mathrm{Tr}\big(\bar{\Gamma}^2\big)}{2}\,, \quad C_3 = -\frac{i}{2}(\mathrm{Tr}\big(\bar{\Gamma}^3\big) + \mathrm{Tr}\big(\bar{\Gamma}\big)). \tag{3.36}$$

Specifying to the case of density matrices ρ that are invariant under translations and reflections around a site we have

$$\mathrm{Tr}\big(\bar{\Gamma}\big) = \ell\,\mathrm{Tr}(\Pi_0') = 2\ell g_0, \tag{3.37}$$

$$\begin{aligned} \mathrm{Tr}\big(\bar{\Gamma}^2\big) &= \ell\,\mathrm{Tr}\left(\sum_{j=0}^{\ell-1}(2(\ell-j)-\ell\delta_{j0})\Pi_j'\Pi_{-j}'\right) = 2\ell\sum_{j=0}^{\ell-1}(2(\ell-j)-\ell\delta_{j0})(g_j g_{-j} + f_j f_{-j}) \\ &= 2\ell\left(\sum_{j=1}^{\ell-1}(2(\ell-j))(g_j g_{-j} + f_j f_{-j}) + \ell g_0^2\right) = 2\mathrm{Tr}\big(F^2+G^2\big)\,, \end{aligned} \tag{3.38}$$

$$\mathrm{Tr}\big(\bar{\Gamma}^3\big) = 2\mathrm{Tr}\big(G^3 + 3F^2G\big)\,, \tag{3.39}$$

where F and G are the $\ell \times \ell$ Toeplitz matrices

$$G = \begin{pmatrix} g_0 & g_{-1} & \cdots & g_{1-\ell} \\ g_1 & g_0 & & \vdots \\ \vdots & & \ddots & \vdots \\ g_{\ell-1} & \cdots & \cdots & g_0 \end{pmatrix}, \qquad F = \begin{pmatrix} f_0 & f_{-1} & \cdots & f_{1-\ell} \\ f_1 & f_0 & & \vdots \\ \vdots & & \ddots & \vdots \\ f_{\ell-1} & \cdots & \cdots & f_0 \end{pmatrix}. \tag{3.40}$$

For the first three cumulants we obtain

$$C_1 = i\ell g_0 \ , \quad C_2 = \ell + \mathrm{Tr}\big(F^2 + G^2\big) \ , \quad C_3 = -i(\mathrm{Tr}\big(G^3 + 3F^2G\big) + \ell g_0) \ . \tag{3.41}$$

It is straightforward to generalise these considerations to higher cumulants because $\mathrm{Tr}\big(\bar{\Gamma}^n\big)$ can always be written as the sum of the traces of products of F and G.

3.2 Full counting statistics in equilibrium

In this section we analyse the generating function $\chi^{(u)}(\lambda, \ell)$ obtained from (3.25) and the associated probability distribution in equilibrium configurations. We first consider the ground state FCS, which has been previously studied by Cherng and Demler in [33]. We then turn to the FCS in finite temperature equilibrium states, which to the best of our knowledge has not been considered in the literature.

3.2.1 Full counting statistics in the ground state

According to the discussion in 2.4.3, the ground state density matrix is Gaussian. The generating function is therefore of the form (3.31), (3.32) with entries

$$f_l = 0, \tag{3.42}$$

$$g_l = -i \int_{-\pi}^{\pi} \frac{dk}{2\pi} e^{-ikl} e^{i\theta_k} \ , \tag{3.43}$$

where θ_k is the Bogoliubov angle (2.40). By rearranging rows and columns, $\bar{\Gamma}$ can be brought to a block diagonal form with $\ell \times \ell$ matrices G and G^T (3.40) on the diagonal and zero otherwise. This allows us to express the generating function as

$$\begin{aligned} \chi^{(u)}(\lambda, \ell) =& (2\cos\lambda)^{\ell} \sqrt{\det\left(\frac{1 - \tan(\lambda)G}{2}\right) \det\left(\frac{1 - \tan(\lambda)G^T}{2}\right)} \\ =& \det\left(\cos\lambda - \sin(\lambda)G\right) \ , \end{aligned} \tag{3.44}$$

This is precisely the result previously obtained by Cherng and Demler [33] by a different technique. They considered the generating function

$$\begin{aligned}\chi_{CD}(\lambda,\ell) =& \langle \mathrm{GS}|e^{i\lambda\sum_{j=1}^{\ell}\frac{1-\sigma_j^z}{2}}|\mathrm{GS}\rangle = e^{i\lambda\ell/2}\chi^{(u)}(-\lambda/2,\ell)\\ =& \det\left(\frac{1+e^{i\lambda}}{2}+\frac{1-e^{i\lambda}}{2}iG\right)\,. \end{aligned} \tag{3.45}$$

The Toeplitz determinant (3.44) can be analysed by standard methods [33]. The symbol of the Toeplitz matrix is defined as in Appendix 3.A. In the case under consideration it is given by

$$\tau(e^{ik}) = \cos\lambda + ie^{i\theta_k}\sin\lambda. \tag{3.46}$$

As long as the symbol has zero winding number a straightforward application of Szegő's Lemma gives, *cf.* Appendix 3.A

$$\lim_{\ell\to\infty}\frac{\ln\chi^{(u)}(\lambda,\ell)}{\ell} = \int_0^{2\pi}\frac{dk}{2\pi}\ln(\cos\lambda + ie^{i\theta_k}\sin\lambda)\,. \tag{3.47}$$

For $h<1$ and $\lambda>\lambda_c(h)$ the winding number of the symbol is 1 and the above result gets modified accordingly [35]. For a detailed analysis we refer to Ref. [35]. We note that all cumulants can be obtained from (3.47) since they are defined by the expansion close to $\lambda=0$. Consequently, the first cumulants are given by

$$\begin{aligned} C_1 &= \int_{-\pi}^{\pi}\frac{dk}{2\pi}e^{i\theta_k},\\ C_2 &= \int_{-\pi}^{\pi}\frac{dk}{2\pi}(1-e^{2i\theta_k}),\\ C_3 &= \int_{-\pi}^{\pi}\frac{dk}{2\pi}2(e^{3i\theta_k}-e^{i\theta_k}),\\ C_4 &= \int_{-\pi}^{\pi}\frac{dk}{2\pi}2(-1+4e^{2i\theta_k}-3e^{4i\theta_k}). \end{aligned} \tag{3.48}$$

The non-zero values of C_3 and C_4 show that the probability distribution is non-Gaussian.

3.2.2 Full counting statistics at finite temperature

We now turn to the FCS in finite temperature equilibrium states, which are particular examples of Gaussian states, and for which we are not aware of any results

in the literature. In this case, the correlation matrix has the same structure as for the ground state, but now

$$f_l = 0, \tag{3.49}$$

$$g_l = -i \int_{-\pi}^{\pi} \frac{dk}{2\pi} e^{-ikl} e^{i\theta_k} \tanh(\beta\epsilon_k/2)\,, \tag{3.50}$$

where ϵ_k is the dispersion relation (2.43). Since $f_l = 0$, the same simplifications as in the ground state case apply and the generating function can be expressed as

$$\chi^{(u)}(\lambda, \ell) = \det\left(\cos\lambda - \sin(\lambda) G\right). \tag{3.51}$$

In Fig. 3.1 we show $P_w^{(u)}(m)$ for subsystem size $\ell = 20$ and several different temper-

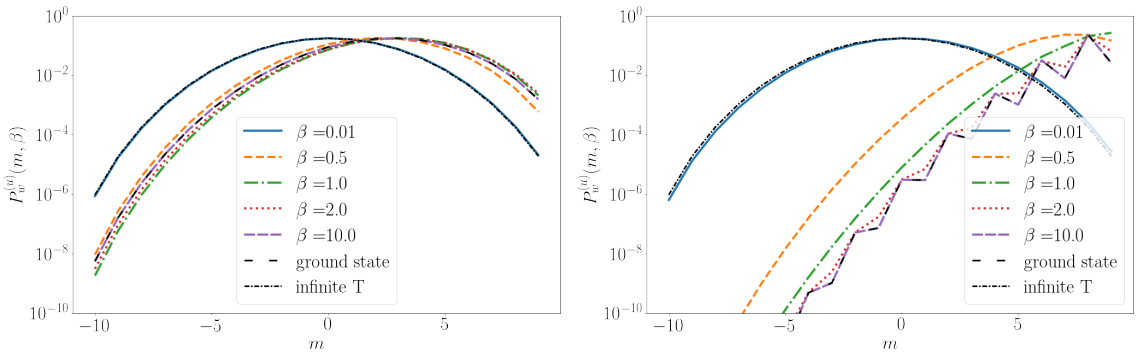

(a) (b)

Figure 3.1: Probability distribution as a function of m for $\ell = 20$ and several temperatures at (a) $h = 0.5$; (b) $h = 2$.

atures. We employ a log-linear plot in order to make the deviations of the probability distributions from a Gaussian form (which would correspond to a parabolic form) more apparent. We can see from Fig. 3.1 (a) that the temperature dependence for $h < 1$, corresponding to the ferromagnetically ordered phase at zero temperature, is not very pronounced. In contrast we see a much stronger temperature dependence in the paramagnetic phase, *cf.* Fig. 3.1 (b). At low temperatures the probability distribution is as expected asymmetric as a result of the applied field and is seen to display an even/odd structure. The latter disappears quickly as temperature is increased, whereas the asymmetry remains until the temperature exceeds the scale set by the magnetic field.

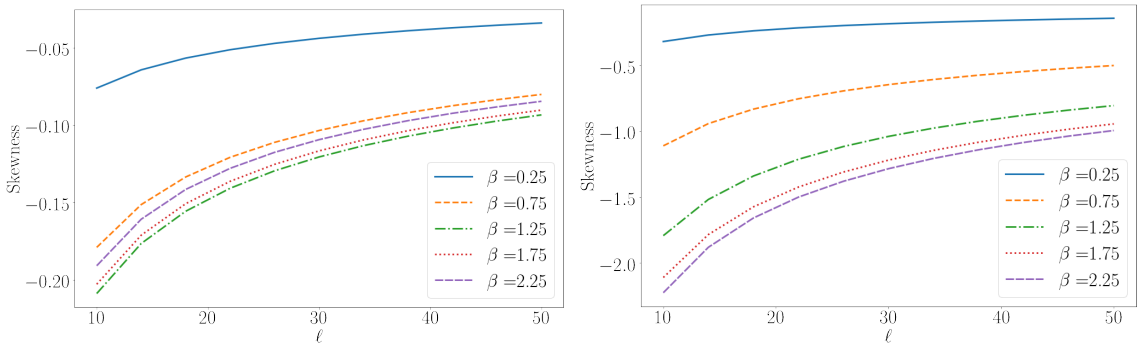

(a) (b)

Figure 3.2: Skewness as a function of ℓ for several values of β at (a) $h = 0.5$ and (b) $h = 2$.

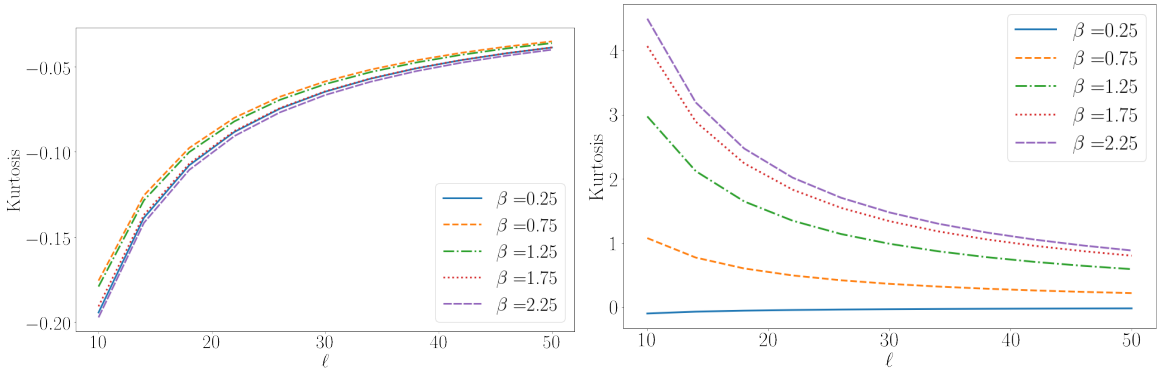

(a) (b)

Figure 3.3: Excess kurtosis as a function of subsystem size ℓ for several temperatures and (a) $h = 0.5$ and (b) $h = 2$.

In Figs 3.2 and 3.3 we show the skewness and excess kurtosis of the probability distribution as a function of subsystem size ℓ for a range of temperatures. These are defined as the thermal expectation values

$$\left\langle \left[\frac{X}{\sqrt{\langle X^2 \rangle_\beta}} \right]^3 \right\rangle_\beta , \quad \left\langle \left[\frac{X}{\sqrt{\langle X^2 \rangle_\beta}} \right]^4 \right\rangle_\beta - 3 , \quad X = S^z_u(\ell) - \langle S^z_u(\ell) \rangle_\beta . \tag{3.52}$$

Both skewness and excess kurtosis are non-vanishing for finite β and ℓ, which establishes that the distribution is not Gaussian. A very peculiar feature is that at fixed ℓ skewness and excess kurtosis are non-monotonic functions of the temperature in the ferromagnetic phase (cf. Fig. 3.4). Furthermore, we observe that at a fixed temperature they both tend to zero as the subsystem size ℓ is increased.

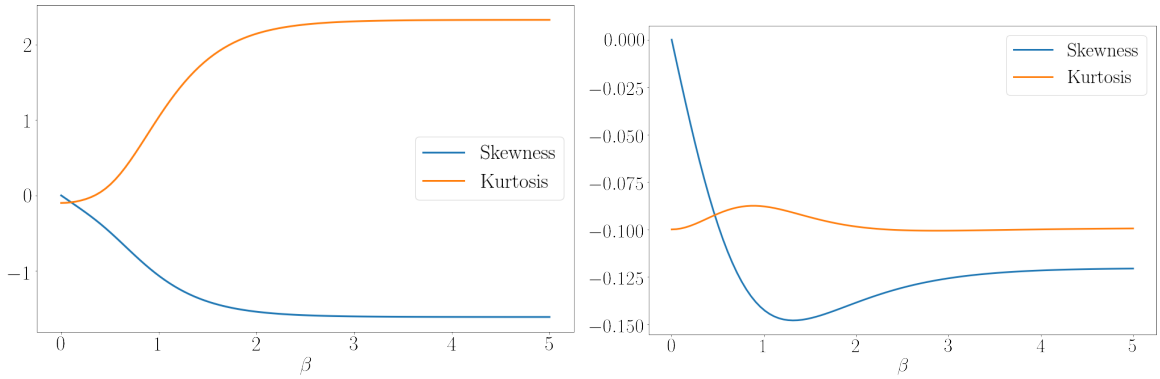

(a) (b)

Figure 3.4: Skewness and excess kurtosis as a function of β at fixed subsystem size $\ell = 20$ in (a) the paramagnetic regime at $h = 2$ and (b) in the ferromagnetic regime at $h = 0.5$. In the ferromagnetic regime we see non-monotonicities in β.

This signals that the corresponding probability distribution approaches a Gaussian. This is expected as for large subsystem sizes the laws of thermodynamics apply and the probability distribution is then approximately Gaussian with a standard deviation that scales as $\sqrt{\ell}$.

3.3 Full counting statistics after a quantum quench

We now turn to the time evolution of the characteristic function $\chi^{(u,s)}(\lambda, t)$ after quantum quenches. We consider two different classes of initial states:

- We initialize the system in the ground state of $H(h_0)$ and time evolve with $H(h)$. Such transverse field quenches have been studied in detail in the literature [75, 80–87, 93–102].

- We initialize the system in the Néel state $|\uparrow\downarrow\uparrow\downarrow \ldots \uparrow\downarrow\rangle$, thus breaking translational symmetry by one site. This symmetry is restored at late times after the quench and it is an interesting question how this is reflected in the probability distributions of observables.

3.3.1 Transverse field quench $h_0 \longrightarrow h$

In this quench protocol both the Hamiltonian and the initial state are translationally invariant. The characteristic function has the determinant representation (3.31), (3.32) with [85]

$$g_l = -i \int_{-\pi}^{\pi} \frac{\mathrm{d}k}{2\pi} e^{-ikl} e^{i\theta_k} \left(\cos \Delta_k - i \sin \Delta_k \cos(2\varepsilon_k t)\right) \tag{3.53}$$

$$f_l = \int_{-\pi}^{\pi} \frac{\mathrm{d}k}{2\pi} e^{-ikl} \sin \Delta_k \sin(2\varepsilon_k t) \ , \tag{3.54}$$

where

$$e^{i\theta_k} = \frac{h - e^{ik}}{\sqrt{1 + h^2 - 2h\cos k}} \ , \quad \cos \Delta_k = 4 \frac{hh_0 - (h + h_0)\cos k + 1}{\varepsilon_h(k)\varepsilon_{h_0}(k)} \ . \tag{3.55}$$

Using Szegő's Lemma it is straightforward to obtain the large-ℓ asymptotics in the initial ($t = 0$) and stationary ($t = \infty$) states. The $t = 0$ result corresponds to a ground state at field h_0 and has been discussed earlier.

3.3.1.1 Behaviour in the stationary state

The late time asymptotics of the generating function can be determined from Szegő's Lemma. For quenches into the paramagnetic phase $h > 1$ it takes the form

$$\lim_{t\to\infty} \frac{\ln \chi^{(u)}(\lambda, \ell, t)}{\ell} = \int_0^{2\pi} \frac{\mathrm{d}k}{2\pi} \ln\left(\cos\lambda + i \sin\lambda \cos\Delta_k e^{i\theta_k}\right) + \mathcal{O}(1/\ell) \ , \quad \ell \gg 1. \tag{3.56}$$

The $\mathcal{O}(\ell^{-1})$ corrections also follow from Szegő's Lemma. The real and imaginary parts of $\chi^{(u)}(\lambda, \ell, t)$ (with $\mathcal{O}(\ell^{-1})$ corrections included) are shown for a transverse field quench from $h_0 = 5$ to $h = 2$ and subsystem size $\ell = 100$ in Fig. 3.5.

For quenches into the ferromagnetic phase and $\lambda < \lambda_c(h_0, h)$, Eq. (3.56) continues to hold. However, for $\lambda > \lambda_c(h_0, h)$ the symbol exhibits non-zero winding number and the analysis needs to be modified, *cf.* Appendix 3.A. The probability distribution in the stationary state is obtained by Fourier transforming $\chi^{(u)}(\lambda, \ell, t)$. Examples for several transverse field quenches are shown in Fig. 3.6. We again

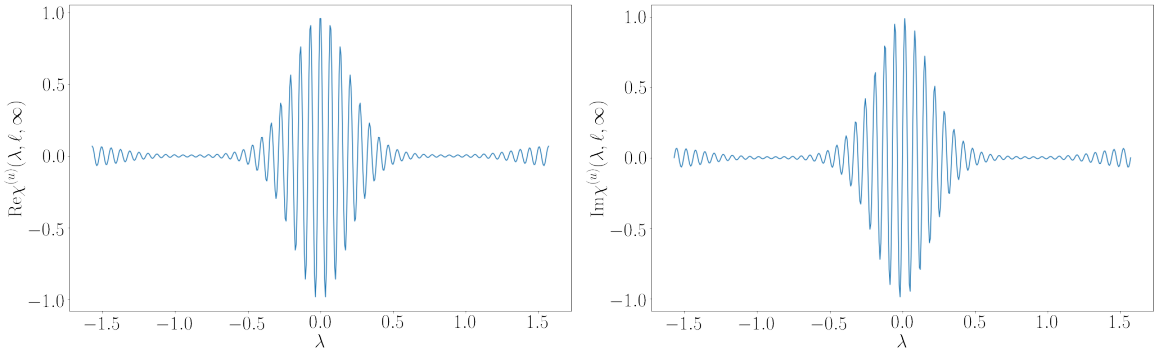

(a) (b)

Figure 3.5: (a) $\mathrm{Re}\chi^{(u)}(\lambda,\ell,\infty)$ and $\mathrm{Im}\chi^{(u)}(\lambda,\ell,\infty)$ for a quench from $h=5$ to $h=2$ and subsystem size $\ell=100$.

employ a logarithmic scale to make the deviations from a Gaussian form more apparent. In Figs 3.7 we plot the skewness and the excess kurtosis of the steady

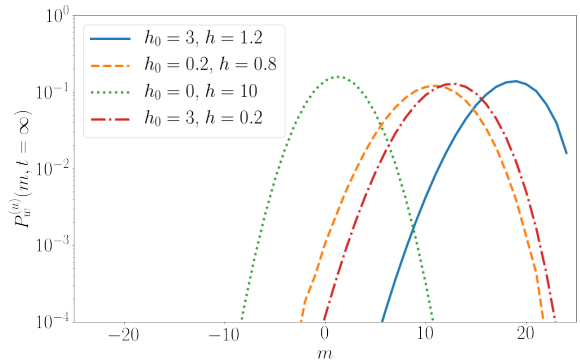

Figure 3.6: Stationary state probability distribution $P_w^{(u)}(m,\infty)$ for a subsystem of size $\ell=70$ for several transverse field quenches.

state probability distributions for a number of transverse field quenches. We observe that in all cases both skewness and excess kurtosis tend to zero for large subsystem sizes. This signals that the probability distributions approach Gaussians in the large-ℓ limit. While the steady states are non-thermal now, they still exhibit finite correlation lengths. Employing the same arguments as for finite temperature ensembles then implies that the cumulants of $S_u^z(\ell)$ are proportional to ℓ in the large-ℓ limit. This in turn suggests that skewness and excess kurtosis should scale as $\ell^{-1/2}$ and ℓ^{-1} respectively, while the standard deviation scales as $\ell^{1/2}$. These expectations are in perfect agreement with our findings (cf. Fig. 3.8).

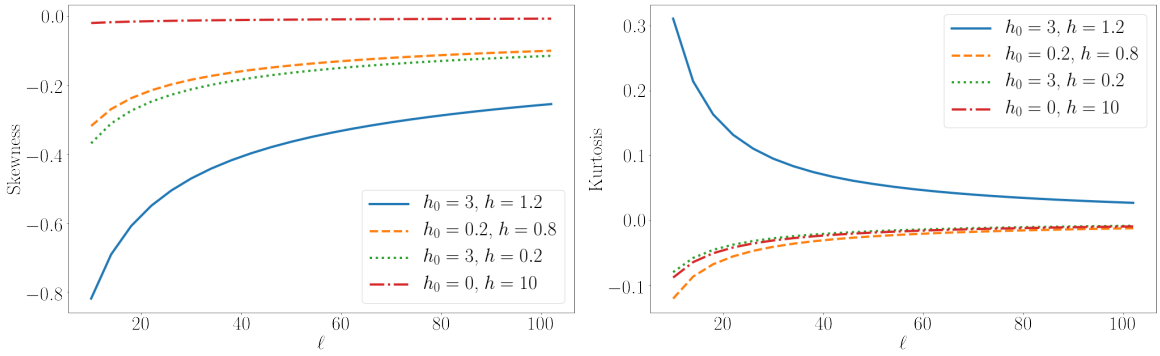

(a) (b)

Figure 3.7: (a) Skewness and (b) Excess kurtosis of the steady state probability distribution as functions of subsystem size ℓ for a number of transverse field quenches.

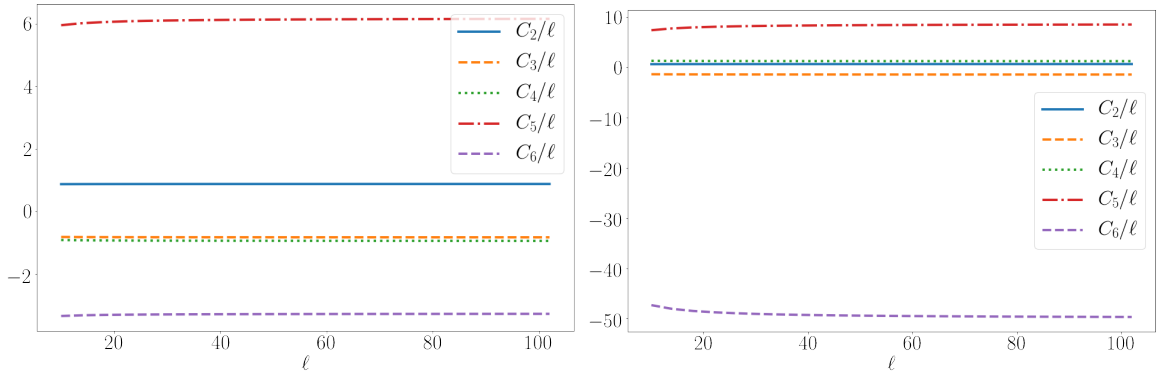

(a) (b)

Figure 3.8: Cumulants C_2 to C_6 over subsystem size ℓ for a quench from (a) $h = 0.2$ to $h = 0.8$ and (b) $h = 3$ to $h = 1.2$. The cumulants are seen to be linear in the subsystem size ℓ.

3.3.1.2 Scaling collapse

At finite times the FCS and the probability distribution can be computed efficiently from the determinant representation (3.31). Importantly we observe that for sufficiently large values of ℓ and t there is scaling collapse

$$\chi^{(u)}(\lambda, \ell, t) \approx \exp\left(\ell f(\lambda, t/\ell)\right) \ , \quad t, \ell \gg 1. \tag{3.57}$$

The property (3.57) is an important ingredient in the analytic calculation of the FCS described in Section 3.4. Several examples of the scaling behaviour of the real part of the generating function are shown in Figs 3.9, 3.10. The imaginary parts exhibit

a similar scaling collapse.

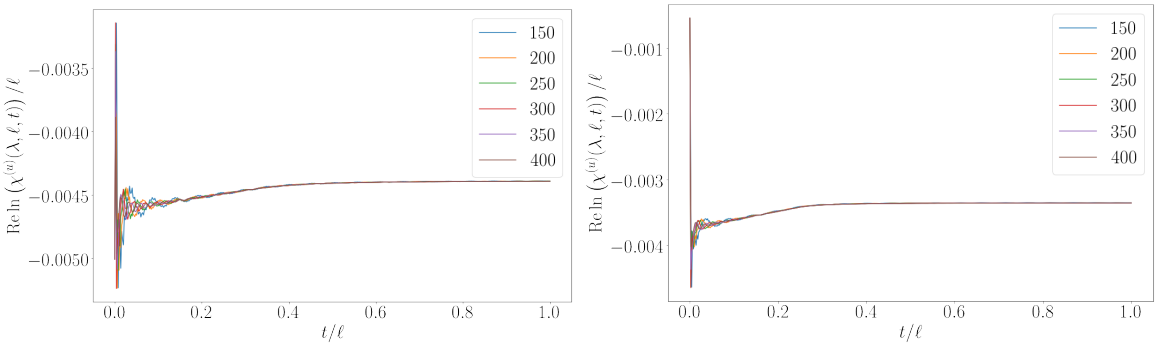

(a) (b)

Figure 3.9: $\mathrm{Re}\ln\chi^{(u)}(0.1,\ell,t)/\ell$ for several values of ℓ for a quench from (a) $h=0.2$ to $h=0.8$ and (b) $h=3$ to $h=1.2$. The data for different subsystem sizes are seen to collapse at sufficiently late times.

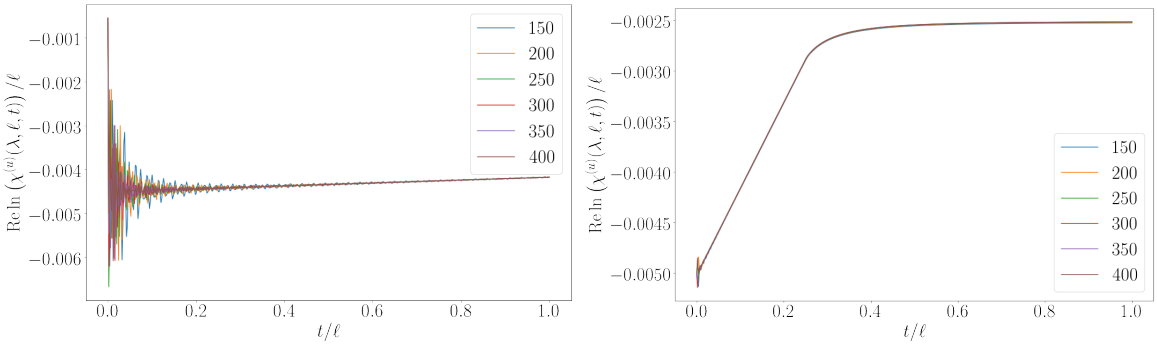

(a) (b)

Figure 3.10: $\mathrm{Re}\ln\chi^{(u)}(0.1,\ell,t)/\ell$ for several values of ℓ for a quench from (a) $h=3$ to $h=0.2$ and (b) $h=0$ to $h=20$. The data for different subsystem sizes are seen to collapse at sufficiently late times.

For quenches *towards* the ferromagnetic regime the scaling collapse for general values of λ can be significantly worse, and then really only emerges at rather large subsystem sizes ℓ, *cf.* Fig. 3.11. Like in the case of the stationary state discussed above, *c.f.* Section 3.3.1.1, there exists a critical value $\hat{\lambda}_c(h_0,h)$ of the counting parameter such that for $\lambda<\hat{\lambda}_c(h_0,h)$ the scaling collapse is excellent, while for $\lambda>\hat{\lambda}_c(h_0,h)$ no collapse is observed at the times and subsystem sizes of interest here. Instead after a rapid evolution for short times, an ℓ and λ dependent slow drift towards the stationary value can be seen for very long times (cf. Fig. 3.12). For

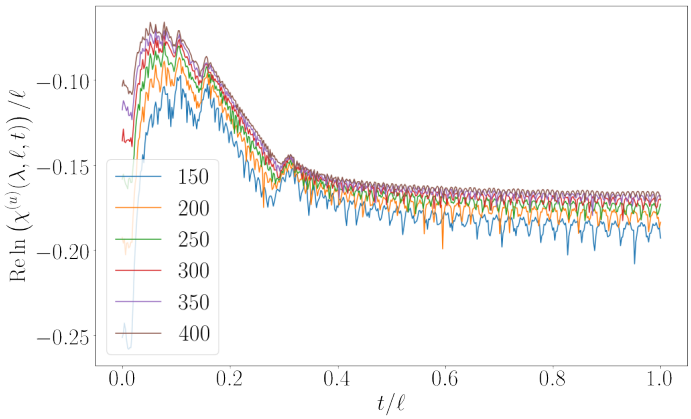

Figure 3.11: $\mathrm{Re}\ln\chi^{(u)}(1.4,\ell,t)/\ell$ for several values of ℓ for a quench from $h=0.2$ to $h=0.8$. The data for different subsystem sizes are seen to collapse at sufficiently late times only for very large subsystem sizes ℓ.

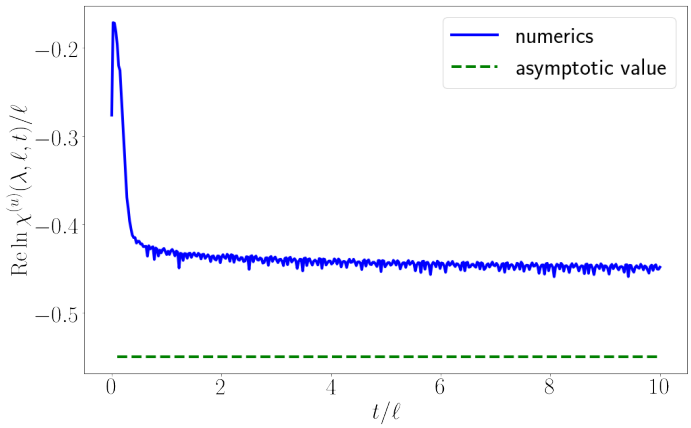

Figure 3.12: $\mathrm{Re}\ln\chi^{(u)}(\lambda,\ell,t)/\ell$ at $\lambda=1.1$ for a quench in the ferromagnetic phase from $h_0=0$ to $h=0.8$ as a function of t as well as the stationary value at $t\to\infty$. After a period of short time decay we see a very slow relaxation towards the stationary value.

the cases we have considered $\hat{\lambda}_c(h_0,h)$ coincides with $\lambda_c(h_0,h)$, which is the value of the counting parameter above which the symbol has non-zero winding number. We note however, that in cases like the one shown in Fig. 3.11 the generating function itself is extremely small and will not give a significant contribution to the corresponding probability distribution.

3.3.1.3 Time dependence of the probability distribution

There are basically four different kinds of transverse field quenches and we now consider them in turn.

1. Quenches within the ferromagnetic phase. For such quenches the probability distribution remains very narrow and approximately Gaussian throughout, *cf.* Fig. 3.13. For the parameters considered the average relaxes quickly towards its stationary value.

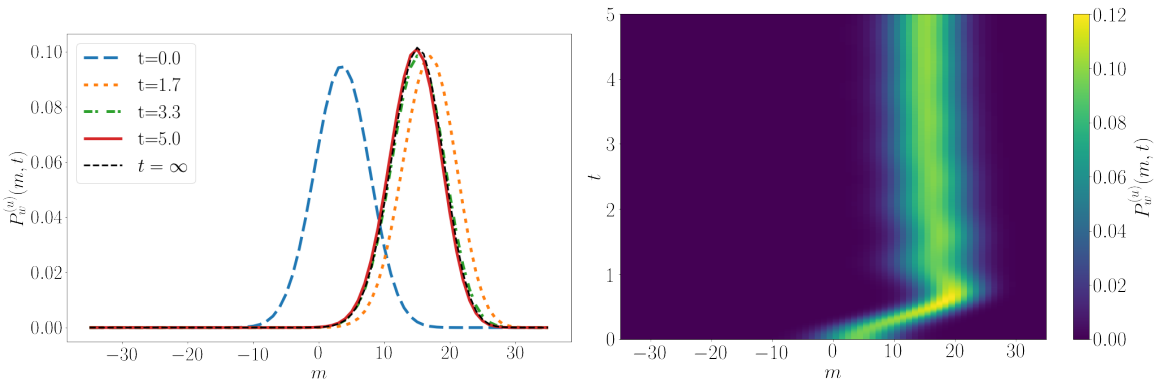

Figure 3.13: (a) Probability distribution $P_w^{(u)}(m,t)$ at times $t = 0, 1.7, 3.3, 5.0$ after a quench from $h = 0.2$ to $h = 0.8$ for subsystem size $\ell = 70$. (b) Probability distribution $P_w^{(u)}(m,t)$ for the same parameters.

2. Quenches within the paramagnetic phase.

   Here the initial probability distribution exhibits an even/odd structure. This can be understood by doing perturbation theory around the large h_0 limit, *cf.* Appendix 3.B. After the quench the mean of the probability distribution broadens and shifts towards smaller values of m. The alternating structure is initially preserved but then gets smoothed out. At late times $P_w^{(u)}(m,t)$ is well described by a Gaussian.

3. Quenches from the paramagnetic to the ferromagnetic phase.

   Here the probability distribution is initially peaked at a large value of m and displays an even/odd structure. At later times it broadens and becomes

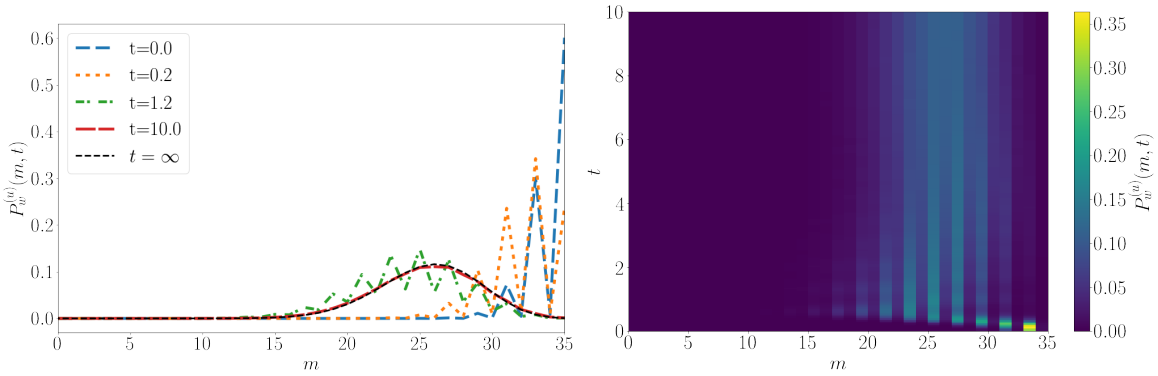

(a) (b)

Figure 3.14: (a) Probability distribution $P_w^{(u)}(m,t)$ at times $t = 0, 0.2, 1.2, 10.0$ after a quench from $h = 3$ to $h = 1.2$ for subsystem size $\ell = 70$. (b) Probability distribution $P_w^{(u)}(m,t)$ for the same parameters.

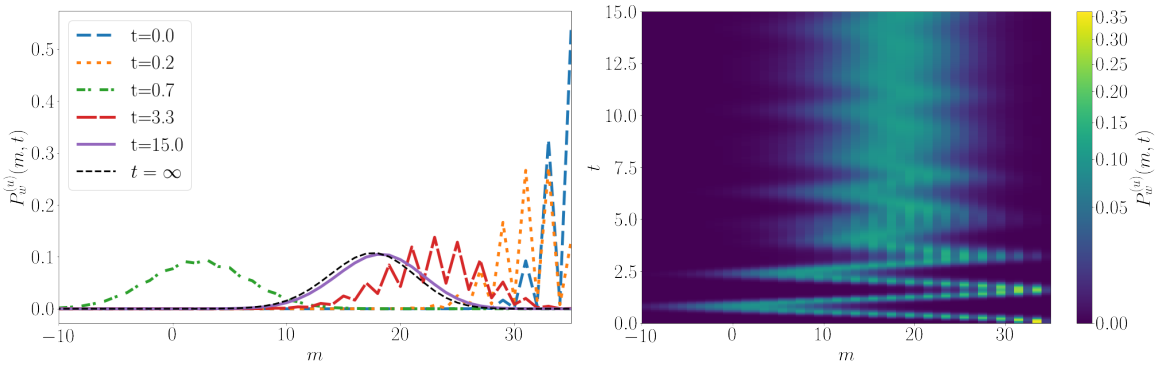

(a) (b)

Figure 3.15: (a) Probability distribution $P_w^{(u)}(m,t)$ at times $t = 0, 0.2, 0.7, 3.3, 15.0$ after a quench from $h = 3$ to $h = 0.2$ for subsystem size $\ell = 70$. (b) Probability distribution $P_w^{(u)}(m,t)$ for the same parameters.

smooth, while relaxing towards its stationary profile in an strongly oscillatory manner.

4. Quenches from the ferromagnetic to the paramagnetic phase.

   In this case the probability distribution shows very little variation in time and remains narrow and approximately Gaussian throughout the evolution. It was pointed out in Ref. [99] that the return amplitude exhibits a non-analyticity at some finite time t^* after the quantum quench. This phenomenon was termed a "dynamical phase transition". Local operators are known to be

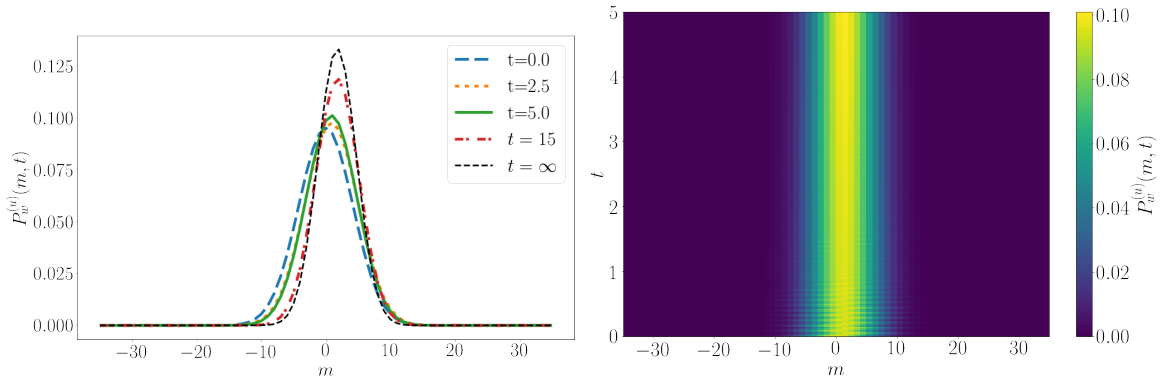

(a) (b)

Figure 3.16: (a) Probability distribution $P_w^{(u)}(m,t)$ at times $t = 0, 2.5, 5.0$ after a quench from $h = 0$ to $h = 10$ for subsystem size $\ell = 70$. (b) Probability distribution $P_w^{(u)}(m,t)$ for the same parameters.

insensitive to this phenomenon [75, 82, 83]. We have investigated the behaviour of $P_w^{(u)}(m,t)$ in the vicinity of t^* but have not observed any unusual effects (cf. Fig. 3.17). We conclude that the probability distribution for the smooth subsystem magnetization in the transverse field direction is also insensitive to the "dynamical phase transition".

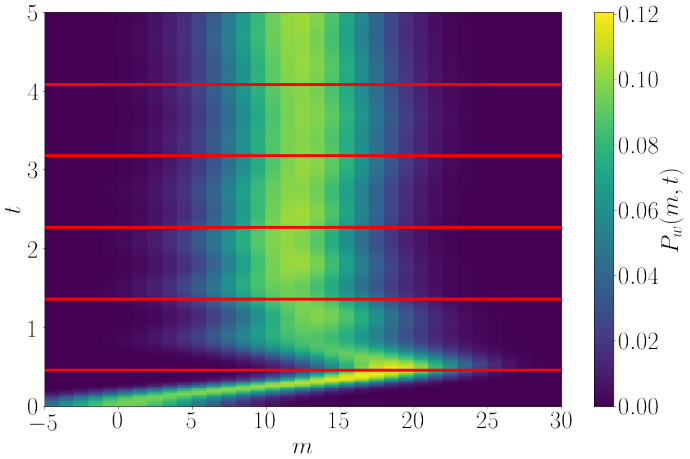

Figure 3.17: Probability distribution $P_w^{(u)}(m,t)$ after a quench from $h = 0$ to $h = 2$ for subsystem size $\ell = 30$. The red lines indicate the times at which the non-analyticities occur in the Loschmidt echo in a quench across the critical point (cf. [99])

Again as a measure for non-Gaussianities of the probability distribution during

the time evolution we can plot Skewness and Kurtosis as a function of time in Fig. 3.18 for all four quenches. We see that for quenches starting in the paramagnetic regime Skewness and Kurtosis are large and quickly relax to the values in the stationary state. This is related to the even-odd effects in the probability distribution for quenches starting from this phase. For quenches originating in the ferromagnetic phase both Skewness and Kurtosis are always approximately of the value in the stationary state.

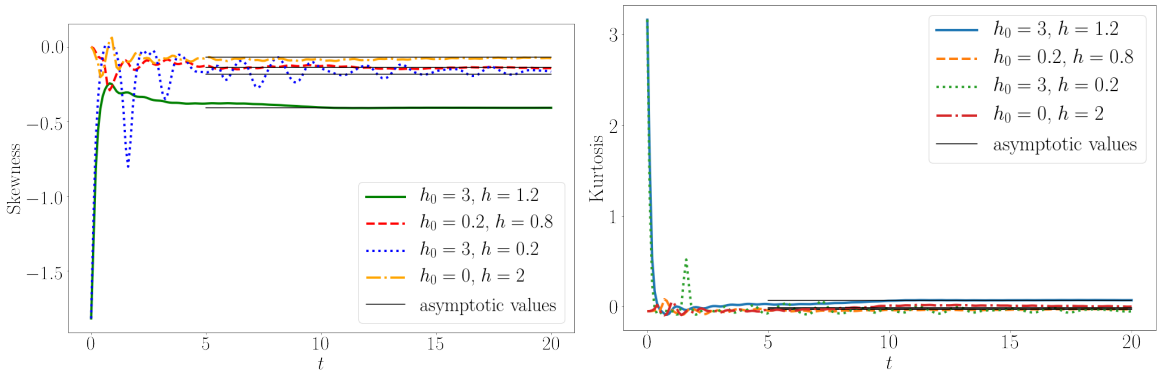

(a) (b)

Figure 3.18: (a) Skewness and (b) Kurtosis as a function of time for quenches between the different phases at subsystem size $\ell = 20$.

3.3.2 Quench from the Néel state

We now turn to the time evolution of $P_w^{(u,s)}(m,t)$ when the system is initialized in the Néel state $|\psi_0\rangle = |\uparrow\downarrow\uparrow\downarrow\ldots\uparrow\downarrow\rangle$. This explicitly breaks translational invariance by one site, but retains invariance under translation by two sites. As a result the subsystem correlation matrix is now a 4×4 block-Toeplitz matrix

$$\Gamma^A_{\text{Néel}} = \begin{pmatrix} \Pi_0^{\text{Néel}} & \Pi_{-1}^{\text{Néel}} & \cdots & \Pi_{1-\ell/2}^{\text{Néel}} \\ \Pi_1^{\text{Néel}} & \Pi_0^{\text{Néel}} & & \vdots \\ \vdots & & \ddots & \vdots \\ \Pi_{\ell/2-1}^{\text{Néel}} & \cdots & \cdots & \Pi_0^{\text{Néel}} \end{pmatrix}, \tag{3.58}$$

where we have assumed the subsystem size ℓ to be even and

$$\Pi_l^{\text{Néel}} = \begin{pmatrix} \langle a_1 a_{4l+1}\rangle - \delta_{0l} & \langle a_2 a_{4l+1}\rangle & \langle a_3 a_{4l+1}\rangle & \langle a_0 a_{4l-3}\rangle \\ \langle a_1 a_{4l+2}\rangle & \langle a_2 a_{4l+2}\rangle - \delta_{l0} & \langle a_3 a_{4l+2}\rangle & \langle a_0 a_{4l-2}\rangle \\ \langle a_1 a_{4l+3}\rangle & \langle a_2 a_{4l+3}\rangle & \langle a_3 a_{4l+3}\rangle - \delta_{l0} & \langle a_0 a_{4l-1}\rangle \\ \langle a_1 a_{4l+4}\rangle & \langle a_2 a_{4l+4}\rangle & \langle a_3 a_{4l+4}\rangle & \langle a_0 a_{4l}\rangle - \delta_{l0} \end{pmatrix}. \tag{3.59}$$

Here the number of degrees of freedom can again be reduced by the symmetries of the Hamiltonian and initial state, namely translation symmetry by two sites and reflection symmetry by a site. Using this analogously to the translation invariant case we obtain

$$\Pi_l^{\text{Néel}} = \begin{pmatrix} -f_l^{(1)} & g_l^{(1)} & f_l^{(3)} & g_l^{(2)} \\ -g_{-l}^{(1)} & f_l^{(1)} & -g_{-l+1}^{(2)} & f_{-l+1}^{(3)} \\ -f_{-l}^{(3)} & g_{l-1}^{(2)} & -f_l^{(2)} & g_l^{(3)} \\ -g_{-l}^{(2)} & -f_{l-1}^{(3)} & -g_{-l}^{(3)} & f_l^{(2)} \end{pmatrix} - \delta_{l,0}\mathbb{1} \tag{3.60}$$

where

$$f_l^{(1)} = \langle a_2 a_{4l+2}\rangle \tag{3.61}$$

$$f_l^{(2)} = \langle a_0 a_{4l}\rangle \tag{3.62}$$

$$f_l^{(3)} = \langle a_3 a_{4l+1}\rangle \tag{3.63}$$

$$g_l^{(1)} = \langle a_2 a_{4l+1}\rangle \tag{3.64}$$

$$g_l^{(2)} = \langle a_0 a_{4l-3}\rangle \tag{3.65}$$

$$g_l^{(3)} = \langle a_0 a_{4l-1}\rangle\,. \tag{3.66}$$

Additionally, the initial state is invariant under translation by one site and subsequent spin flip on all spins, given by action of the operator $\Sigma = \prod_j \sigma_j^x$. The Hamiltonian is not invariant under this operation, however one gets

$$\Sigma H(h)\Sigma = H(-h), \tag{3.67}$$

relating different two-point functions at opposite magnetic field value. As an example we obtain

$$f_l^{(1)}(h) = f_l^{(2)}(-h). \tag{3.68}$$

Explicit calculation of the two-point functions shows that these are anti-symmetric in $h \leftrightarrow -h$ and we see that $g_l^{(1)} = -g_l^{(3)}$, $g_l^{(2)} = 0$, $f_l^{(3)} = f_{-l}^{(3)}$ and $f_l^{(2)} = -f_l^{(1)}$. Therefore there are three remaining independent two point functions and we can write

$$\Pi_l^{\text{Néel}} = \begin{pmatrix} -f_l & g_l & h_l & 0 \\ -g_{-l} & f_l & 0 & h_l \\ -h_{-l} & 0 & f_l & -g_l \\ 0 & -h_{-l} & g_{-l} & -f_l \end{pmatrix} - \delta_{l,0}\mathbb{1} \ , \tag{3.69}$$

where the two-point functions are given by

$$\begin{aligned} f_l - \delta_{l0} &= i\int_0^{2\pi} \frac{\mathrm{d}k}{2\pi} e^{-2ijk}\Big[e^{i\theta_k}\cos\big(\varepsilon(k+\pi)t\big)\sin\big(\varepsilon(k)t\big) - \\ &\qquad e^{-i\theta_{k+\pi}}\cos\big(\varepsilon(k)t\big)\sin\big(\varepsilon(k+\pi)t\big)\Big] \ , \\ g_l &= i\int_0^{2\pi} \frac{\mathrm{d}k}{2\pi} e^{-2ijk}\Big[\cos\big(\varepsilon(k)t\big)\cos\big(\varepsilon(k+\pi)t\big) + \\ &\qquad e^{i(\theta_k+\theta_{k+\pi})}\sin\big(\varepsilon(k)t\big)\sin\big(\varepsilon(k+\pi)t\big)\Big], \\ h_l &= i\int_0^{2\pi} \frac{\mathrm{d}k}{2\pi} e^{-i(2j-1)k}\Big[e^{-i\theta_k}\cos\big(\varepsilon(k+\pi)t\big)\sin\big(\varepsilon(k)t\big) - \\ &\qquad e^{i\theta_{k+\pi}}\cos\big(\varepsilon(k)t\big)\sin\big(\varepsilon(k+\pi)t\big)\Big]. \end{aligned} \tag{3.70}$$

In the following we will determine the characteristic functions

$$\chi^{(u)}(\lambda,\ell,t) = \langle\psi_0(t)|e^{i\lambda S_u^z(\ell)}|\psi_0(t)\rangle \ , \qquad \chi^{(s)}(\lambda,\ell,t) = \langle\psi_0(t)|e^{i\lambda S_s^z(\ell)}|\psi_0(t)\rangle \ , \tag{3.71}$$

where again we have defined

$$S_u^z(\ell) = \sum_{j=1}^{\ell}\sigma_j^z \ , \quad S_s^z(\ell) = \sum_{j=1}^{\ell}(-1)^j\sigma_j^z \ . \tag{3.72}$$

According to our general discussion in Section 3.1 they have determinant representations of the form

$$\begin{aligned} \chi^{(u)}(\lambda,\ell,t) &= \pm\big(2\cos(\lambda)\big)^{\ell}\sqrt{\det\left(\frac{1+\Gamma^A_{\text{Néel}}\tilde{\Gamma}}{2}\right)} \ , \\ \chi^{(s)}(\lambda,\ell,t) &= \pm\big(2\cos(\lambda)\big)^{\ell}\sqrt{\det\left(\frac{1+\Gamma^A_{\text{Néel}}\tilde{\Gamma}^{\pi}}{2}\right)} \ , \end{aligned} \tag{3.73}$$

where $\tilde{\Gamma}^{\pi}_{2j,2j-1} = -\tilde{\Gamma}^{\pi}_{2j-1,2j} = -\tan(\lambda)(-1)^j$ and $\tilde{\Gamma}_{2j,2j-1} = -\tilde{\Gamma}^{\pi}_{2j-1,2j} = -\tan(\lambda)$ respectively.

3.3.2.1 Behaviour in the stationary state

We first consider the probability distributions for a finite subsystem of even size ℓ in the late time limit. As we will now show, the stationary state for the Néel quench is locally equivalent to an infinite temperature state. To see this we first note that the energy of the Néel state is

$$\langle\psi_0|H(h)|\psi_0\rangle = 0. \tag{3.74}$$

We can also look at expectation values of all higher conservation laws. In terms of spins their explicit representation is given by [76]

$$I^{(1,+)} = H(h), \tag{3.75}$$

$$I^{(n>1,+)} = -J\sum_j \left(S^{xx}_{j,j+n} + S^{yy}_{j,j+n-2}\right) + h\left(S^{xx}_{j,j+n-1} + S^{yy}_{j,j+n-1}\right), \tag{3.76}$$

$$I^{(n,-)} = -J\sum_j \left(S^{xy}_{j,j+n} - S^{yx}_{j,j+n}\right), \tag{3.77}$$

where $n \geq 1$ and

$$S^{\alpha\beta}_{j,j+\ell} = \sigma^\alpha_j \left[\prod_{k=1}^{\ell-1}\sigma^z_{j+k}\right]\sigma^\beta_{j+\ell}, \qquad S^{yy}_{j,j} = -\sigma^y_j. \tag{3.78}$$

From these expressions it can immediately be seen that

$$\langle\psi_0|I^{(n,\pm)}|\psi_0\rangle = 0. \tag{3.79}$$

The vanishing of the expectation value of Hamiltonian and all higher conserved quantities in the Néel state implies that the conserved Bogoliubov mode occupation numbers are given by

$$\langle\psi_0|\alpha^\dagger_k\alpha_k|\psi_0\rangle = \frac{1}{2}. \tag{3.80}$$

These characterize an infinite temperature equilibrium state. We conclude that the system will relax locally [76] to an infinite temperature steady state at late times after the quench. Using this observation it is then straightforward to work out the probability distributions $P^{(u)}(m, t=\infty)$ of $S^z_u(\ell) = \sum_{j=1}^{\ell}\sigma^z_j$ and $P^{(s)}(m,\infty)$

of $S_s^z(\ell) = \sum_{j=1}^{\ell} (-1)^j \sigma_j^z$. As shown in the introduction we have

$$P^{(u,s)}(m, t=\infty) = \begin{cases} 2\sum_{r\in\mathbb{Z}} \delta(m-2r+\ell) P_w^{(u,s)}(r-\frac{\ell}{2}, \infty) & \ell \text{ odd} \\ 2\sum_{r\in\mathbb{Z}} \delta(m-2r) P_w^{(u,s)}(r, \infty) & \ell \text{ even} \end{cases} . \tag{3.81}$$

As we are dealing with an infinite temperature state, we may calculate $P_w(r)$ by using a grand canonical ensemble and working in the simultaneous eigenbasis of the σ_j^z's. This reduces the calculation of $P_w(r)$ to the combinatorial problem of how many eigenstates there are for a given eigenvalue of $S_u^z(\ell)$ or $S_s^z(\ell)$. This is easily solved in terms of the binomial distribution

$$P_w^{(u)}(m, \infty) = P_w^{(s)}(m, \infty) = \frac{1}{2^\ell} \binom{\ell}{\ell/2 - m} \sim \sqrt{\frac{2}{\ell\pi}} \exp\left(-\frac{2m^2}{\ell}\right) . \tag{3.82}$$

The result (3.82) for large ℓ is of course reproduced by applying Szegő's Lemma for block Toeplitz matrices to the determinant representations (3.73). This gives

$$\lim_{t\to\infty} \frac{\ln \chi^{(u)}(\lambda, \ell, t)}{\ell} = \frac{1}{2} \ln\left(\cos^2(\lambda)\right) + \mathcal{O}(1/\ell) = \lim_{t\to\infty} \frac{\ln \chi^{(s)}(\lambda, \ell, t)}{\ell} , \quad \ell \gg 1. \tag{3.83}$$

Fourier transforming gives the Gaussian form of $P_w^{(u,s)}(m, \infty)$ in (3.82).

3.3.2.2 Time dependence

The time dependence of the probability distributions for both $S_u^z(\ell)$ and $S_s^z(\ell)$ can now be determined numerically from the determinant representation (3.73). Results for two values of the transverse field ($h = 0.2$ and $h = 2$) are shown in Figs 3.19, 3.20, 3.21 and 3.22. The probability distribution of $S_u^z(\ell)$ initially has a single peak at $m = 0$. At later times this peak broadens and relaxes towards the Gaussian profile (3.82). When quenching to the ferromagnetic phase, *cf.* Fig. 3.19, an additional feature emerges: an even/odd structure evolves at short times after the quench.

The probability distribution of $S_s^z(\ell)$ is useful for investigating the restoration of the translational symmetry. In the initial state $P_w^{(s)}(m, t=0)$ features a single peak at $m = -\ell/2$, which is a characteristic fingerprint of the classical Néel state (in z-direction). We first discuss quenches into the ferromagnetic phase. Here at short

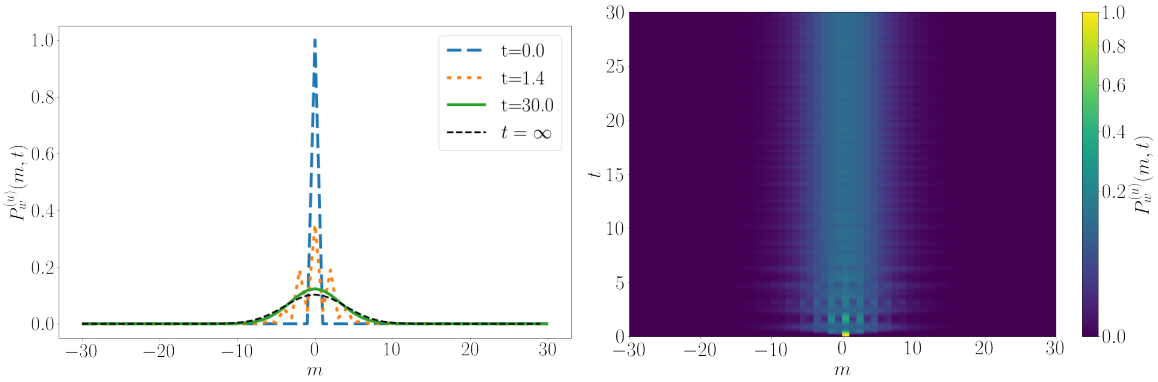

(a) (b)

Figure 3.19: $P_w^{(u)}(m,t)$ for a subsystem of size $\ell = 60$ at times $t = 0, 1.4, 30.0$ for a system initialized in a Néel state and time evolved with $H(h = 0.2)$. The dotted lines are the asymptotic probability distributions given in (3.82).

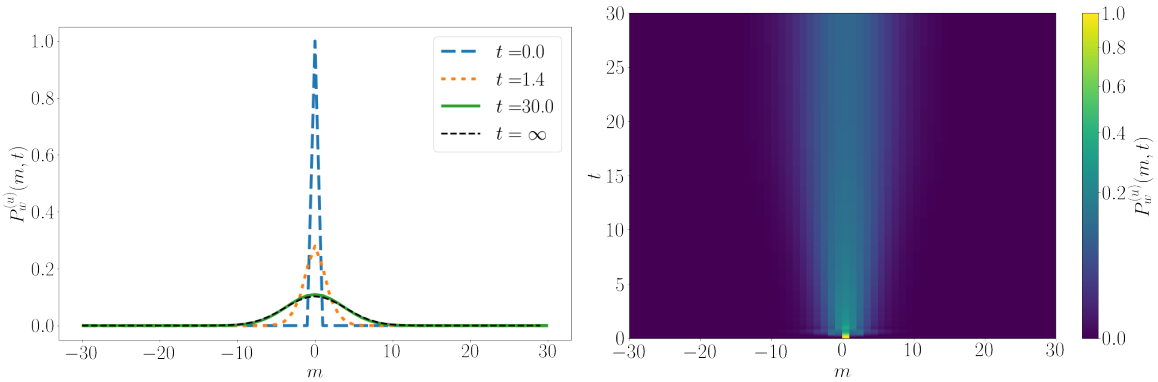

(a) (b)

Figure 3.20: $P_w^{(u)}(m,t)$ for a subsystem of size $\ell = 60$ at times $t = 0, 1.4, 30.0$ for a system initialized in a Néel state and time evolved with $H(h = 2)$. The dotted lines are the asymptotic probability distributions given in (3.82).

times after the quench $P_w^{(s)}(m,t)$ develops an even/odd structure and broadens significantly. The average of the probability distribution oscillates strongly in time and decays very slowly to its stationary value, which is a Gaussian distribution centred around $m = 0$. This shows that translational symmetry is restored very slowly.

The behaviour for quenches into the paramagnetic phase is broadly similar. An even/odd structure develops at early times, but is less pronounced that for quenches to the ferromagnetic phase. The average of $P_w^{(s)}(m,t)$ again oscillates

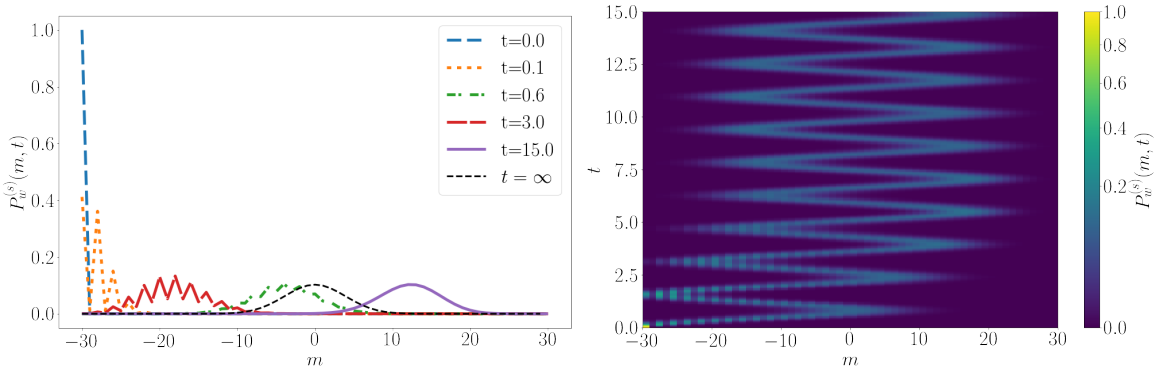

(a) (b)

Figure 3.21: $P_w^{(s)}(m,t)$ for a subsystem of size $\ell = 60$ at times $t = 0, 1.4, 30.0$ for a system initialized in a Néel state and time evolved with $H(h = 0.2)$. The dotted lines are the asymptotic probability distributions given in (3.82).

strongly around $m = 0$, but is seen to relax much more quickly than for quenches to the ferromagnetic phase. Approximate translational symmetry gets restored more rapidly.

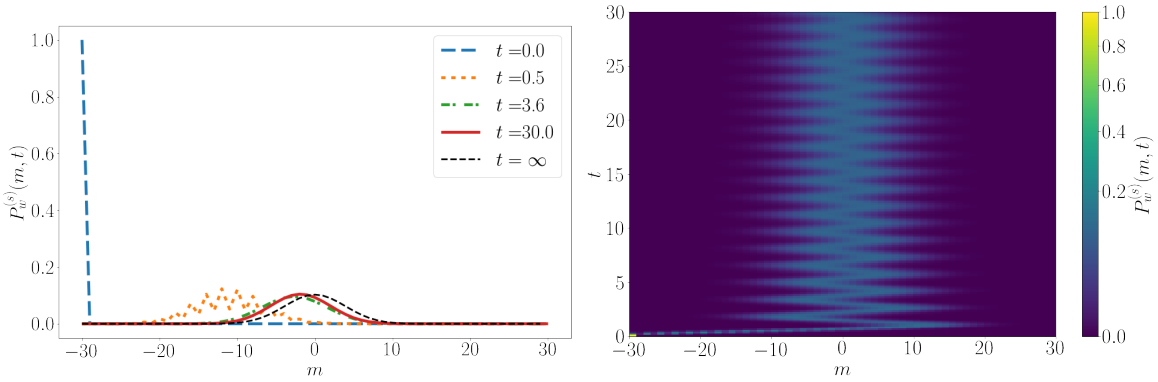

(a) (b)

Figure 3.22: $P_w^{(s)}(m,t)$ for a subsystem of size $\ell = 60$ at times $t = 0, 1.4, 30.0$ for a system initialized in a Néel state and time evolved with $H(h = 2)$. The dotted lines are the asymptotic probability distributions given in (3.82).

3.4 Analytic results for the probability distribution

We now restrict our discussion to the particular case of transverse field quenches. As we have seen above, in this case the characteristic functions $\chi^{(u)}(\lambda, \ell, t)$ exhibit

a scaling collapse at late times, *cf.* (3.57). This suggests that it might be possible to obtain analytic results for the late time asymptotics by a suitable generalization of the multi-dimensional stationary state approximation method previously used to determine the asymptotics of the order parameter two-point function [82] and the entanglement entropy [86]. As we will see, such a generalization is indeed possible, even though the case at hand is significantly more complicated.

Our starting point is the following expression

$$\ln \chi^{(u)}(\lambda, \ell, t) = \ell \ln(\cos\lambda) + \frac{1}{2}\mathrm{Tr}(\ln(1 - \tan\lambda\, \Gamma')) \ , \tag{3.84}$$

which is derived from (3.31) by using the identity $\ln(\det A) = \mathrm{Tr}(\ln(A))$. The second term in (3.84) can be expanded in a power series

$$\frac{1}{2}\mathrm{Tr}(\ln(1 - \tan\lambda\, \Gamma')) = -\frac{1}{2}\sum_{n=1}^{\infty} \frac{\big(\tan(\lambda)\big)^n}{n}\, \mathrm{Tr}\big[(\Gamma')^n\big] \ . \tag{3.85}$$

This then leads us to examine integer powers $(\Gamma')^n$ of the correlation matrix. Unlike in the case of the order parameter two-point function analysed in [75] odd powers do not vanish because Γ' is not a real anti-symmetric matrix. The *symbol* $t'(k)$ corresponding to the correlation matrix Γ' is defined by

$$(\Gamma')_{ln} = \int_{-\pi}^{\pi} \frac{\mathrm{d}k}{2\pi} e^{i(l-n)k}\ \hat{t}'(k) \ . \tag{3.86}$$

Its explicit expression for a magnetic field quench from h_0 to h is

$$\hat{t}'(k) = \begin{pmatrix} -ie^{i\theta_k}(\cos\Delta_k - i\sin\Delta_k\cos(2\varepsilon_k t)) & \sin\Delta_k \sin(2\varepsilon_k t) \\ \sin\Delta_k\sin(2\varepsilon_k t) & -ie^{-i\theta_k}(\cos\Delta_k + i\sin\Delta_k\cos(2\varepsilon_k t)) \end{pmatrix} , \tag{3.87}$$

where θ_k and Δ_k have been previous defined in (3.55). Following Ref. [75] we can represent the trace of powers of the correlation matrix as multiple integrals. For this let us first look at the second moment. The block matrix elements of Γ^2 can be written as

$$\big(\Gamma'^2\big)_{lm} = \sum_{m=1}^{\ell} \Gamma'_{lm}\Gamma'_{mn} = \int_{-\pi}^{\pi}\int_{-\pi}^{\pi} \frac{\mathrm{d}^2k}{(2\pi)^2} e^{i(lk_1 - nk_2)} \hat{t}'(k_1)\hat{t}'(k_2) \sum_{m=1}^{\ell} e^{im(k_1-k_2)}. \tag{3.88}$$

Evaluating the sum in a geometric series we can rewrite the sum as an integral:

$$\begin{aligned} e^{-i(\ell+1)k/2}\sum_{m=1}^{\ell} e^{imk} =& \frac{e^{ik}-e^{i(\ell+1)k}}{1-e^{ik}} e^{-i(\ell+1)k/2} \\ =& \frac{e^{-i\ell k/2}-e^{i\ell k/2}}{e^{-ik/2}-e^{ik/2}} \\ =& \frac{\ell}{2}\int_{-1}^{1} \mathrm{d}\xi \ \frac{k}{2\sin(k/2)} e^{i\ell\xi k/2}. \end{aligned} \tag{3.89}$$

This is easy to generalise to general n and one gets

$$\begin{aligned} \mathrm{Tr}\big[(\Gamma')^n\big] =& \left(\frac{\ell}{2}\right)^n \int_{-\pi}^{\pi} \frac{dk_1\dots dk_n}{(2\pi)^n} \int_{-1}^{1} d\xi_1\dots d\xi_n \\ & C\big(\vec{k}\big)\ F\big(\vec{k}\big)\ \exp\left(i\ell\sum_{j=0}^{n-1}\frac{\xi_j}{2}(k_{j+1}-k_j)\right), \end{aligned} \tag{3.90}$$

where we have defined $k_0 \equiv k_n$ and

$$C(\vec{k}) = \prod_{j=0}^{n-1} \frac{k_j - k_{j-1}}{2\sin\left[(k_j-k_{j-1})/2\right]}\ , \qquad F(\vec{k}) = \mathrm{Tr}\left(\prod_{i=0}^{n-1}\hat{t}'(k_i)\right)\ . \tag{3.91}$$

We now change variables

$$\zeta_0 = \xi_1\ , \quad \zeta_i = \xi_{i+1} - \xi_i\ ,\ i = 1,\dots,n-1\ . \tag{3.92}$$

The integration ranges in the ζ variables is determined by the constraints

$$-1 \le \sum_{j=0}^{k-1}\zeta_j \le 1\ , \quad k = 1,\dots,n. \tag{3.93}$$

The integral over ζ_0 can now be carried out as the integrand does not depend on it. This gives

$$\begin{aligned} \mathrm{Tr}\big[(\Gamma')^n\big] =& \left(\frac{\ell}{2}\right)^n \int_{-\pi}^{\pi} \frac{dk_1\dots dk_n}{(2\pi)^n} \int_{-1}^{1} d\zeta_1\dots d\zeta_{n-1}\ \mu(\vec{\zeta}) \\ & C\big(\vec{k}\big)\ F\big(\vec{k}\big)\ \exp\left(-i\ell\sum_{j=1}^{n-1}\frac{\zeta_j}{2}(k_j-k_0)\right), \end{aligned} \tag{3.94}$$

where $\mu(\{\zeta\})$ is the size of the range of ζ_0 under the constraints (3.93)

$$\mu(\vec{\zeta}) = \max\left[0, \min_{0\le j\le n-1}\left(1-\sum_{k=1}^{j}\zeta_k\right) + \min_{0\le j\le n-1}\left(1+\sum_{k=1}^{j}\zeta_k\right)\right]. \tag{3.95}$$

3.4.1 Multi-dimensional stationary phase approximation

For large values of ℓ the integrals can be carried out using a multi-dimensional stationary phase approximation. As the symbol is independent of ζ_j the stationarity conditions for the ζ_j's implies that the leading contribution to (3.94) derives from the region

$$k_j \approx k_0 \ , \quad j = 1, \ldots, n-1 \ . \tag{3.96}$$

We may thus replace k_j with k_0 everywhere except in rapidly oscillating terms in the symbol such as $e^{2i\varepsilon(k_j)t}$. In [75] this procedure was referred to as *localisation rule*. As in [82] application of this rule gives

$$C(\vec{k}) \approx 1 \ . \tag{3.97}$$

Obtaining a closed form expression for $F(\vec{k})$ is however much more involved than for the order-parameter two point function studied in Ref. [75]. Looking at the first terms, here e.g. the first three moments $\Pi_n = \mathrm{Tr}\left(\prod_{i=0}^{n-1} \hat{t}'(k_i)\right)$

$$\Pi_1 = -2iA\cos(c) + 2iB\cos(a_0)\sin(c) \tag{3.98}$$

$$\begin{aligned}\Pi_2 =& AB\left(2\cos\left(a_0\right)\sin(2c) + 2\cos\left(a_1\right)\sin(2c)\right) \\ &+ B^2\left(2\cos\left(a_0\right)\cos\left(a_1\right)\cos(2c) + 2\sin\left(a_0\right)\sin\left(a_1\right)\right) - 2A^2\cos(2c)\end{aligned} \tag{3.99}$$

$$\begin{aligned}\Pi_3 =& A^2B\left(-2i\cos\left(a_0\right)\sin(3c) - 2i\cos\left(a_1\right)\sin(3c) - 2i\cos\left(a_2\right)\sin(3c)\right) \\ &+ AB^2(-2i\cos\left(a_0\right)\cos\left(a_1\right)\cos(3c) - 2i\cos\left(a_2\right)\cos\left(a_1\right)\cos(3c) \\ &- 2i\cos\left(a_0\right)\cos\left(a_2\right)\cos(3c) - 2i\sin\left(a_0\right)\sin\left(a_1\right)\cos(c) \\ &- 2i\sin\left(a_0\right)\sin\left(a_2\right)\cos(c) - 2i\sin\left(a_1\right)\sin\left(a_2\right)\cos(c)) \\ &+ B^3\left(2i\cos\left(a_0\right)\cos\left(a_1\right)\cos\left(a_2\right)\sin(3c) + 2i\sin\left(a_0\right)\sin\left(a_1\right)\cos\left(a_2\right)\sin(c)\right. \\ &+2i\sin\left(a_0\right)\sin\left(a_2\right)\cos\left(a_1\right)\sin(c) + 2i\sin\left(a_1\right)\sin\left(a_2\right)\cos\left(a_0\right)\sin(c)) \\ &+ 2iA^3\cos(3c),\end{aligned} \tag{3.100}$$

where $a_i = 2\varepsilon(k_i)t$, $c = \theta_{k_0}$, $A = \cos\Delta_{k_0}$ and $B = -\sin\Delta_{k_0}$, we conjecture that application of the localization rule to $F(\vec{k})$ results in

$$F(\vec{k})\Big|_{\rm loc} = 2\sum_{A_1,A_2,A_3} \mathrm{sign}(A_1\cup A_2)(-i)^{n+S(A_1,A_2)}\,(\cos\Delta_{k_0})^{|A_3|}(\sin\Delta_{k_0})^{|A_1|+|A_2|} \times\cos\Big([n-2q(A_1)]\theta_{k_0}-\frac{\pi(|A_1|+|A_2|)}{2}\Big)\prod_{i\in A_1}\sin(2\varepsilon(k_i)t)\prod_{j\in A_2}\cos(2\varepsilon(k_j)t)\;. \tag{3.101}$$

Here the sum is over all partitions of the set of integers $\{0,1,\ldots,n-1\}$ into three sets A_1, A_2 and A_3, where the number of elements in A_1 is constrained to be even. The size of the set $B=\{b_1,b_2,\ldots\}$ is denoted by $|B|$ and we have defined

$$\begin{aligned} q(B) &= \mod_n\Big[\sum_{i=1}^{|B|}(-1)^{i+1}b_i\Big], \\ S(A_1,A_2) &= \begin{cases} 2 & \text{if } q(A_1)\le\frac{n}{2}, \quad \mod_2\big[\,|A_1\cup A_2|\,\big]=1 \text{ and } |A_1|>0 \\ 0 & \text{else.}\end{cases}\end{aligned} \tag{3.102}$$

Finally, $\mathrm{sign}(A)$ is the sign of the permutation required to bring the (integer) elements of the set A into ascending order. We have explicitly checked (3.101) for $1\le n\le 15$ but have not been able to find a rigorous proof for it.

We now use the identity (for even k)

$$\prod_{i=1}^{k}\sin(x_i)\prod_{j=k+1}^{k+m}\cos(x_j) = \frac{(-1)^{\frac{k}{2}}}{2^{k+m}}\sum_{i_1=0}^{1}\sum_{i_2=0}^{1}\cdots\sum_{i_{k+m}=0}^{1}\exp\left(i\sum_{j=1}^{k+m}(-1)^{i_j}x_j+i\pi\sum_{j=1}^{k}i_j\right)\;, \tag{3.103}$$

to rewrite the time-dependent factors in (3.101). This gives

$$\begin{aligned} F(\vec{k})\Big|_{\rm loc} =& 2\sum_{A_1,A_2,A_3}\mathrm{sign}(A_1\cup A_2)\,\frac{(-i)^{S(A_1,A_2)+n+|A_1|}}{2^{|A_1|+|A_2|}}(\cos\Delta_{k_0})^{|A_3|}(\sin\Delta_{k_0})^{|A_1|+|A_2|} \\ &\times\cos\Big([n-2q(A_1)]\theta_{k_0}-\frac{\pi(|A_1|+|A_2|)}{2}\Big) \\ &\times\sum_{p_1=0}^{1}\cdots\sum_{p_{|A_1|+|A_2|}=0}^{1}\exp\left(2it\sum_{r=1}^{|A_1|+|A_2|}(-1)^{p_r}\varepsilon(k_{(A_1\cup A_2)_r})+i\pi\sum_{r=1}^{|A_1|}p_r\right)\;, \end{aligned} \tag{3.104}$$

where $(A)_r$ is the r'th element of the set A and

$$(A_1\cup A_2)_r = \begin{cases}(A_1)_r & \text{if } r\le|A_1|,\\ (A_2)_{r-|A_1|} & \text{if } |A_1|<r\le|A_1|+|A_2|.\end{cases} \tag{3.105}$$

Application of the localization rule to (3.94) hence results in an expression of the form

$$\begin{aligned}\mathrm{Tr}\big[(\Gamma')^n\big]\Big|_{\mathrm{loc}} &= 2\left(\frac{\ell}{2}\right)^n \sum_{A_1,A_2,A_3} \mathrm{sign}(A_1\cup A_2)\,\frac{(-i)^{S(A_1,A_2)+n+|A_1|}}{2^{|A_1|+|A_2|}} \\ &\times(\cos\Delta_{k_0})^{|A_3|}(\sin\Delta_{k_0})^{|A_1|+|A_2|}\cos\left([n-2q(A_1)]\theta_{k_0}-\frac{\pi(|A_1|+|A_2|)}{2}\right) \\ &\times\sum_{p_1=0}^{1}\cdots\sum_{p_{|A_1|+|A_2|}=0}^{1}(-1)^{\sum_{r=1}^{|A_1|}p_r}\int_{-1}^{1}d\zeta_1\ldots d\zeta_{n-1}\;\mu(\vec{\zeta})\int_{-\pi}^{\pi}\frac{dk_1\ldots dk_n}{(2\pi)^n} \\ &\times\exp\left(2it\sum_{r=1}^{|A_1|+|A_2|}(-1)^{p_r}\varepsilon(k_{(A_1\cup A_2)_r})-i\ell\sum_{j=1}^{n-1}\frac{\zeta_j}{2}(k_j-k_0)\right)\;. \quad (3.106)\end{aligned}$$

In the next step we carry out a multi-dimensional stationary phase approximation for the $2n-2$ integrals over $\zeta_1,\ldots,\zeta_{n-1}$ and $k_1,\ldots,k_{n-1}$. We will assume that there is a single saddle point and use

$$\begin{aligned}&\int dx_1\ldots dx_k\;p(x_1,\ldots,x_k)e^{i\ell q(x_1,\ldots,x_k)}\approx \\ &\qquad\left(\frac{2\pi}{\ell}\right)^{k/2}\frac{p(x_1^{(0)},\ldots,x_k^{(0)})}{\sqrt{|\det A|}}\exp\left(i\ell q(x_1^{(0)},\ldots,x_k^{(0)})+\frac{i\pi\sigma_A}{4}\right), \quad (3.107)\end{aligned}$$

where σ_A the signature of the matrix A (i.e. the difference between the numbers of positive and negative eigenvalues), which is the Hessian of the function q evaluated at the saddle point

$$A_{ij}=\frac{\partial}{\partial x_i}\frac{\partial}{\partial x_j}\bigg|_{\vec{x}=\vec{x}^{(0)}} q(x_1,\ldots,x_k)\;. \quad (3.108)$$

In our case the saddle point conditions are

$$\begin{aligned}k_j^{(0)} &= k_0\;,\quad j=1,\ldots,n-1\;, \\ \zeta_j^{(0)} &= \begin{cases}\gamma_{A_1\cup A_2,k} & \text{if } j\in A_1\cup A_2\;,\\ 0 & \text{else}\;,\end{cases} \quad (3.109)\end{aligned}$$

where $\gamma_{A,k}=\frac{4t}{\ell}(-1)^{p_{(A)_k^{-1}}}\varepsilon'(k_0)$ and $(A_1\cup A_2)^{-1}$ is the inverse of the index-function $(A_1\cup A_2)_j$ defined above. The Hessian A is a matrix of the form

$$A=\frac{1}{2}\begin{pmatrix}0 & I\\ I & M\end{pmatrix}\;, \quad (3.110)$$

and hence we have $\det A = -4^{1-n}$ and $\sigma_A = 0$. The value of $\mu(\vec{\zeta})$ at the saddle point for a given sequence $\{p_1, p_2, \ldots, p_{|A_1|+|A_2|}\}$ is

$$\mu(\vec{\zeta}^{(0)}) = \max\left[0, \min_{0\le j\le |B|}\left(1-\sum_{k=1}^{j}\gamma_{B,k}\right) + \min_{0\le j\le |B|}\left(1+\sum_{k=1}^{j}\gamma_{B,k}\right)\right], \tag{3.111}$$

where $B = A_1 \cup A_2 - \{0\}$. The saddle point approximation thus gives

$$\begin{aligned}\mathrm{Tr}\big[(\Gamma')^n\big] \;\approx\; & \ell \sum_{A_1,A_2,A_3} \mathrm{sign}(A_1\cup A_2)\, \frac{(-i)^{S(A_1,A_2)+n+|A_1|}}{2^{|A_1|+|A_2|}} (\cos\Delta_{k_0})^{|A_3|}(\sin\Delta_{k_0})^{|A_1|+|A_2|} \\ & \times \cos\Big([n-2q(A_1)]\theta_{k_0} - \frac{\pi(|A_1|+|A_2|)}{2}\Big) \sum_{p_1=0}^{1}\cdots\sum_{p_{|A_1|+|A_2|}=0}^{1} (-1)^{\sum_{r=1}^{|A_1|} p_r} \\ & \times \int_{-\pi}^{\pi}\frac{dk_0}{2\pi}\,\mu(\vec{\zeta}^{(0)})\,\exp\left(-2it\varepsilon(k_0)\sum_{r=1}^{|A_1\cup A_2|}(-1)^{p_r}\right).\end{aligned} \tag{3.112}$$

The leading contribution to the final integral can then also be determined by a stationary phase approximation. This shows that all terms with $\sum_{r=1}^{|A_1\cup A_2|}(-1)^{p_r} \neq 0$ are suppressed at late times by a factor of $1/\sqrt{t}$. Conversely, the leading contribution to $\chi^{(u)}(\lambda,\ell,t)$ at late times arises from terms with $\sum_{r=1}^{|A_1\cup A_2|}(-1)^{p_r} = 0$, which requires $|A_1|+|A_2|$ to be even.

3.4.1.1 Structure of $\mu(\vec{\zeta}^{(0)})$

At this point it is useful to investigate the structure of $\mu(\vec{\zeta}^{(0)})$ for a given term in the multiple sum over $p_1, \ldots, p_{|A_1|+|A_2|}$ in more detail. For simplicity we focus on a particular example

$$|A_1| = |A_2| = 2\,, \quad \{p_{(A_1\cup A_2)_k^{-1}} | k = 1,\ldots,4\} = \{0,1,0,1\}. \tag{3.113}$$

In this case we have

$$\begin{aligned}\mu(\vec{\zeta}^{(0)}) &= \max\Big(0, \min(1, 1-\frac{4t}{\ell}\varepsilon'(k_0)) + \min(1, 1+\frac{4t}{\ell}\varepsilon'(k_0))\Big) \\ &= \max\Big(0, 2-\frac{4t}{\ell}\,|\varepsilon'(k_0)|\,\Big) = \Theta(\ell - 2\,|v_{k_0}|\,t)\Big(2-4\frac{t\,|v_{k_0}|}{\ell}\Big),\end{aligned} \tag{3.114}$$

where $v_{k_0} = \varepsilon'(k_0)$ is the group velocity of Bogoliubov fermions at momentum k_0 and $\Theta(x)$ is the Heaviside step function. The step function in (3.114) is reminiscent

of the light-cone structure found for two point correlation functions of local operators [14, 103–105] and entanglement entropies [85, 106, 107]. Repeating the above exercise for

$$|A_1| = |A_2| = m \ , \quad \{p_{(A_1 \cup A_2)_k^{-1}} | k = 1, \dots, 2m\} = \{\underbrace{1, 1, \dots, 1}_{m}, 0, 0, \dots, 0\} \ , \tag{3.115}$$

leads to the result

$$\mu(\vec{\zeta}^{(0)}) = \Theta(\ell - 2m\,|v_{k_0}|\,t)\Big(2 - 4m\frac{t\,|v_{k_0}|}{\ell}\Big) \ . \tag{3.116}$$

All other cases can be worked out analogously and lead to Heaviside step functions $\Theta(\ell - 2m\,|v_{k_0}|\,t)$ with $m \in \mathbb{N}_0$. We can calculate the moments $\mathrm{Tr}((\Gamma')^n)$ numerically as a first check of the validity of the saddle point approximation. As we sill have a sum over the partitions of n numbers for moment $\mathrm{Tr}((\Gamma')^n)$, calculation of large n becomes computationally expensive very quickly. The moments for $n = 5$ and $n = 6$ are shown in Fig. 3.23 and Fig. 3.24

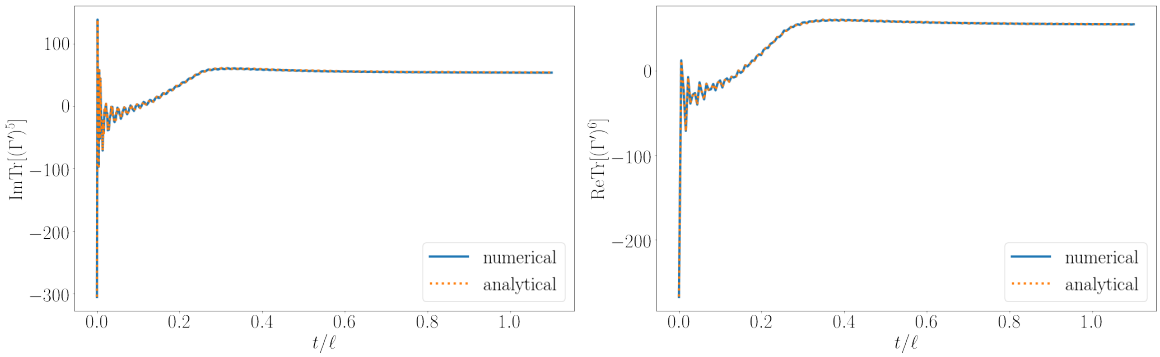

(a) (b)

Figure 3.23: Moments $\mathrm{Tr}((\Gamma')^n)$ for (a) $n = 5$ and (b) $n = 6$ for a transverse field quench from $h_0 = 5$ to $h = 1.5$. For moment 5 the imaginary part, whereas for moment 6 the real part is plotted, the respective other part is 0. The analytic approximation gives a very good description for almost all times.

3.4.2 Result for $\chi(\lambda, \ell, t)$

In order to obtain the logarithm of the characteristic function $\chi(\lambda, \ell, t)$ we now need to sum over all contributions (3.112) with coefficients given in (3.85). This is

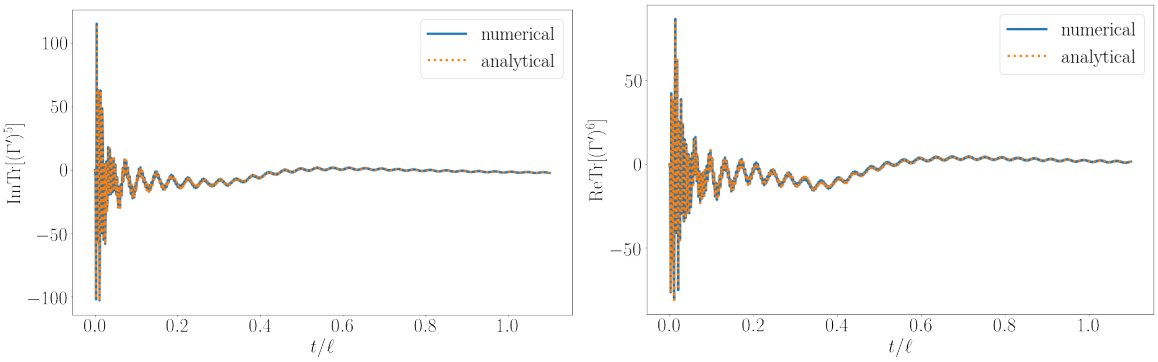

(a) (b)

Figure 3.24: Moments $\mathrm{Tr}((\Gamma')^n)$ for (a) $n = 5$ and (b) $n = 6$ for a transverse field quench from $h_0 = 0$ to $h = 0.8$. For moment 5 the imaginary part, whereas for moment 6 the real part is plotted, the respective other part is 0. The analytic approximation gives a very good description for almost all times.

a formidable task. It turns out that the structure of Heaviside step functions discussed above provides a very useful way of organizing the complicated summation required. The full result can be expressed in the form

$$\ln \chi^{(u)}(\lambda, \ell, t) \approx \ell \ln(\cos\lambda) + \frac{\ell}{2} \sum_{n=0}^{\infty} \int_0^{2\pi} \frac{dk_0}{2\pi} \Theta(\ell - 2n|v_k|t) \left[1 - \frac{2n|v_k|t}{\ell}\right] \times \sum_{m=0}^{n+1} \cos\left(2m\varepsilon(k_0)t\right) f_{n,m}(\lambda, k_0) + \mathcal{C} \,. \tag{3.117}$$

Here $\mathcal{C}$ is a constant that is beyond the accuracy of the stationary phase approximation and the functions $f_{n,m}(\lambda, k_0, t)$ are given in terms of infinite series. Based on the first 15 terms in these series we conjecture the following explicit expressions

$$\begin{aligned}
f_{0,0}(\lambda, k_0) &= 2\ln\left(1 + i\cos\Delta_{k_0}\tan\lambda e^{i\theta_{k_0}}\right) , \\
f_{1,0}(\lambda, k_0) &= \ln\left[1 - \frac{\sin^2\Delta_{k_0}\tan^2\lambda(\cos\theta_{k_0} + i\cos\Delta_{k_0}\tan\lambda)^2}{\left(\sin^2\theta_{k_0} + (\cos\theta_{k_0} + i\cos\Delta_{k_0}\tan\lambda)^2\right)^2}\right] , \\
f_{2,0}(\lambda, k_0) &= \ln\Bigg[1 + \\
&\frac{\sin^4\Delta_{k_0}\tan^4\lambda\sin^2\theta_{k_0}(\cos\theta_{k_0} + i\cos\Delta_{k_0}\tan\lambda)^2}{\left(\left(\sin^2\theta_{k_0} + (\cos\theta_{k_0} + i\cos\Delta_{k_0}\tan\lambda)^2\right)^2 - \sin^2\Delta_{k_0}\tan^2\lambda(\cos\theta_{k_0} + i\cos\Delta_{k_0}\tan\lambda)^2\right)^2}\Bigg] .
\end{aligned} \tag{3.118}$$

In principle one could determine further terms $f_{n,0}$ but their contribution turns out to be negligible for all cases we have considered. The contributions $f_{n,m>0}(\lambda, k_0, t)$ are more difficult to simplify. While the term $f_{0,1}$ can still be obtained without further approximations, in order to obtain closed form expressions for $m > 1$ we have resorted to an expansion in powers of $\sin(\Delta_{k_0})$. This is expected to give very accurate results for small quenches, which are defined as producing a small density of elementary excitations through the quench [75, 82]. The leading terms are then conjectured to be of the form

$$\begin{aligned} f_{0,1} &= -i \tan\Delta_{k_0} \ln\left[\frac{1+ie^{i\theta_{k_0}}\cos\Delta_{k_0}\tan\lambda}{1+ie^{-i\theta_{k_0}}\cos\Delta_{k_0}\tan\lambda}\right] , \\ f_{1,1} &= \tan\Delta_{k_0}\Bigg(i\ln\left[\frac{1+ie^{i\theta_{k_0}}\cos\Delta_{k_0}\tan\lambda}{1+ie^{-i\theta_{k_0}}\cos\Delta_{k_0}\tan\lambda}\right] \\ &\qquad -\frac{4\cos\Delta_{k_0}\tan\lambda\sin\theta_{k_0}}{\sin^2\theta_{k_0}+(\cos\theta_{k_0}+i\cos\Delta_{k_0}\tan\lambda)^2}\Bigg)+\mathcal{O}(\sin^3(\Delta_{k_0})). \end{aligned} \tag{3.119}$$

The expansion coefficient $f_{1,1}$ is known to order $\sin^3\Delta_{k_0}$, with unknown $\mathcal{O}(\sin^5\Delta_{k_0})$ corrections. As we will see below, the contributions described by (3.118) and (3.119) are sufficient to obtain an extremely accurate description of $\chi^{(u)}(\lambda,\ell,t)$. The constant $\mathcal{C}$ can be fixed by comparing the $t\to\infty$ limit of (3.117) to the result obtained previously for the behaviour in the stationary state. For later convenience we define two approximations as

$$\begin{aligned} \ln\chi_a^{(u)}(\lambda,\ell,t) = \; & \ell\ln(\cos\lambda)+\tfrac{\ell}{2}\textstyle\sum_{n=0}^{2}\int_0^{2\pi}\frac{dk_0}{2\pi}\Theta(\ell-2n|v_k|t)\left[1-\frac{2n|v_k|t}{\ell}\right] \\ & \times\textstyle\sum_{m=0}^{a}\cos\left(2m\varepsilon(k_0)t\right)f_{n,m}(\lambda,k_0)+\mathcal{C}\ , \end{aligned} \tag{3.120}$$

where $a=1,2$ and where we set $f_{2,1}=0$.

3.5 Accuracy of the asymptotic result

Our analytic result (3.117), (3.118), (3.119) gives the leading contributions in the *space-time scaling limit* [75] $\ell,t\to\infty$, ℓ/t fixed. An important question is how good this asymptotic result describes the behaviour of $\chi^{(u)}(\lambda,\ell,t)$ at small and intermediate times and subsystem sizes. In order to answer this question we now turn to

a comparison between our analytical results (3.120) and a direct numerical evaluation of the determinant representation (3.31), (3.32). The numerical errors in the latter are negligible.

3.5.1 Small-λ regime

A representative comparison between the analytical results $\chi^{(u)}_{1,2}(\lambda,\ell,t)$ for small values of λ and numerics is shown in Fig 3.25 and 3.26. We see that $\chi^{(u)}_{1}(\lambda,\ell,t)$

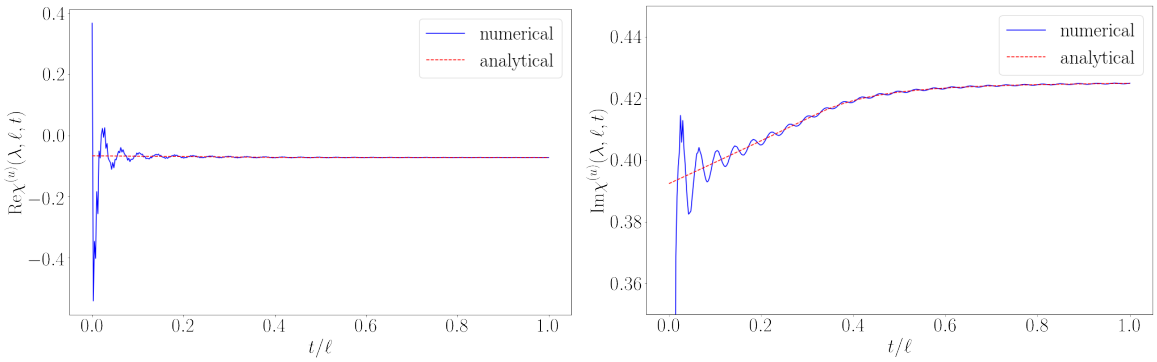

(a) (b)

Figure 3.25: Real and imaginary parts of the leading approximation $\chi^{(u)}_{1}(\lambda=0.1,\ell=200,t)$ for a transverse field quench quench from $h=0$ to $h=0.8$. The analytic approximation gives a good description only at late times.

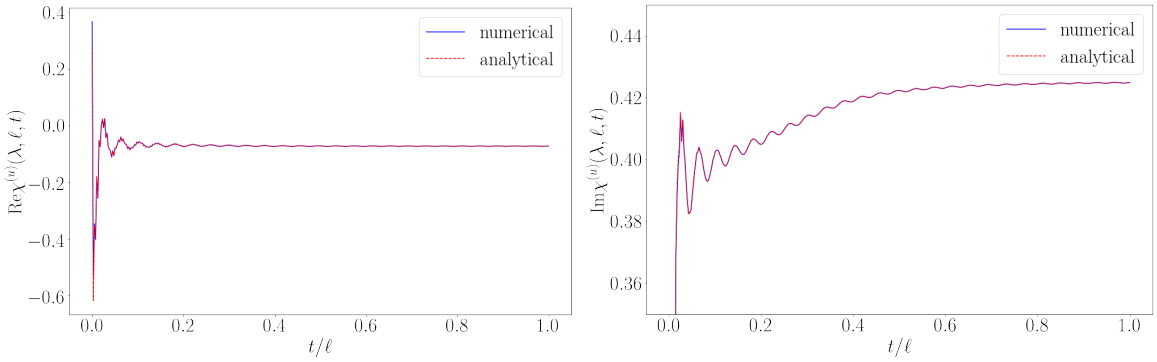

(a) (b)

Figure 3.26: Real and imaginary parts of $\chi^{(u)}_{2}(\lambda=0.1,\ell=200,t)$ for a transverse field quench quench from $h=0$ to $h=0.8$. The analytical expression (red dashed line) is seen to be in excellent agreement with the numerical results, which have negligible errors on the scale of the figure.

reproduces the numerics very well at late times after the quench. In contrast,

the oscillatory behaviour at short times is clearly not captured. The improved approximation $\chi_2^{(u)}(\lambda, \ell, t)$ (3.120) is seen to be in excellent agreement with the numerics.

By construction the oscillatory part of the analytic result is most accurate over the entire range of the "counting parameter" λ when $\sin \Delta_{k_0}$ is small, i.e. for small quenches. For quenches where $\sin \Delta_{k_0}$ is no longer small we still find excellent agreement between the analytic and numerical results as long as $\tan(\lambda)$ is small. This can be understood by noting that for such values of λ the infinite sum in (3.85) is dominated by the first few terms, i.e. small values of n. On the other hand, higher orders of $\sin \Delta_{k_0}$ only emerge for larger values of n. Therefore the leading order result in $\sin \Delta_{k_0}$ already provides a very good approximation in the small-$\tan(\lambda)$ regime even when $\sin \Delta_{k_0}$ is not small. This observation is of significant practical importance: As shown in Fig. 3.27 in a particular example $|\mathrm{Re}\chi^{(u)}(\lambda, \ell, t)|$

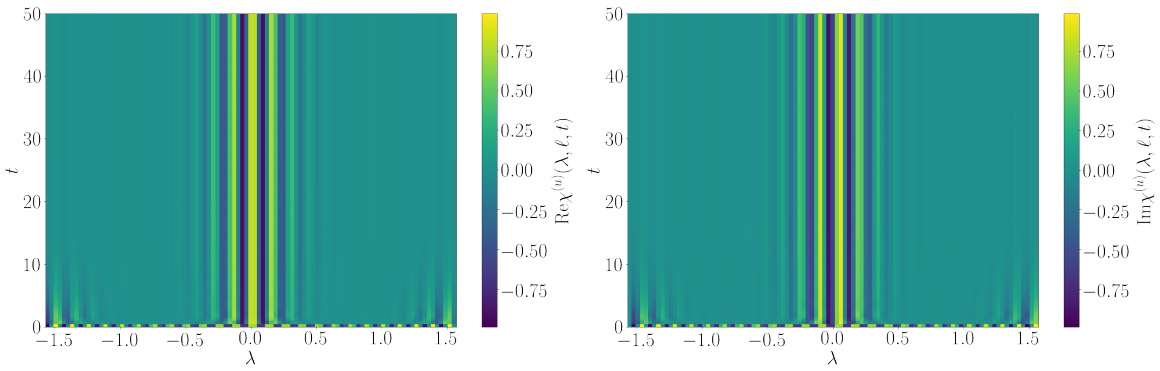

(a) (b)

Figure 3.27: (a) Real and (b) imaginary parts of $\chi^{(u)}(\lambda, \ell = 50, t)$ as functions of λ and t for a transverse field quench from $h = 5$ to $h = 1.5$. We observe that the characteristic function is small unless λ is small. The behaviour for quenches within the ferromagnetic phase and quenches between the phases is similar.

and $|\mathrm{Im}\chi^{(u)}(\lambda, \ell, t)|$ are largest in the vicinity of $\lambda = 0$ (except at short times). This implies that the corresponding probability distribution, which is the object we are ultimately interested in, will be dominated by the small-λ regime. As a consequence (3.117), (3.118), (3.119) provide a good approximation for the calculation of $P_w^{(u)}(m)$ for all quenches.

3.5.2 Large-λ regime

In the large-λ regime we have to distinguish between the cases where the symbol in the stationary state has zero or non-zero winding number, *c.f.* Section 3.3.1.1. The first case covers quenches to the paramagnetic phase. Here we find that our analytic result is again in good agreement with numerics. The second scenario applies to quenches to the ferromagnetic phase and $\lambda > \lambda_c(h_0, h)$. We have shown in Section 3.3.1.2 that there is no good scaling collapse in this regime of counting parameters for the moderate subsystem sizes and times of interest here. It should therefore not come as a surprise that the asymptotic result does not provide a good approximation in this regime. Presumably (3.117), (3.118), (3.119) no longer hold in this regime because the analytic continuation of the power series expansion of the logarithm (3.85) becomes non-trivial in this case. In practice the failure of the analytic approach to give a good account of the generating function in this parameter regime is irrelevant as $\chi^{(u)}(\lambda, \ell, t)$ itself is extremely small and makes a negligible contribution to the probability distribution. As shown in Fig. 3.28, the main contribution to the latter, which after all is our object of interest, arises from the small-λ regime of the generating function, which is well approximated by our analytic expressions.

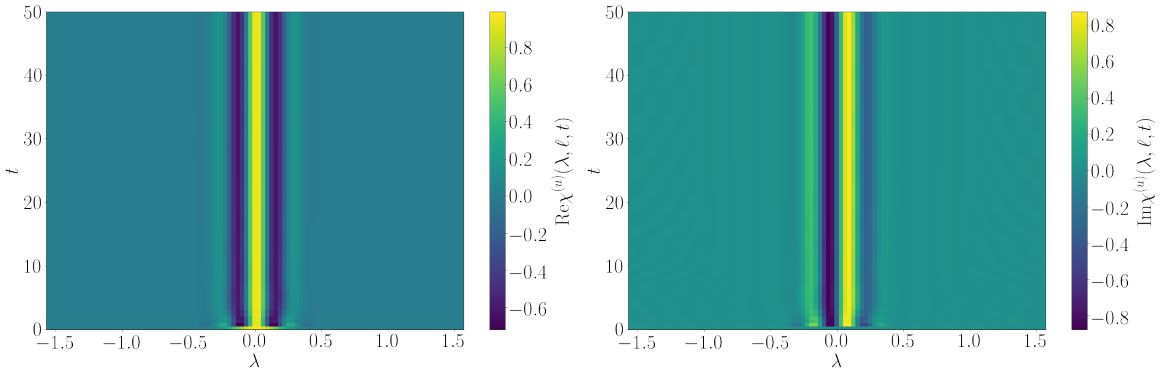

(a) (b)

Figure 3.28: Real (a) and imaginary (b) parts of $\chi^{(u)}(\lambda, \ell = 50, t)$ for a quench within the ferromagnetic phase from $h_0 = 0.2$ to $h = 0.8$. The dominant contribution to the probability distribution arises from the small-λ regime.

3.5.3 Relative errors

In order to provide a more quantitative discussion of the quality of the approximate results (3.120) we consider the relative errors

$$r_{1,2}(\lambda,\ell,t)=\left|1-\frac{\ln\left(\chi^{(u)}_{1,2}(\lambda,\ell,t)\right)}{\ln\left(\chi^{(u)}_{\rm num}(\lambda,\ell,t)\right)}\right|\,, \tag{3.121}$$

where $\chi^{(u)}_{1,2/\rm num}(\lambda,\ell,t)$ are respectively the analytic approximations (3.120) and the result of the numerical computation of the determinant representation (3.31), (3.32).

In Fig. 3.29 we plot the time dependence of the relative errors for a quench from

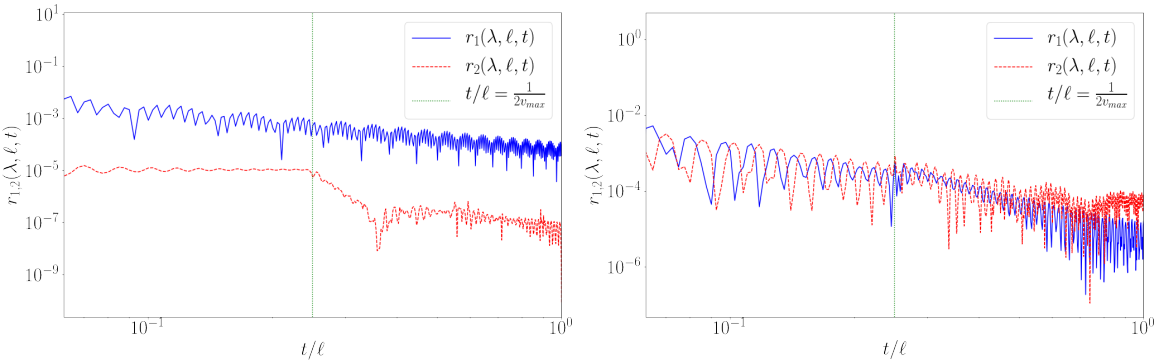

(a) (b)

Figure 3.29: (a) Relative errors $r_{1,2}(\lambda=0.1,\ell=200,t)$ for a quench within the paramagnetic phase from $h_0=5$ to $h=1.5$. (b) same for $r_{1,2}(\lambda=1.4,\ell=200,t)$.

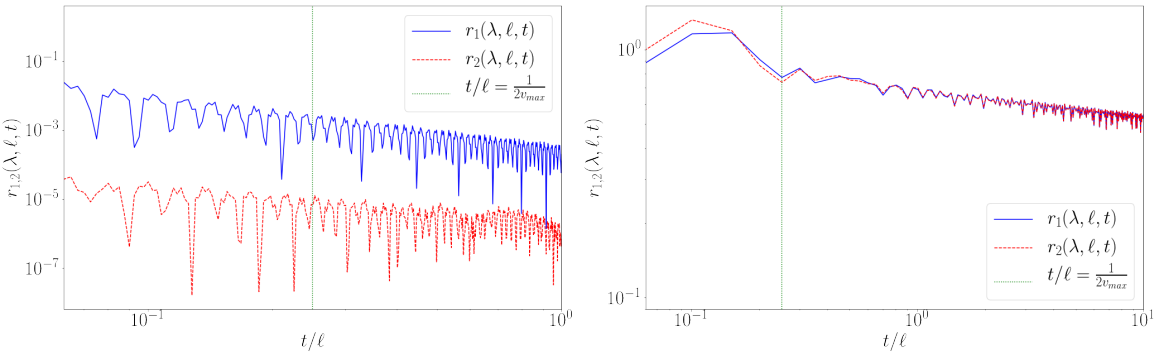

(a) (b)

Figure 3.30: (a) Relative errors $r_{1,2}(\lambda=0.1,\ell=200,t)$ for a quench within the ferromagnetic phase from $h_0=0$ to $h=0.8$. (b) same for $r_{1,2}(\lambda=1.4,\ell=200,t)$.

$h_0=5$ to $h=1.5$ for a subsystem of size $\ell=200$ and two values of the counting

parameter λ. The maximal value of $\sin(\Delta_{k_0})$ within the domain of integration approximately 0.54, which means that higher orders in $f_{1,1}$ can be important. As we have argued above, this will be the case if $\tan(\lambda)$ is not small. In Fig. 3.29 (a) $\lambda = 0.1$ is taken to be small, and the quality of both approximations $\chi^{(u)}_{1,2}(\lambda, \ell, t)$ is seen to be excellent. In Fig. 3.29 (b) the counting parameter $\lambda = 1.4$ is taken to be large. This leads to a significantly larger error, which is however still fairly small and also decays in time. We see that the analytic results provide a good approximation for all values of λ.

We now turn to a parameter regime, in which our analytic results no longer provide a uniformly good approximation for all values of the counting parameter λ. Fig. 3.30 shows results for a quench from $h_0 = 0.2$ to $h = 0.8$. The maximal value of $\sin \Delta_{k_0}$ in the integration range is now 0.71 so that higher orders in $f_{1,1}$ can again be important. For small values of λ the relative errors of both analytical approximations are small and decreasing in time. On the other hand $\chi^{(u)}_{1,2}(\lambda, \ell, t)$ cease to provide accurate approximations for large values of λ with $\lambda > \lambda_c(h_0, h)$ as can be seen in Fig. 3.30 (b). However, we want to stress once more that $\chi^{(u)}(\lambda, 200, t)$ itself is extremely small in this parameter regime and makes only a negligible contribution to the probability distribution.

3.5.4 Probability distributions

An asymptotic expansion for the probability distribution $P^{(u)}_w(m, t)$ can be obtained by Fourier transforming the generating function, *cf.* Eq. (2.57). As expected on the basis of the discussion above, we find that the analytic result becomes very accurate at sufficiently late times for *all* quenches. At intermediate and short times we still find excellent agreement between the analytical and numerical results for quenches originating the ferromagnetic, see e.g. Fig. 3.31 (a). For quenches from the paramagnetic phase the analytic result is in excellent agreement with numerics at short and intermediate times as long as the quench is "small". In practice this covers all quenches within the paramagnetic phase as long as h is not very close

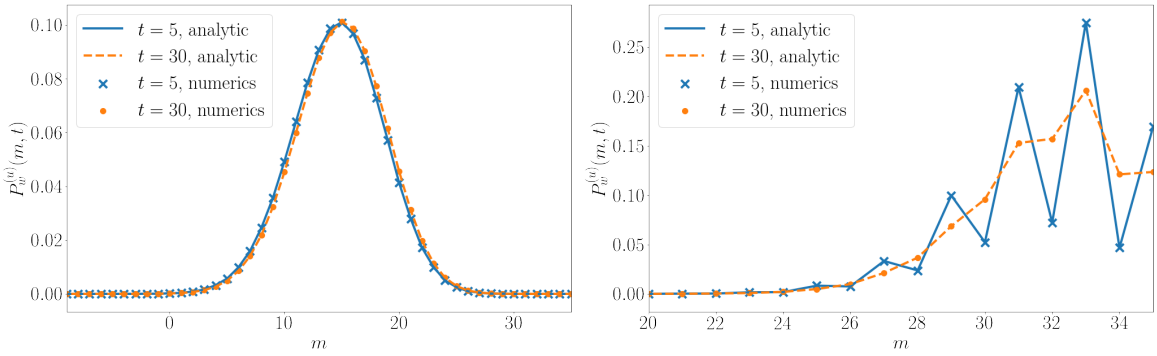

Figure 3.31: Comparison of the asymptotic expression for $P_w^{(u)}(m,t)$ at $\ell = 70$ obtained from Eqns (3.117), (3.118), (3.119) (solid lines) to numerics (symbols) for transverse field quenches with (a) $h_0 = 0.2$ and $h = 0.8$ and (b) $h_0 = 5$ and $h = 2$. The agreement is seen to be excellent.

to 1. For other quenches the corrections to the $f_{1,1}$ term in (3.119) will become significant at short and intermediate times. For quenches across the critical point we again have to distinguish between quenches originating in the paramagnetic and ferromagnetic phase. For quenches originating in the ferromagnetic phase similarly to a quench within the ferromagnetic phase $\chi(\lambda, \ell, t)$ is non-vanishing only close to $\lambda = 0$ and therefore all quenches, independent on the size of $\sin \Delta_{k_0}$ are well described (cf. Fig. 3.32). For quenches originating in the paramagnetic phase for small times there is a non-vanishing contribution around $\lambda = \frac{\pi}{2}$ as there was for quenches within the paramagnetic phase. As for quenches across the critical point $\sin \Delta_{k_0}$ is always large, $f_{1,1}$ can not be well described as an expansion in $\sin \Delta_{k_0}$. Therefore short times do not show excellent agreement any more, however we see that the smooth part still gives a good description of the numerics.

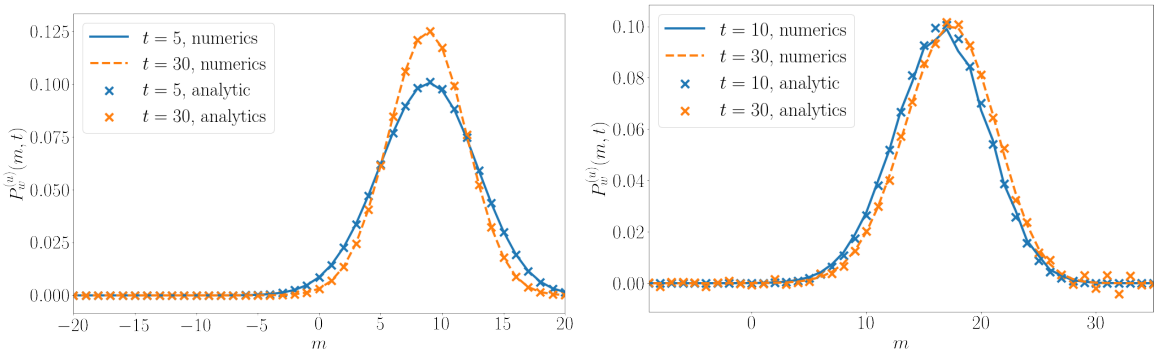

(a) (b)

Figure 3.32: Comparison of the asymptotic expression for $P_w^{(u)}(m,t)$ at $\ell = 70$ obtained from Eqns (3.117), (3.118), (3.119) (solid lines) to numerics (symbols) for transverse field quenches with (a) $h_0 = 0$ and $h = 2$ and (b) $h_0 = 3$ and $h = 0.2$. The agreement is seen to be excellent in the case for a quench from the ferromagnetic to the paramagnetic regime. For the quench from the paramagnetic to the ferromagnetic regime the agreement is slightly worse.

3.A Asymptotics of block Toeplitz matrices

Let T_ℓ be a block Toeplitz matrix with elements $(T_\ell)_{ln} = t_{l-n}$. The *symbol* $\tau(e^{ik})$ of T_ℓ is defined by

$$t_n \equiv \int_0^{2\pi} \frac{dk}{2\pi} \tau(e^{ik}) e^{-ink}. \tag{3.122}$$

In cases where the symbol has winding number zero, the large-ℓ asymptotics of the determinant of T_ℓ is (under certain conditions) given by [108]

$$\ln \det T_\ell = \ell \int_0^{2\pi} \frac{dk}{2\pi} \ln \det \left(\tau(e^{ik})\right) + \det \left(T(\tau^{-1})T(\tau)\right) + o(1). \tag{3.123}$$

Here $T(\tau)$ denotes an infinite Toeplitz matrix with symbol τ. In the case where the block-size is 1, this reduces to the Szegő limit theorem

$$\ln \det T_\ell = \ell \int_0^{2\pi} \frac{dk}{2\pi} \ln \tau(e^{ik}) + \sum_{q\geq 1} q \, (\ln \tau)_q (\ln \tau)_{-q} + o(1), \tag{3.124}$$

where

$$(\ln \tau)_q = \int_0^{2\pi} \frac{dk}{2\pi} \ln \tau(e^{ik}) e^{-ikq} \, . \tag{3.125}$$

The large ℓ asymptotics of Toeplitz determinants in cases where the symbol τ has winding number ± 1 is given by [75, 109]

$$\ln \det T_\ell = \ell \int_0^{2\pi} \frac{dk}{2\pi} \ln a(e^{ik}) + \sum_{q\geq 1} q\ (\ln a)_q (\ln a)_{-q} + \ln \int_0^{2\pi} \frac{\mathrm{d}k}{2\pi} e^{-i\ell k} \frac{a_-(e^{ik})}{a_+(e^{ik})} + o(1)\ , \tag{3.126}$$

where

$$a(e^{ik}) \equiv -e^{\mp ik}\tau(e^{ik}) = \exp\left(\sum_{j=1}^{\infty} (\ln a)_{\pm j} e^{\pm ijk}\right)\ . \tag{3.127}$$

3.B Perturbation theory around the $h \to \infty$ limit

We have seen that the probability distributions $P^{(u,s)}(m,t)$ exhibit an even/odd structure in m for short times after quenches starting in the paramagnetic phase. In this appendix we show that this structure can be understood in perturbation theory around the $h \to \infty$ limit. For simplicity we consider the probability distribution $P^{(u)}(m)$ in the ground state at $h \gg 1$. In the limit $h \to \infty$ the ground state is the saturated ferromagnetic state along the transverse field direction

$$|0\rangle^{(0)} = |\uparrow \ldots \uparrow\rangle\ . \tag{3.128}$$

Hence

$${}^{(0)}\langle 0|e^{i\lambda S^z_u(\ell)}|0\rangle^{(0)} = e^{i\lambda\ell}\ . \tag{3.129}$$

The corresponding probability distribution is a delta function at $m = \ell/2$. The other eigenstates of $\sum_j \sigma^z_j$ are denoted by $|n\rangle^{(0)}$. The leading correction to the generating function arises at second order in perturbation theory in $H_1 = \sum_j \sigma^x_j \sigma^x_{j+1}$. The relevant corrections to the ground state are

$$|0\rangle^{(2)} = |0\rangle^{(0)} + \sum_{n\neq 0} |n\rangle^{(0)} \frac{{}^{(0)}\langle n|H_1|0\rangle^{(0)}}{E_0^{(0)} - E_n^{(0)}} - \frac{1}{2}|0\rangle^{(0)} \sum_{n\neq 0} \frac{\left|{}^{(0)}\langle n|H_1|0\rangle^{(0)}\right|^2}{\left(E_n^{(0)} - E_0^{(0)}\right)^2} + \ldots \tag{3.130}$$

Substituting this into the expression for the generating function gives

$$\begin{aligned} {}^{(2)}\langle 0|e^{i\lambda S_u^z(\ell)}|0\rangle^{(2)} &= e^{i\lambda\ell}\left[1-\sum_{n\neq 0}\frac{\left|{}^{(0)}\langle n|H_1|0\rangle^{(0)}\right|^2}{\left(E_n^{(0)}-E_0^{(0)}\right)^2}\right] \\ &\quad +\sum_{n\neq 0}{}^{(0)}\langle n|e^{i\lambda S_u^z(\ell)}|n\rangle^{(0)}\left|\frac{{}^{(0)}\langle n|H_1|0\rangle^{(0)}}{E_0^{(0)}-E_n^{(0)}}\right|^2. \end{aligned} \quad (3.131)$$

In order for ${}^{(0)}\langle n|H_1|0\rangle^{(0)}$ to be non-zero the product state $|n\rangle^{(0)}$ must have precisely two overturned spins. Let us denote their positions by j and $j+1$. For $\ell \geq 2$ we then have

$${}^{(0)}\langle n|e^{i\lambda S_u^z(\ell)}|n\rangle^{(0)} = \begin{cases} e^{i\lambda(\ell-4)} & \text{if } 1\leq j<\ell \\ e^{i\lambda(\ell-2)} & \text{if } j=0 \text{ or } \ell \\ e^{i\lambda\ell} & \text{else.} \end{cases} \quad (3.132)$$

This gives

$${}^{(2)}\langle 0|e^{i\lambda S_u^z(\ell)}|0\rangle^{(2)} = e^{i\lambda\ell}\left[1-\frac{\ell+1}{16h^2}\right]+\frac{2}{16h^2}e^{i\lambda(\ell-2)}+\frac{\ell-1}{16h^2}e^{i\lambda(\ell-4)}. \quad (3.133)$$

The corresponding probability distribution is

$$\begin{aligned} P^{(u)}(m)\Big|_{\mathrm{PT}} &= \left[1-\frac{\ell+1}{16h^2}\right]\delta(m-\ell/2) \\ &\quad +\frac{2}{16h^2}\delta(m+1-\ell/2)+\frac{\ell-1}{16h^2}\delta(m+2-\ell/2). \end{aligned} \quad (3.134)$$

This is seen to exhibit an even/odd effect as the corrections for $m=\ell/2 \bmod 2$ are proportional to the subsystem size. The comparison to the exact probability distribution is shown in Fig. 3.33.

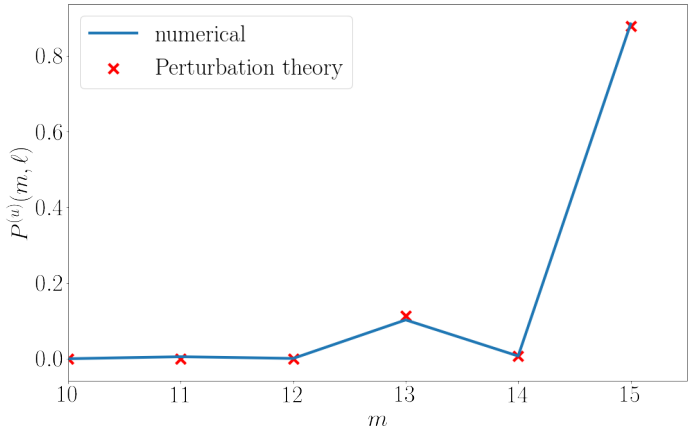

Figure 3.33: Comparison of the exact numerical probability distribution to the perturbation theory result in the paramagnetic ground state at $h = 4$ at subsystem size $\ell = 30$. It can be seen that the perturbation theory correctly reproduces the staggering of the probability distribution.

II

Weak integrability breaking

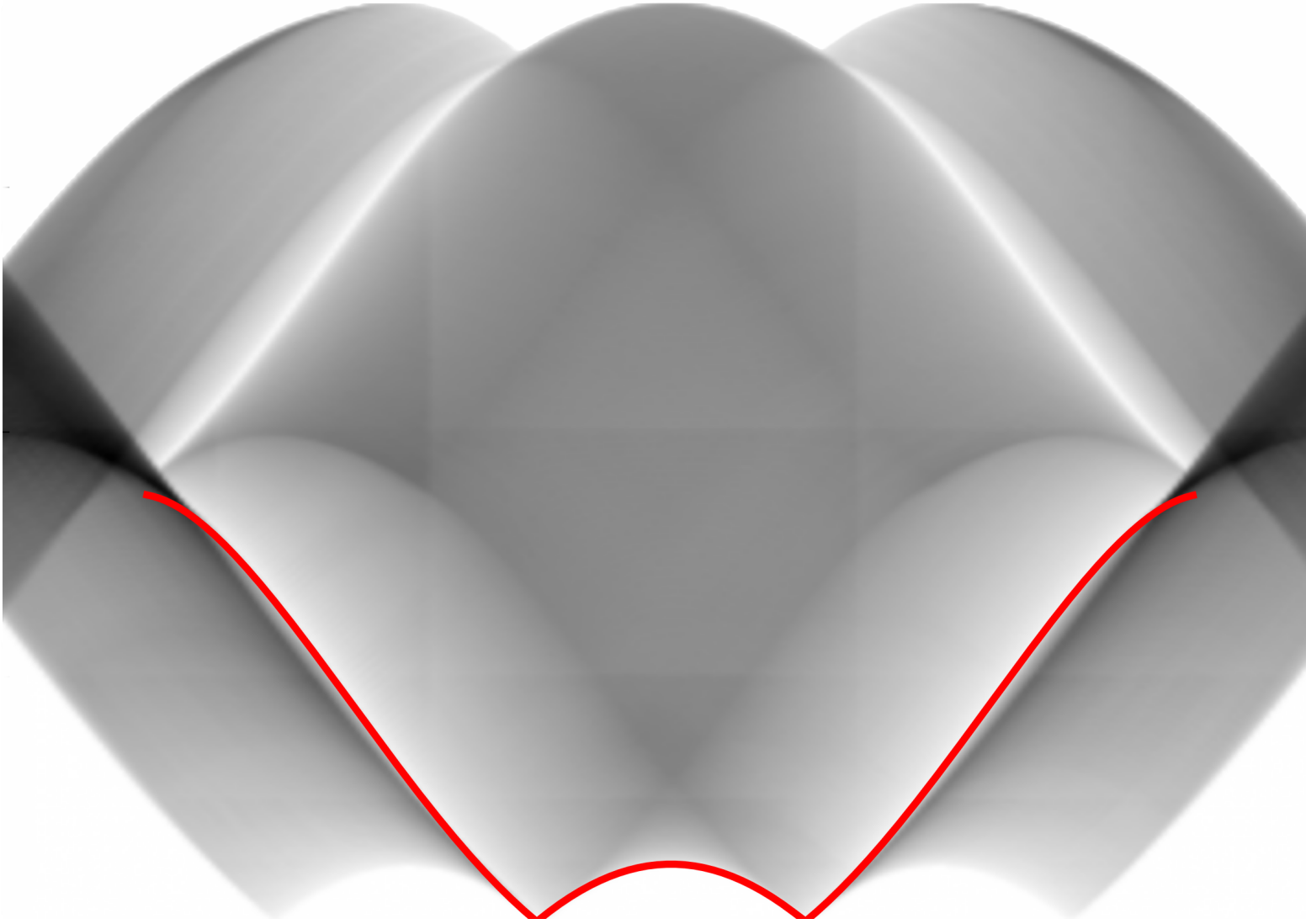

4

Integrability, stability of excitations and the XXX-Heisenberg model

Contents

4.1 1D is special: Interactions and integrability

Dimensionality plays an important rôle in interacting quantum systems. One of the key paradigms in three dimensions is Fermi liquid theory. In a nutshell, introducing weak interactions to a free fermionic theory dresses the bare particles of the free theory to quasi-particles with the same quantum numbers and a finite, however very long life time close to the Fermi surface. Importantly, parametrically decreasing the interaction, the quasi-particle adiabatically goes over to the bare particle of the theory [23]. All physical quantities in the vicinity of the free theory point in parameter space are then very well described using these quasi-particles. In contrast to this, introducing interactions in a one dimensional free fermionic theory can have dramatic effects on the elementary excitations. At low energies these can not be described by dressed bare particles with the same quantum numbers, but they in fact have a bosonic character. This is known as Luttinger Liquid theory [3].

Another important distinction of one dimensional quantum systems is the existence of special points in parameter space, where the system is strongly interacting, yet elementary excitations have infinite life time. In three dimensions this

is a quality only of free theories. These theories are called integrable theories and they are generally characterized by the existence of a macroscopic number of mutually commuting conserved quantities with (quasi-) local [110, 111] densities

$$\left[\hat{H}^{(n)}, \hat{H}^{(m)}\right] = 0 \tag{4.1}$$

where $\hat{H}^{(1)}$ is the Hamiltonian and $\hat{H}^{(0)}$ the translation operator.

Elementary excitations are generally complicated superpositions of the bare particles of the theory [19]. They are simultaneous eigenstates of all the conserved quantities $\hat{H}^{(n)}$ and can for large system sizes be described in terms of dressed momenta p and energies $\varepsilon(p)$, which are additive [19, 112]. These excitations are eigenstates of not only energy and momentum operators, but also of the higher order conserved quantities. Like for energy and momentum the corresponding eigenvalues are additive.

4.2 Stability of excitations in integrable systems

In this section we want to briefly motivate why the elementary excitations of an integrable theory are stable. To this end we consider a one-parameter excitation of an integrable theory. For a generic theory, where the only conserved quantities are energy and momentum (or quasi-momentum), the stability of any such excitation is determined by the overlap of the one-parameter excitation with the continuum of higher-order excitations in the energy-momentum plane. If the overlap is non-zero, the one-parameter excitation will generally decay into the higher-order excitations it has overlap with.

We can now look at the energy-momentum relation in an integrable theory. In general the one-parameter elementary excitation will overlap the continuum of higher-order excitations (cf. 4.1 in the XXX-model) and the decay is allowed kinematically. However in the integrable theory there exist not only energy and momentum conservation, but as mentioned above, there is a macroscopic number of conserved quantities. For example looking at the potential decay of the

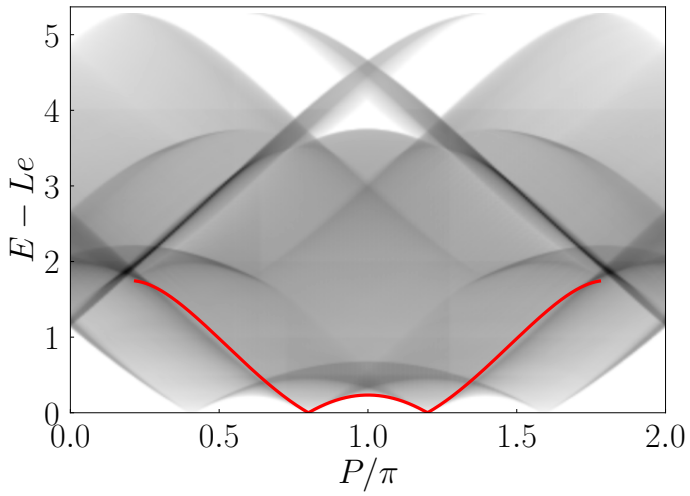

Figure 4.1: Energy and momentum of a one-parameter excitation in the XXX-model in red as well as a continuum of three particle excitations. The shading reflects the density of states of the three-parameter excitations. The explicit construction will be introduced later. The one-parameter excitation overlaps the three-particle continua, which for a generic model would imply a finite decay rate for the one-parameter excitation. The energy of the excitations are $\mathcal{O}(1)$ corrections to the $\mathcal{O}(L)$ ground state energy, where L is the size of the system. The plot is normalized to 0 by subtracting the ground state energy Le.

one-parameter excitation with momentum p and energy $\varepsilon(p)$ into a three-particle excitation with momenta p_1, p_2 and p_3, we not only have energy and momentum conservation

$$P: \qquad p = p_1 + p_2 + p_3 \tag{4.2}$$

$$E: \qquad \varepsilon(p) = \varepsilon(p_1) + \varepsilon(p_2) + \varepsilon(p_3) \tag{4.3}$$

but conservation of all the higher conservation laws $H^{(n)}$ with $n > 1$

$$\hat{H}^{(n>1)}: \qquad H^{(n>1)}(p) = H^{(n>1)}(p_1) + H^{(n>1)}(p_2) + H^{(n>1)}(p_3). \tag{4.4}$$

For the decay to be allowed, there must exist a set of momenta p_1, p_2, p_3 for a given incoming momentum p, such that all these equations are satisfied simultaneously. This constitutes an infinite system of equations for only four unknowns, which is highly over-constrained. As the densities are independent of each other a solution generically is highly unlikely. For the XXX-model the constraint of the first higher order conserved quantity is pictorially shown in Fig. 4.2. This motivates why exci-

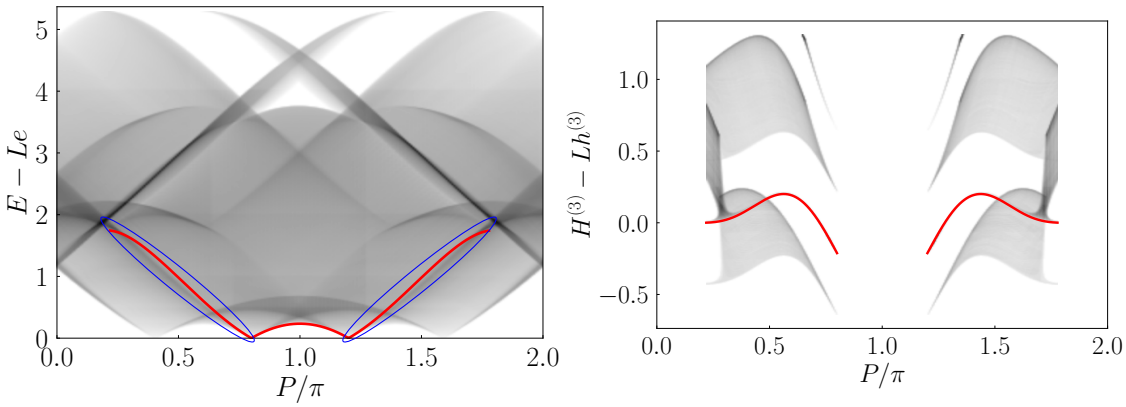

Figure 4.2: Revisiting the energy of the one-parameter excitation over momentum in red and the three particle continua in grey in the left figure, the allowed decay channels are states of the one-parameter excitations on the red line into three particle states that overlap the states on the red line in the energy-momentum plot. These are encircled in blue. The conservation of energy and momentum therefore restricts the possible decay channels and we can focus on the remaining one-parameter excitations and three particle states for and into which decay is allowed. For these allowed states we plot the third conserved quantity over momentum in the right figure. The one-parameter excitation is again plotted as a red line, while the three particle continua, which are allowed by energy-momentum conservation, are given by the grey continuum, the shading again signifying the density of states. We can clearly see that for every new conservation law the range of momenta where a one particle excitation can decay into three particles is shrinking. Going to even higher conserved quantities it can be expected that the allowed phase space for decay shrinks further until no decay is allowed.

tations in integrable systems are stable. The higher order conservation laws are however only present directly at the integrable point. Any integrability breaking perturbation will break these higher conservation laws and we expect that excitations, which are stable in the integrable theory but whose decay is kinematically allowed, to decay. In the following we will specialize to a specific integrable theory, the XXX-Heisenberg model and will specifically construct excitations on top of the ground state.

4.3 The antiferromagnetic XXX-Heisenberg model and Bethe Ansatz

The spin-$\frac{1}{2}$ antiferromagnetic XXX-Heisenberg model [6] in a magnetic field is a paradigm of integrability in strongly interacting quantum systems. While in three dimensions it is a basic model for magnetism, the Mermin-Wagner/Hohenberg [113, 114] theorem forbids breaking of continuous symmetry in in $1D$-systems and magnetic long range order can not develop. Instead quasi long range order is forming, defined as algebraically decaying two-point spin functions [3, 115]. This signifies an infinite correlation length and therefore that the system is at a critical point. The Heisenberg model in $1D$ shows very interesting physics, like quantum critical behaviour, fractionalisation of quantum numbers or domain wall excitations [3, 115, 116], all of which will be important to us in the following. The spin-$\frac{1}{2}$ Heisenberg model as a model of a $1D$ spin chain can be seen to arise from a strong repulsive interaction between fermions with spin at half filling, described by the Hubbard model, a simple model for a Mott insulator [18]. Although the Heisenberg model is a $1D$ quantum spin chain, it is not only interesting from a theoretical standpoint, but there are many experimental realisations in metals and crystals [117–120]. In these experiments materials are used where the interaction between spins is mainly in one preferred direction, forming a number of quasi-$1D$ chains within the materials. There is some residual interaction between the chains, but as long as the energies at which the spin chains are probed is much larger than the interactions between spin chains these interactions can be taken into account by perturbation theory and the system behaves as if it was one dimensional.

In the following we will briefly sketch the solution of the model, the construction of eigenstates at finite system sizes and in the thermodynamic limit, as well as a mathematical tool we will use to calculate matrix elements in the theory.

We start out considering the more general spin-$\frac{1}{2}$ XXZ-Heisenberg model given

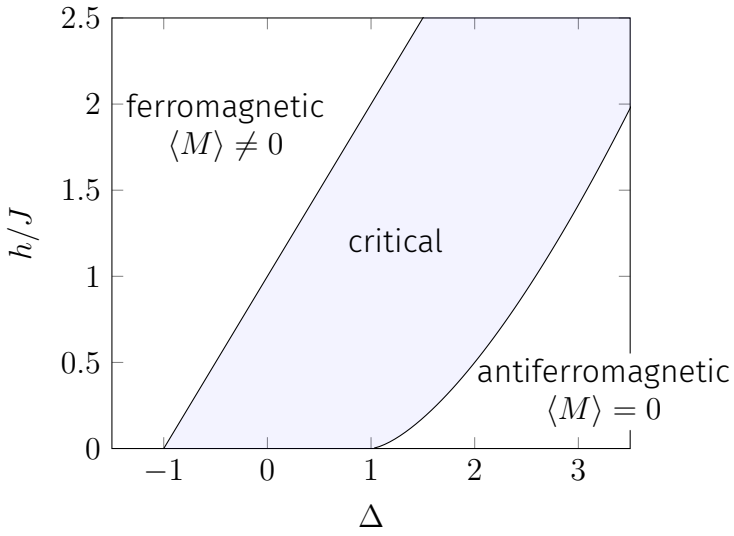

Figure 4.3: Sketch of the $T = 0$ phase diagram of the spin-$\frac{1}{2}$ XXZ Heisenberg chain in a magnetic field. In the following we will focus on $\Delta = 1$, where the model is gapless and critical.

by the Hamiltonian

$$H(J, \Delta, h) = J \sum_{j=1}^{L} \left(S_j^x S_{j+1}^x + S_j^y S_{j+1}^y + \Delta S_j^z S_{j+1}^z \right) - h \sum_{j=1}^{L} S_j^z \ . \tag{4.5}$$

Here $J > 0$ and S_j^α are spin operators with commutation relations

$$[S_i^\alpha, S_j^\beta] = i \delta_{ij} \varepsilon_{\alpha\beta\gamma} S_i^\gamma \ . \tag{4.6}$$

The spectrum of (4.5) is gapless for $|\Delta| \leq 1$ and $|h| < J(1 + \Delta)$ [19, 112] (cf. Fig. 4.3). The model can be solved by Bethe Ansatz [6, 121]. The antiferromagnetic XXX-model we are interested in is recovered from (4.5) by setting $\Delta = 1$.

4.3.1 Coordinate Bethe Ansatz

Eigenstates of the XXZ Hamiltonian (4.5) can be constructed by means of the Bethe Ansatz [6] for any value of the anisotropy Δ. As S^z commutes with the Hamiltonian it is convenient to work in a sector with a fixed number of down-spins N with respect to the ferromagnetic state

$$|0\rangle := \left| S^z = \frac{L}{2} \right\rangle = \bigotimes_{j=1}^{L} |\uparrow\rangle_j \ , \tag{4.7}$$

which will be used as a reference state in the following. Energy eigenstates with N down-spins take the form

$$|N\rangle = \sum_{j_1,\ldots,j_N=1}^{L} a(j_1,\ldots,j_N) \prod_{a=1}^{N} S^-_{j_a} |0\rangle \ , \tag{4.8}$$

where $1 \leq j_1 < j_2 < \cdots < j_N \leq L$. The wave functions have Bethe Ansatz form [6, 19, 112, 121, 122]

$$\begin{aligned} a(j_1,\ldots,j_N) &= \sum_{P\in S_N} (-1)^{[P]} \mathcal{A}_P \exp\left(i \sum_{a=1}^{N} k_{Pa} j_a \right) \ , \\ \mathcal{A}_P &= \prod_{a<b} \left(e^{i(k_{P_a}+k_{P_b})} + 1 - 2\Delta e^{ik_{P_a}} \right) . \end{aligned} \tag{4.9}$$

The energy of the state with wave function (4.9) is given by

$$E = J \sum_{a=1}^{N} (\cos k_a - \Delta) - h \left(\frac{L}{2} - N \right) . \tag{4.10}$$

4.3.2 Bethe equation for the XXX model

Imposing periodic boundary conditions on the wave functions (4.9) leads to quantization conditions for the wave numbers k_a known as *Bethe Ansatz equations*

$$e^{ik_a L} = \prod_{a\neq b}^{N} \left[-\frac{2\Delta e^{ik_a} - e^{ik_a+ik_b} - 1}{2\Delta e^{ik_b} - e^{ik_a+ik_b} - 1} \right] . \tag{4.11}$$

From here on we set $\Delta = 1$. It is convenient to introduce rapidity variables λ_a defined by

$$e^{ik_a} = \frac{\lambda_a - i/2}{\lambda_a + i/2} . \tag{4.12}$$

In terms of the rapidity variables the Bethe Ansatz equations read

$$\left(\frac{\lambda_a - i/2}{\lambda_a + i/2} \right)^L = \prod_{\substack{b=1 \\ b\neq a}}^{N} \frac{\lambda_a - \lambda_b - i}{\lambda_a - \lambda_b + i} \ , \ a = 1,\ldots,N. \tag{4.13}$$

A standard way of analysing (4.13) is by employing the *string hypothesis*. The string hypothesis is an Ansatz for the general solution of the Bethe Ansatz equations and

can be motivated by looking at fixed N and large L [115]. For $N = 2$ and a solution λ_a with $\mathrm{Im}\lambda_a > 0$, the left hand side of the Bethe Ansatz equations (4.13) gets very large

$$\left|\frac{\lambda_a - i/2}{\lambda_a + i/2}\right|^L \gg 1. \tag{4.14}$$

From the right hand side we then see that $\lambda_a - \lambda_b \approx i$, hinting at a structure of the solutions in the complex plane. Generalising to larger N the string hypothesis assumes that all solutions of (4.13) are composed of strings of the form

$$\lambda_\alpha^{n,j} = \lambda_\alpha^n + \frac{i}{2}(n + 1 - 2j) + \delta_\alpha^{n,j}, \quad j = 1, \ldots, n. \tag{4.15}$$

Here $\delta_\alpha^{n,j}$ are deviations from "ideal" strings and are assumed to be exponentially small in system size. While not all solutions can be exactly described by the string hypothesis [6, 123–125], energy eigenstates at finite magnetisation are believed to follow the string hypothesis [115].

Let us now consider a solution to (4.13) that contains M_n strings of length n with corresponding string centres λ_α^n (this implies that $\sum_n M_n n = N$). Substituting (4.15) into (4.13) and neglecting the deviations we obtain a set of coupled equations for the set $\{\lambda_\alpha^n\}$. Taking logarithms we arrive at

$$L\theta\left(\frac{\lambda_\alpha^n}{n}\right) = 2\pi I_\alpha^n + \sum_{(m,\beta)\neq(n,\alpha)} \theta_{nm}(\lambda_\alpha^n - \lambda_\beta^m). \tag{4.16}$$

Here I_α^n are integer or half-odd integers numbers (arising from taking logarithms), $\theta(x) = 2\arctan(2x)$, and

$$\theta_{nm}(x) = \begin{cases} \theta\left(\frac{x}{2n}\right) + 2\sum_{j=1}^{n-1}\theta\left(\frac{x}{2j}\right) & \text{for } m = n \\ \theta\left(\frac{x}{|n-m|}\right) + 2\theta\left(\frac{x}{|n-m|+2}\right) + \ldots + 2\theta\left(\frac{x}{n+m-2}\right) + \theta\left(\frac{x}{n+m}\right) & \text{for } m \neq n \end{cases}. \tag{4.17}$$

Equations (4.16) are called *Takahashi's equations*. They relate the solutions of the BAE to a set of integer or half-odd integer numbers, which therefore can be considered as quantum numbers of our problem. The permitted ranges of the I_α^n are [112]

$$|I_\alpha^n| \leq \frac{1}{2}\left[L - 1 - \sum_{m=1}^{\infty}(2\min(m,n) - \delta_{n,m})\, M_m\right]. \tag{4.18}$$

Energy and momentum of solutions to (4.16) are given by

$$\begin{aligned} E &= \sum_{m=1}^{\infty}\sum_{\beta=1}^{M_m}\left(-\pi J a_n(\lambda_\beta^m)+mh\right)-\frac{hL}{2}\,, \\ P &= \pi\sum_{m=1}^{\infty}M_m+\sum_{m=1}^{\infty}\sum_{\beta=1}^{M_m}\frac{2\pi I_\beta^m}{L} \end{aligned} \tag{4.19}$$

where we have defined

$$a_n(x)=\frac{1}{2\pi}\frac{n}{x^2+(n/2)^2}\,. \tag{4.20}$$

All solutions to Takahashi's equations correspond to highest weight states of the spin SU(2) algebra [126]

$$S^+|\{\lambda_\alpha^n\}\rangle=0. \tag{4.21}$$

A complete set of energy eigenstates is then obtained by acting with the spin lowering operator on these highest weight states

$$\left(S^-\right)^m|\{\lambda_\alpha^n\}\rangle\,,\quad m=0,1,\ldots,L-2\sum_n nM_n. \tag{4.22}$$

4.3.3 Thermodynamic limit and integral equations

We want to consider excitations in the thermodynamic limit of large system sizes and macroscopic many particles (cf. [19, 112, 115])

$$L,N\to\infty,\qquad \frac{N}{L}=n=\text{fixed}. \tag{4.23}$$

In this limit and under the string hypothesis many microscopic states are locally indistinguishable. They can be described by one class of macroscopic state, which, analogously to ideal Fermi gases, are characterized by densities of particles and holes. If the number of string centers for a certain string n is of $\mathcal{O}(L)$, the solutions of (4.16) for the string centers λ_a^n are lying dense on the real line.

$$\lambda_{a+1}^n-\lambda_a^n=\mathcal{O}(L^{-1}). \tag{4.24}$$

In the same way as for free fermions on a lattice, the particle and hole densities are defined as

- $\rho_{n,p}(\lambda)\Delta\lambda =$ number of particles in $[\lambda, \lambda + \Delta\lambda]$
- $\rho_{n,h}(\lambda)\Delta\lambda =$ number of holes in $[\lambda, \lambda + \Delta\lambda]$

where the total density of roots $\rho_n = \rho_{n,p} + \rho_{h,p}$ contrary to free fermions is not constant, but due to the interactions is a function of λ [127]. Let us define the so called *counting function*

$$z_n(\lambda) = \theta\left(\frac{\lambda}{n}\right) - \frac{1}{L}\sum_{(m,\beta)\neq(n,\alpha)} \theta_{nm}(\lambda_\alpha^n - \lambda_\beta^m). \tag{4.25}$$

Looking at the Bethe equation (4.16), it is defined such that

$$z_n(\lambda_\alpha^n) = \frac{2\pi I_\alpha^n}{L} \tag{4.26}$$

and therefore $z_n(\lambda_\alpha^n) - z_n(\lambda_\beta^n)$ counts the number of roots between λ_α^n and λ_β^n. Going to the thermodynamic limit the counting function can be written as

$$z_n(\lambda) = \theta\left(\frac{\lambda}{n}\right) - \sum_{m=1}^{\infty}\int_{-\infty}^{\infty} d\mu\theta_{nm}(\lambda - \mu)\rho_{m,p}(\mu), \tag{4.27}$$

where now $z_n(\lambda) - z_n(\lambda + \Delta\lambda)$ counts the number of root between λ and $\lambda + \Delta\lambda$. It is therefore related to the density of roots ρ_n by

$$\frac{dz_n(\lambda)}{d\lambda} = 2\pi\rho_n(\lambda). \tag{4.28}$$

Taking the derivative of (4.27) we obtain

$$\rho_{n,p}(\lambda) + \rho_{n,h}(\lambda) = a_n(\lambda) - \sum_{m=1}^{\infty}\int_{-\infty}^{\infty} \mathrm{d}\mu\, T_{nm}(\lambda - \mu)\rho_{m,p}(\mu) \tag{4.29}$$

with

$$T_{nm}(\lambda) = (1 - \delta_{mn})a_{|n-m|}(\lambda) + 2a_{|n-m|+2}(\lambda) + \cdots + 2a_{n+m-2}(\lambda) + a_{n+m}(\lambda). \tag{4.30}$$

The energy density of this state is given as

$$e(\{\rho_{n,p}\}) = \sum_{n=1}^{\infty}\int_{-\infty}^{\infty} d\lambda\rho_{n,p}(\lambda)(-\pi J a_n(\lambda) + nh). \tag{4.31}$$

where

$$\varepsilon_{n,0}(\lambda) = (-\pi J a_n(\lambda) + nh) \tag{4.32}$$

is the bare energy of the bare particles.

4.3.4 Elements of the Algebraic Bethe Ansatz

Within the Bethe Ansatz framework it is also possible to determine matrix elements in some integrable theories. These can be obtained using the Algebraic Bethe Ansatz [19]. In this chapter we will consider the XXZ case with anisotropy parameter $\Delta = \cos\gamma$. We can then easily specialize to the isotropic limit $\Delta = 1$ later. A key object is the monodromy matrix

$$T(\lambda) = \begin{pmatrix} A(\lambda) & B(\lambda) \\ C(\lambda) & D(\lambda) \end{pmatrix} , \tag{4.33}$$

where A, B, C, D are operators acting on the Hilbert space of the chain and λ is known as spectral parameter. The monodromy matrix fulfils the Yang-Baxter equation

$$\begin{aligned} R(\lambda-\mu)(T(\lambda)\otimes 1)(1\otimes T(\mu)) = \\ (1\otimes T(\mu))(T(\lambda)\otimes 1)R(\lambda-\mu) , \end{aligned} \tag{4.34}$$

where the R-matrix has the form

$$R(\lambda,\mu) = \begin{pmatrix} 1 & 0 & 0 & 0 \\ 0 & b(\lambda,\mu) & c(\lambda,\mu) & 0 \\ 0 & c(\lambda,\mu) & b(\lambda,\mu) & 0 \\ 0 & 0 & 0 & 1 \end{pmatrix} . \tag{4.35}$$

If we now choose

$$b(\lambda) = \frac{\sinh(\lambda)}{\sinh(\lambda+i\gamma)}, \tag{4.36}$$

$$c(\lambda) = \frac{\sinh(i\gamma)}{\sinh(\lambda+i\gamma)}, \tag{4.37}$$

it can be shown [19] that the trace of the monodromy matrix T generates all (strictly) local conservation laws of the XXZ-chain with the Hamiltonian being one of them.

The Yang-Baxter algebra determines intertwining relations for the operators

A, B, C, D. For the following, four important ones thereof are given by [19]:

$$[B(\lambda), B(\mu)] = 0 \tag{4.38}$$

$$[C(\lambda), C(\mu)] = 0 \tag{4.39}$$

$$A(\lambda)B(\mu) = b^{-1}(\lambda - \mu)\left(B(\mu)A(\lambda) - c(\lambda - \mu)B(\lambda)A(\mu)\right) \tag{4.40}$$

$$D(\lambda)B(\mu) = b^{-1}(\mu - \lambda)\left(B(\mu)D(\lambda) - c(\mu - \lambda)B(\lambda)D(\mu)\right) \tag{4.41}$$

Due to the Hamiltonian commuting with the trace of the monodromy matrix, eigenstates of (4.5) can be constructed as

$$|\lambda_1, \ldots, \lambda_N\rangle = \prod_{i=1}^{N} B(\lambda_i)\,|0\rangle \ , \tag{4.42}$$

where the set of rapidities $\{\lambda_i\}_{i\in\{1,\ldots,N\}}$ are solutions to the Bethe equations

$$\frac{a(\mu_j)}{d(\mu_j)} = \prod_{k\neq j} \frac{b(\mu_k - \mu_j)}{b(\mu_j - \mu_k)} \ , \quad j = 1, \ldots, N. \tag{4.43}$$

Here the functions $a(\lambda)$ and $d(\lambda)$ arise from the action of the monodromy matrix on the reference state

$$A(\lambda)\,|0\rangle = a(\lambda)\,|0\rangle \qquad D(\lambda)\,|0\rangle = d(\lambda)\,|0\rangle \qquad C(\lambda)\,|0\rangle = 0 \ . \tag{4.44}$$

In the case at hand the functions $a(\lambda)$ and $d(\lambda)$ are given by

$$a(\mu) = 1 \qquad\qquad d(\mu) = \left(b(\mu - i\frac{\gamma}{2})\right)^L. \tag{4.45}$$

where L is the length of the system. The isotropic limit $\Delta = 1$ corresponds to taking $\gamma \to 0$, while rescaling the spectral parameters

$$\mu_j = \gamma\lambda_j \ , \quad \lambda_j \text{ fixed.} \tag{4.46}$$

This recovers the Bethe Ansatz equations (4.13) from (4.43). The global spin lowering operator is obtained as [126]

$$-\,i \lim_{\lambda\to\infty} \lambda\, B(\lambda) = S^-. \tag{4.47}$$

Matrix elements of physical operators can then be calculated by a mapping of the physical operator to the algebraic Bethe Ansatz operators A, B, C, D, the so called

inverse scattering problem and subsequent calculation of expectation values of these utilizing the known commutation relations (4.41). For the XXZ model the inverse scattering relations for the local spin operators are given by [128]:

$$S_j^- = 2\prod_{i=1}^{j-1}(A+D)(\xi_i)B(\xi_j)\prod_{i=j+1}^{L}(A+D)(\xi_i), \tag{4.48}$$

$$S_j^+ = 2\prod_{i=1}^{j-1}(A+D)(\xi_i)C(\xi_j)\prod_{i=j+1}^{L}(A+D)(\xi_i), \tag{4.49}$$

$$S_j^z = -2\prod_{i=1}^{j-1}D(\xi_j)\prod_{i=j+1}^{L}(A+D)(\xi_i)+1, \tag{4.50}$$

where ξ_i are inhomogeneity parameters, which will be set to $i\gamma/2$ in the end. When calculating matrix elements of these operators, after use of the commutation relations and the action of A, C and D on the reference state $|0\rangle$, one obtains sums of overlaps of states of the form

$$\langle\{\lambda\} \mid \{\mu\}\rangle = \langle\lambda_1,\ldots,\lambda_N|\prod_{i=1}^{N}B(\mu_i)\,|0\rangle \ , \tag{4.51}$$

where only the λ_i satisfy the Bethe equation, whereas in general the μ_i do not. The last step is now to use the Slavnov overlap formula [129]

$$\langle\{\lambda\}|\{\mu\}\rangle = \frac{\det\left(H(\{\lambda\},\{\mu\})\right)}{\prod_{j>k}\phi(\lambda_k-\lambda_j)\prod_{j<k}\phi(\mu_k-\mu_j)}, \tag{4.52}$$

where H is a matrix defined as

$$H_{ab} = \frac{\phi(i\gamma)}{\phi(\lambda_a-\mu_b)}\left(a(\mu_b)\prod_{k\neq a}\phi(\lambda_k-\mu_b+i\gamma) - d(\mu_b)\prod_{k\neq a}\phi(\lambda_k-\mu_b-i\gamma)\right) \tag{4.53}$$

with $\phi(x)=\sinh(x)$. We now have all the ingredients to calculate matrix elements in the XXZ model.

5

Spinon decay in the spin-$\frac{1}{2}$ Heisenberg chain with weak next nearest neighbour exchange

Contents

5.1 Motivation and decay rate

We have seen that integrable many-particle quantum systems are special in that they support stable elementary excitations, which typically are related in very complicated ways to the fundamental degrees of freedom. For example, in the Heisenberg antiferromagnet the elementary excitations are interacting spin-1/2 objects called spinons [126, 130], as introduced before. We have shown that these elementary excitations are protected from decay into multi-particle excitations by the existence of local integrals of motion, even in cases where decay is kinematically allowed. We are now interested in introducing a weak integrability breaking perturbation, which means we will introduce some interaction parametrically small in some constant κ. In such situations we have argued that we expect to

induce particle decay. As the introduction of interactions in one dimensions can have dramatic effects on the quasi-particles, an important question is how large the corresponding decay rates are. If they are small, the elementary excitations of the integrable model will remain a good basis for describing the physics of the perturbed model. Such questions have been investigated in some detail for integrable quantum field theories [131–134]. The case of integrable lattice models is considerably harder, and to the best of our knowledge has not been investigated so far. The added difficulty compared to field theory cases is that the description of the ground and excited states is more complicated, as seen above. The question of what effects weak integrability breaking perturbations have on the excitation spectrum of lattice models is also of importance in so-called mobile impurity approaches to the calculation of threshold singularity exponents in lattice models [135]. As pointed out in Ref. [136] in the context of the Hubbard model, there exist different formulations of mobile impurity models [137], which correspond to different choices of bases of elementary excitations. One may argue that for integrable models the "integrable" basis of elementary excitations ought to be the preferred choice. An obvious question is then whether this remains the case even if integrability is weakly broken. This is intimately related to how large the decay rate of the excitations is once a perturbation is applied. For the Hubbard model the available integrable model technology [18] does not currently permit to answer this question. We therefore consider the simpler case of the spin-$1/2$ Heisenberg XXZ chain of length L in a magnetic field h

$$H(J,\Delta,h) = J\sum_{j=1}^{L}\left(S_j^xS_{j+1}^x + S_j^yS_{j+1}^y + \Delta S_j^zS_{j+1}^z\right) - h\sum_{j=1}^{L}S_j^z. \tag{5.1}$$

as introduced in Chapter 4.3.

A simple way of perturbing the model away from the integrable point is by introducing a next nearest neighbour interaction

$$\delta H = \kappa\sum_j S_j^zS_{j+2}^z\ . \tag{5.2}$$

This interaction destroys integrability, but still commutes with the total spin operator along the z-axis $S^z = \sum_j S^z_j$. Hence the z-component of the total spin remains a good quantum number. In presence of the perturbation spinons cease to be exact elementary excitations and we expect them to acquire a finite life-time. Using Fermi's golden rule for small perturbations the decay rate can be expressed in the form

$$\Gamma = 2\pi \sum_f |\mathcal{M}(i \to f)|^2 \, \rho_f(E_i) \, \delta_{p_f, p_i} \tag{5.3}$$

where E_f and p_f (E_i and p_i) are the energy and momentum of the final (initial) state [138], $\rho_f(E)$ the density of states of the final state and the matrix element $\mathcal{M}$ is given by

$$\mathcal{M} = \langle f | \, \delta H \, | i \rangle \ . \tag{5.4}$$

We are interested in the case where the initial state is an exact one-spinon eigenstate of (4.5), while the final state is any exact eigenstate of the unperturbed system.

Most of our analysis will focus on the isotropic Heisenberg model at $\Delta = 1$ and $h > 0$. Other values of Δ can be treated in the same way. We can consider $h < 0$ by starting with the reference state where all spins point down $|\downarrow\downarrow \cdots \downarrow\rangle$.

We first describe the excited states that contribute to the decay rate in Section 5.2.3. We then use the Algebraic Bethe Ansatz to obtain explicit expressions for the matrix elements describing the spinon decay, *cf.* 5.3. In Section 5.4 we then numerically determine the contributions of various decay channels to the decay rate.

5.2 Excitations in the XXX model

5.2.1 What is a spinon?

We will be interested in the low energy excitations of the XXX Heisenberg model. To get a better understanding, we first present an intuitive way of thinking about

these excitations, before they will be constructed rigorously. This discussion really applies to $\Delta > 1$, however it will still be useful for the construction at $\Delta = 1$. While we saw that eigenstates of the Heisenberg model are complicated superpositions of product states in a certain spin sector, the ground state of the antiferromagnetic Heisenberg model at zero magnetic field can be shown to be "morally", on short length scales, similar to an anti-ferromagnetic Néel state [3]. In this schematic picture the bare "particles" are spinflips, also called magnons.

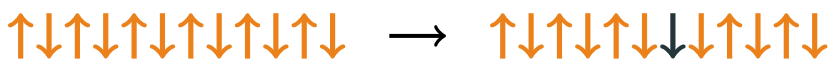

Figure 5.1: Schematic short range order representation of the ground state of the antiferromagnetic Heisenberg model at zero magnetic field on the left and a bare excitation of the model (magnon) on the right.

These spin-1 excitations do however not constitute the elementary low energy excitations of the theory, but these are given by spin-$\frac{1}{2}$ excitations, called spinons [130]. In the schematic short-range order picture, where the ground state is given by the anti-ferromagnetic Néel state, this corresponds to domain wall configurations.

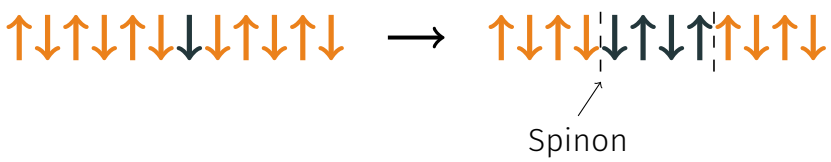

Figure 5.2: Schematic representation of the elementary low energy excitation of the Heisenberg model at short ranges. The excitation is a spin-$\frac{1}{2}$ particle called "spinon", which in the schematic representation corresponds to a domain-wall configuration.

We see from this schematic picture, and it can be seen to be true for the more complicated exact state [112], that spinon excitations come in pairs, as the consecutive spin flips creating the domain walls will always create two domain walls. As we will be interested in the stability of single excitations, one question is how to obtain an odd number of spinon excitations. For this, let us consider putting the chain with an odd number of sites on a ring, such that we have periodic boundary

conditions on the spins. Looking at the schematic picture in Fig. 5.3, we see that due to the antiferromagnetic structure, there has to be an odd number of domain walls for the odd length chain.

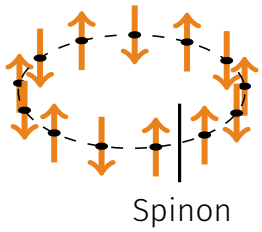

Figure 5.3: Schematic representation of the ground state for an odd length chain with periodic boundary conditions. Due to the anti-ferromagnetic structure of the state, there has to be at least one, and always an odd number of domain walls. This carries over to the more complicated exact energy eigenstates [112].

This can again be shown to be correct also for the more complicated Bethe Ansatz states and at finite magnetic fields [112].

5.2.2 Exact ground state

Let us first explicitly construct the ground state of the XXX-Heisenberg model. As in the schematic discussion we take a chain of even length L. Then the ground state can be shown to be the state with the quantum numbers [112]

$$I^1_\alpha = -\frac{N+1}{2} + \alpha, \quad \alpha = 1, \dots, N. \tag{5.5}$$

Therefore the lowest energy state at a fixed magnetisation is the state where the I_a are symmetric around 0:

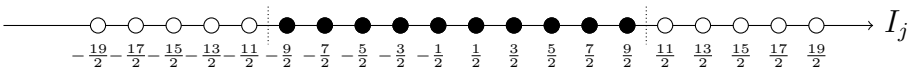

Low lying excitations in the same S^z sector are e.g. particle-hole like excitations created from the ground state and the number of excitations in a chain of even length can be seen to always be even, as discussed before in the schematic discussion of the spinon excitations.

5.2.3 Low lying excitations and spectrum

We are now going to explicitly construct excitations in the finite L XXX-Heisenberg chain at finite magnetic field and show that these excitations can be seen to be quasi-particle excitations with additive energies and momenta when going to the large L limit. In order to have access to single-spinon excitations, as described above, we need to consider odd chain lengths L. As we just saw, for even values of L the lowest excitations involve at least two spinons [126].

5.2.3.1 One particle and one hole excitations

For odd L with an odd number N of down spins there are two degenerate lowest energy states. They are obtained by considering real solutions (1-strings) to the Bethe Ansatz equations and choosing either

$$I_\alpha^1 = -\frac{N}{2} + \alpha, \quad \alpha = 1, \dots, N, \tag{5.6}$$

or

$$I_\alpha^1 = -\frac{N}{2} + 1 + \alpha, \quad \alpha = 1, \dots, N, \tag{5.7}$$

The corresponding configurations of half-odd integers for $N = 11$ look as follows:

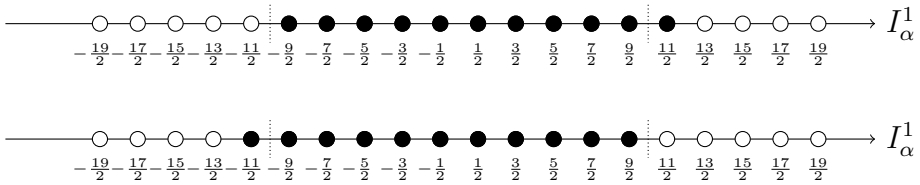

The filled quantum numbers corresponding to the filled circles hereby correspond to the magnon excitations schematically introduced above. The energy density $e(h)$ of these two states in the thermodynamic limit

$$L, N \to \infty, \frac{N}{L} = n = \text{fixed} \tag{5.8}$$

can be expressed, as shown in Chapter 4.3.3, in terms of the solution of a linear integral equation for the root density $\rho_1(\lambda)$, *cf.* Ref. [112]

$$\rho_1(\lambda) = a_1(\lambda) - \int_{-B}^{B} \mathrm{d}\eta \; a_2(\lambda - \eta) \; \rho_1(\eta). \tag{5.9}$$

where here and in the following we have dropped the index p of the particle density. Here the integration boundary B is determined by the density of down spins n through

$$\int_{-B}^{B} \mathrm{d}\lambda\ \rho_1(\lambda) = n. \tag{5.10}$$

The energy per site is then given by

$$e(h) = \int_{-B}^{B} \mathrm{d}\lambda\ \rho_1(\lambda)\varepsilon_1^{(0)}(\lambda), \tag{5.11}$$

where

$$\varepsilon_1^{(0)}(\lambda) = -J\pi a_1(\lambda) + h. \tag{5.12}$$

The two states above are particular limits of one-parameter "particle-like" and "hole-like" excitations. The particle excitation corresponds to I_α^1 configurations of the form

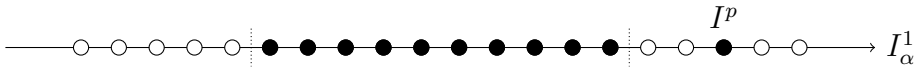

whereas the hole-like excitation is obtained by promoting one half-odd integer I_α^1 in the ground state configuration to the "Fermi edge" that has one fewer half-odd integer:

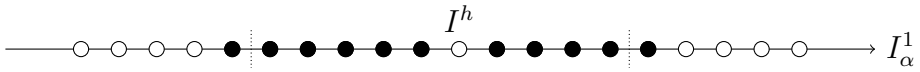

Both types of excitations involve a single parameter: I^p for the particle excitation and I^h for the hole excitation. For asymptotically large system sizes L the energies and momenta of these excitations are given by [112]

$$E^p = Le + \varepsilon_1(\lambda^p) + o(1), \qquad |\lambda^p| > B\ , \tag{5.13}$$

$$P^p = \pi + 2\pi \int_0^{\lambda^p} \mathrm{d}\lambda\ \rho_1(\lambda) + \mathcal{O}(L^{-1})\ , \tag{5.14}$$

$$E^h = Le - \varepsilon_1(\lambda^h) + o(1), \qquad \left|\lambda^h\right| < B\ , \tag{5.15}$$

$$P^h = \pi - 2\pi \int_0^{\lambda^h} \mathrm{d}\lambda\ \rho_1(\lambda) + \mathcal{O}(L^{-1})\ , \tag{5.16}$$

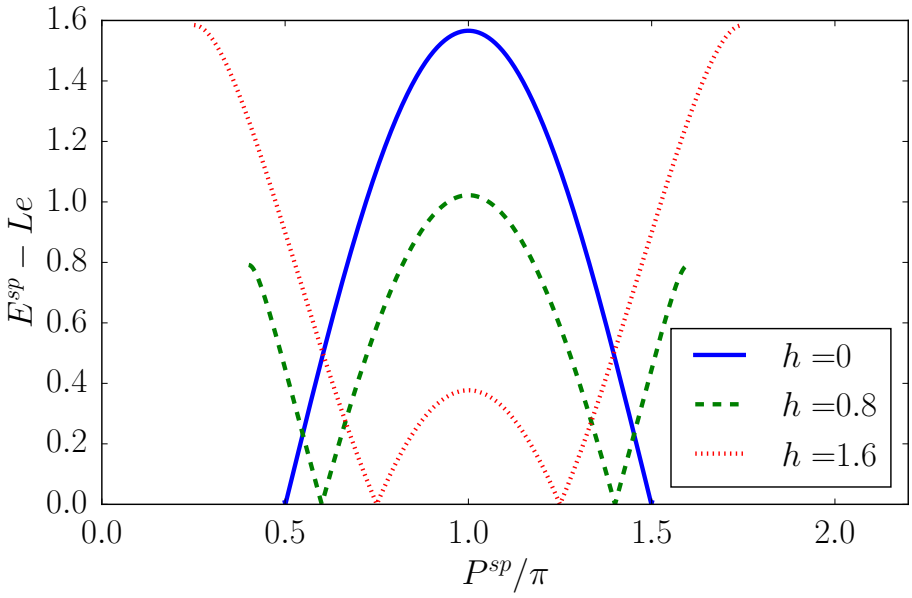

Figure 5.4: Energy-momentum dispersion of the one-parameter excitations for different values of the magnetic field h.

where the *dressed energy* $\epsilon_1(\lambda)$ is a solution to the linear integral equation

$$\varepsilon_1(\lambda) = \varepsilon_1^{(0)}(\lambda) - \int_{-B}^{B} \mathrm{d}\mu \;\; a_2(\mu - \lambda)\, \varepsilon_1(\mu). \tag{5.17}$$

The derivation can be found in Appendix 5.A The rapidities λ^p and λ^h are continuous parameters above and below the "Fermi-edge" respectively. They are related to the parameters I^p and I^h through Takahashi's equations (4.16).

The excitation energy for a one-spinon excitation can now be extracted by simply subtracting the extensive part of the energy (which equals the ground state energy of the Heisenberg chain), which allows us to extract the spinon energy and momentum

$$\epsilon_s(\lambda) = |\varepsilon_1(\lambda)|, \qquad p_s(\lambda) = \pi + 2\pi \,\mathrm{sgn}(|\lambda| - B) \int_0^{\lambda} d\mu \; \rho_1(\mu). \tag{5.18}$$

The corresponding dispersion relation is plotted for several values of magnetic field h in Fig. 5.4. The value for the magnetic field is fixed by imposing $\varepsilon_1(B) = 0$. We note that by construction the spinon dispersion is identical to the one extracted from the two-spinon excitation of the Heisenberg model with even chain lengths L, apart from a shift in momentum by π.

5.2.3.2 Excitations involving several particles and/or holes

As δH commutes with S^z, the decay of the single-particle (hole) excitation described above can only involve excited states with the same S^z quantum number. These are obtained in the following ways:

1. One can consider solutions of Takahashi's equations only involving 1-strings. These will involve additional particle-hole excitations on top of the 1-spinon excitation constructed above.

2. One can consider solutions of Takahashi's equations involving n-strings with $n \geq 2$. As a result of the magnetic field these excitations have a gap.

3. One can consider excitations of the form (4.22) that are not SU(2) highest-weight states. These again have a gap for $h > 0$ because

$$[S^-, H(J, \Delta = 1, h)] = -hS^- \tag{5.19}$$

As we are dealing with an interacting theory, this leaves us with an infinite number of possible decay channels, i.e. even to first order in perturbation theory in κ, a single spinon can decay into excitations involving $3, 5, 7, \ldots$ particles. As in one dimension the accessible phase space shrinks with the number of particles involved [139], it is reasonable to assume that the dominant decay channels will involve excitations with low numbers of particles. In the following we will focus on excitations involving 3 particles. We have considered a class of five-particle excitations where we excite two particle- and hole-type excitations in addition to the one-spinon excitation, and found the corresponding decay rate to be smaller (see Section 5.4).

"pph-excitation" This excitation involves only 1-strings and corresponds to configurations of the (half-odd) integers I^1_α looking as follows

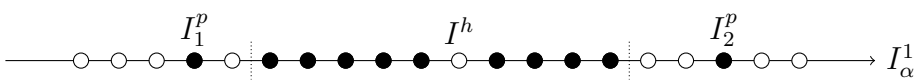

States of this kind can be thought of as a sub-class of 3-spinon excitations that involves two particles and one hole, which are parametrized by I^h and $I^p_{1,2}$ respectively (or equivalently by the corresponding rapidities λ^h, $\lambda^p_{1,2}$). Energy and momentum of this excitation are given by

$$E^{pph} = Le + \epsilon_s(\lambda^p_1) + \epsilon_s(\lambda^p_2) + \epsilon_s(\lambda^h) + o(1) \,, \tag{5.20}$$

$$P^{pph} = p_s(\lambda^p_1) + p_s(\lambda^p_2) + p_s(\lambda^h) + \mathcal{O}(L^{-1}) \,, \tag{5.21}$$

where $\epsilon_s(\lambda)$ and $p_s(\lambda)$ are defined in (5.18). The excitation energy is obtained subtracting the ground state energy, and the corresponding continuum of 3-spinon excited states is shown in Fig. 5.5a. The grey shading reflects the density of excitations at given values of energy and momentum. Darker regions correspond to higher densities. The intensity of the shading is obtained by considering large but finite L and varying I^h and $I^p_{1,2}$ over all allowed values for a given excitation, and calculating approximate values of $\lambda^h, \lambda^p_{1,2}$ by solving the equations

$$p_s(\lambda^h) = \frac{2\pi I^h}{L}, \quad p_s(\lambda^p_j) = \frac{2\pi I^p_j}{L}, \; j = 1, 2. \tag{5.22}$$

The corresponding approximate excitation energy is then obtained by substituting these values into (5.21). Each set $\{I^h, I^p_{1,2}\}$ provides one point in the P^{pph}-E^{pph}-plane and the collection of all these points generates a shading that reflects the density of states.

We see that for momenta $\pi(\frac{1}{2} + m) < p_s(\lambda) < \pi(\frac{3}{2} - m)$ decay of the 1-spinon excitation is kinematically forbidden, while it is allowed for some values in the regions $p_s(\lambda) > \pi(\frac{3}{2} - m)$ and $p_s(\lambda) < \pi(\frac{1}{2} + m)$.

"phh-excitation" This excitation involves only 1-strings and corresponds to configurations of the (half-odd) integers I^1_α looking as follows

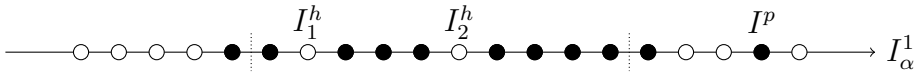

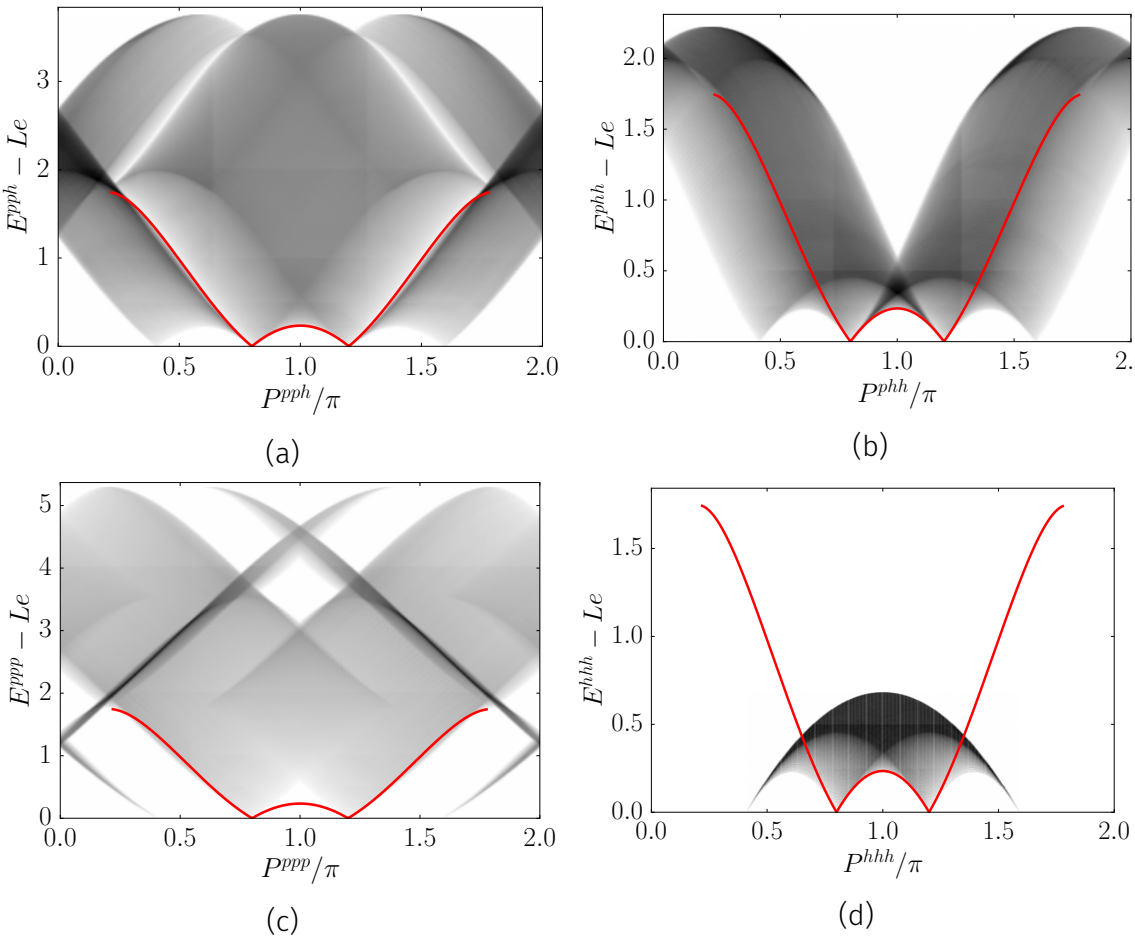

Figure 5.5: Excitation continua (grey) for (a) two particle one hole (b) one particle two holes (c) three particle and (d) three holes at magnetization $m = 3/10$. The 1-spinon dispersion is shown in red. The shading of the continuum reflects the density of states (see main text). Decay of the single spinon is kinematically allowed in part of the Brillouin zone.

States of this kind are a sub-class of 3-spinon excitations that involves one particle and two holes, which are parametrized by I^p and $I^h_{1,2}$ or equivalently by the corresponding rapidities $\lambda^p, \lambda^h_{1,2}$. Energy and momentum of this excitation are given by

$$E^{phh} = Le + \epsilon_s(\lambda^p) + \epsilon_s(\lambda^h_1) + \epsilon_s(\lambda^h_2) + o(1) \,, \tag{5.23}$$

$$P^{phh} = p_s(\lambda^p) + p_s(\lambda^h_1) + p_s(\lambda^h_2) + \mathcal{O}(L^{-1}) \,, \tag{5.24}$$

where $\epsilon_s(\lambda)$ and $p_s(\lambda)$ are defined in (5.18). The excitation energy is again obtained by subtracting the ground state energy and is shown as a function of the total

momentum in Fig. 5.5b.

"ppp-excitations" This excitation involves only 1-strings and corresponds to configurations of the (half-odd) integers I^1_α looking as follows

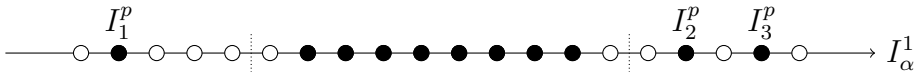

States of this kind are a sub-class of 3-spinon excitations that involves three particles. Energy and momentum of this excitation are

$$E^{ppp} = Le + \sum_{j=1}^{3} \epsilon_s(\lambda_j^p) + o(1) \ , \tag{5.25}$$

$$P^{ppp} = \sum_{j=1}^{3} p_s(\lambda_j^p) + \mathcal{O}(L^{-1}), \tag{5.26}$$

where $\epsilon_s(\lambda)$ and $p_s(\lambda)$ are defined in (5.18). The excitation energy is again obtained by subtracting the ground state energy and is shown as a function of the total momentum in Fig. 5.5c.

"hhh-excitations" This excitation involves only 1-strings and corresponds to configurations of the (half-odd) integers I^1_α looking as follows

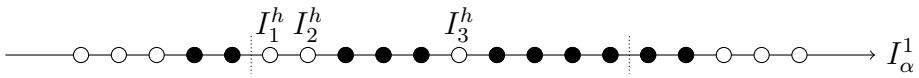

States of this kind are a sub-class of 3-spinon excitations that involves three holes. Energy and momentum of this excitation are

$$E^{hhh} = Le + \sum_{j=1}^{3} \epsilon_s(\lambda_j^h) + o(1) \ , \tag{5.27}$$

$$P^{hhh} = \sum_{j=1}^{3} p_s(\lambda_j^h) + \mathcal{O}(L^{-1}), \tag{5.28}$$

where $\epsilon_s(\lambda)$ and $p_s(\lambda)$ are defined in (5.18). The excitation energy is again obtained by subtracting the ground state energy and is shown as a function of the total momentum in Fig. 5.5d.

Excitations involving a single 2-string We now turn to the simplest excitation involving a single 2-string. This corresponds to solutions of (4.16) with $M_1 = N-2$, $M_2 = 1$ and configurations of the half-odd integers I^1_α, I^2_1 of the kind

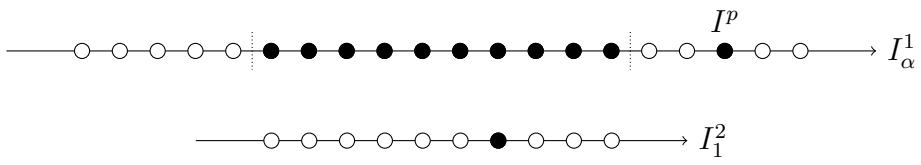

We note that the permitted values for I^2_1 have range

$$|I^2_1| \leq \frac{1}{2}\left[L - 2N\right]. \tag{5.29}$$

The excitation is parametrized by the two half-odd integers I^p, I^2_1 or equivalently the corresponding rapidities λ^p, λ^s. Energy and momentum of this excitation are given by

$$E^{2sp} = Le + \epsilon_s(\lambda^p) + \varepsilon_2(\lambda^s)\,, \qquad |\lambda^p| > B\,, \tag{5.30}$$

$$P^{2sp} = p_s(\lambda^p) + p_2(\lambda^s)\,, \tag{5.31}$$

where ε_2 and $p_2(\lambda)$ are given by [112]

$$\begin{aligned} \varepsilon_2(\lambda^s) &= \varepsilon_{2,0}(\lambda^s) - \int_{-B}^{B} \mathrm{d}\mu\; \varepsilon_1(\mu)\left(a_1(\mu-\lambda^s) + a_3(\mu-\lambda^s)\right). \\ p_s(\lambda) &= \theta\Big(\frac{\lambda}{2}\Big) - \int_{-B}^{B} \mathrm{d}\mu\;\; \theta_{21}(\lambda-\mu)\;\rho_1(\mu) \end{aligned} \tag{5.32}$$

and bare energy $\varepsilon_{2,0}(\lambda)$ from 4.3.3. Excitation continua that encompass the two-particle continuum (5.31) are obtained by adding particle-hole excitations, e.g.

$$E^{2s3p2h} = Le + \sum_{j=1}^{3}\epsilon_s(\lambda^p_j) + \sum_{k=1}^{2}\epsilon_s(\lambda^h_k) + \varepsilon_2(\lambda^s)\,, \qquad \left|\lambda^h_j\right| < B < |\lambda^p_k|\;, \tag{5.33}$$

$$P^{2s3p2h} = \sum_{j=1}^{3} p_s(\lambda^p_j) + \sum_{k=1}^{2} p_s(\lambda^h_k) + p_2(\lambda^s)\,. \tag{5.34}$$

The continuum (5.34) is shown in Fig. 5.6 for several magnetizations. We see that the single spinon excitation cannot decay into the 2-string excitation for kinematic reasons. If we keep on adding particle-hole excitations at small magnetic

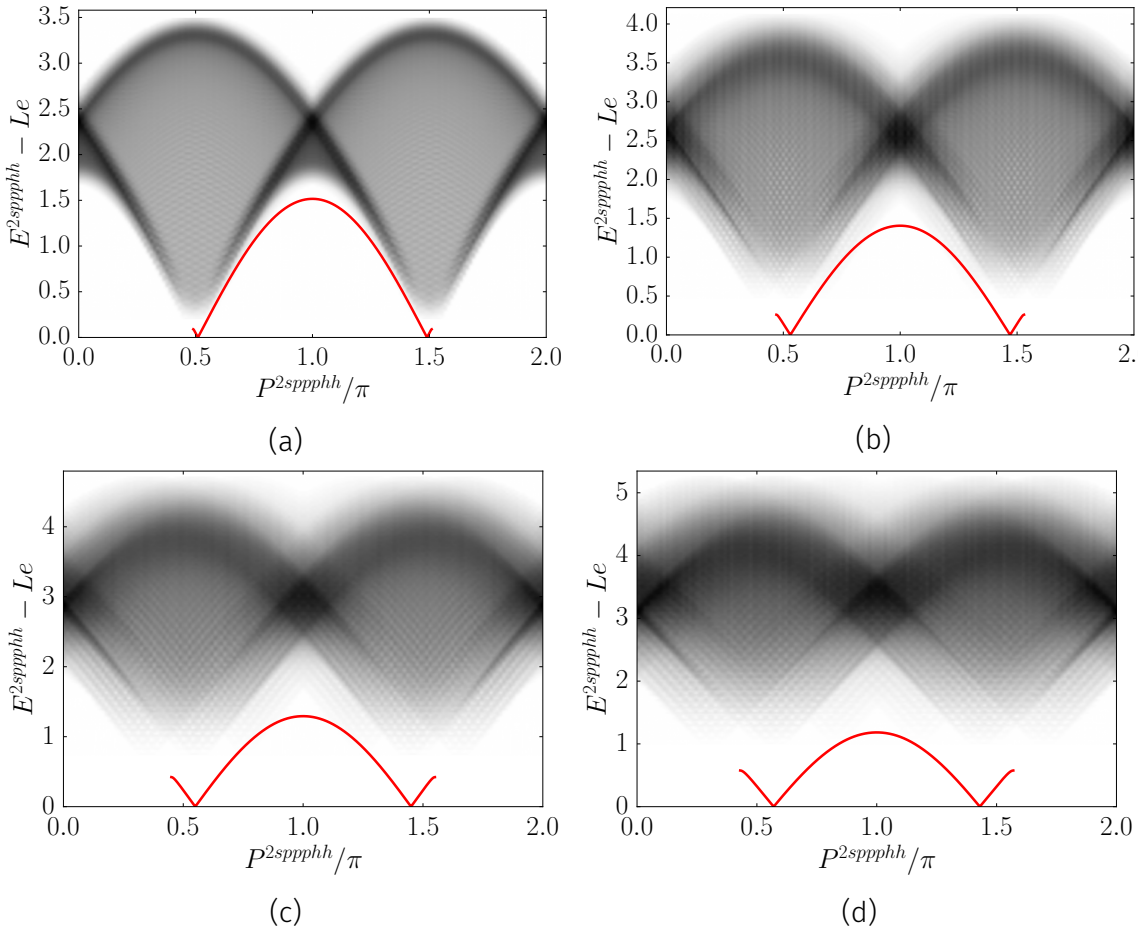

Figure 5.6: One two-string and $3p2h$ excitation continuum (grey) at magnetization (a) $m = 0.01$, (b) $m = 0.03$, (c) $m = 0.05$ and (d) $m = 0.07$, (the corresponding magnetic fields are $h = 0.09$, $h = 0.26$, $h = 0.42$ and $h = 0.58$ respectively). The 1-spinon dispersion is shown in red. The shading of the continuum reflects the density of states (see main text). Decay of the single spinon is kinematically not allowed.

fields decay of the 1-spinon excitation will eventually become kinematically allowed. However, the decay rate is then expected to be negligible on the basis of aforementioned phase-space arguments, *cf.* Ref. [139].

Excitations involving longer strings Excitations involving longer strings have larger gaps at finite magnetic fields [112]. We expect contributions from decay channels involving such excitations to be small for the same reasons we put forward in the 2-string case above.

Excitations that are not highest weight states As mentioned above, excitations which are not highest weight states have gaps that are proportional to the magnetic field h. Nevertheless, decay of a single spinon into excitations that are not highest weight states will generally be allowed at sufficiently small h. As an example let us consider highest-weight states with $M_1 = N - 1$, $M_{n\geq 2} = 0$. The lowest energy states in this sector correspond to integers

$$I^1_\alpha = -\frac{N}{2} + \alpha, \quad \alpha = 1, \ldots, N, \tag{5.35}$$

or

$$I^1_\alpha = -\frac{N}{2} - 1 + \alpha, \quad \alpha = 1, \ldots, N, \tag{5.36}$$

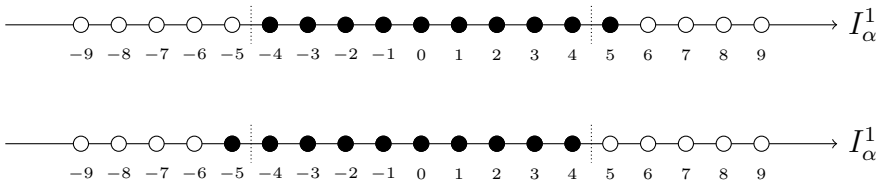

In complete analogy to our discussion above, these can be viewed as particular limits of a 1-spinon excitation. Acting with the spin lowering operator gives a 1-parameter excited state with a dispersion that equals the 1-spinon dispersion shifted upwards in energy by h. Hence decay of our 1-spinon excitation into this particular descendant state is kinematically not allowed. However, if we add an additional particle-hole pair the situation changes. Let us consider configurations of integers such as

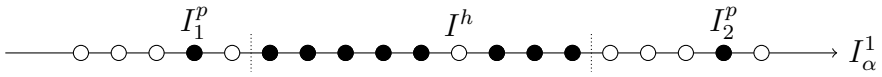

States of this kind can be thought of as a sub-class of 3-spinons. Energy and momentum of the excitation obtained by acting with the spin-lowering operator on this state are given by

$$E^{pph}_{\rm desc} = Le + \epsilon_s(\lambda^p_1) + \epsilon_s(\lambda^p_2) + \epsilon_s(\lambda^h) + h + o(1)\ , \tag{5.37}$$

$$P^{pph}_{\rm desc} = \pi + p_s(\lambda^p_1) + p_s(\lambda^p_2) + p_s(\lambda^h) + \mathcal{O}(L^{-1})\ . \tag{5.38}$$

Inspection of Fig. 5.5a shows that decay of the 1-spinon excitation into this continuum is kinematically allowed at sufficiently weak fields. However, as will be shown in 5.B this decay is strongly suppressed for large system sizes L.

5.3 Determinant Formulas for Matrix Elements in the XXZ chain

In 5.2.3 we have constructed the one spinon quasi-particle excitations with additive energies and momenta that constitute the low energy excitations of the Heisenberg model in the large L limit as complicated superpositions of product states at finite but large L. Using the Algebraic Bethe Ansatz and inverse scattering we can now calculate matrix elements involving quasi-particle spinon excitations. The Algebraic Bethe Ansatz provides a convenient setting for calculating scalar products as well as the norm of Bethe states [129, 140, 141]. Matrix elements can be analysed by utilizing the expression of local spin operators σ_j^z in terms of the operators A, B, C, D, *cf.* Ref. [128]. With the help of these relations matrix elements of spin operators S_j^α between eigenstates of the XXZ Hamiltonian were derived in Ref. [128], and general operators were considered in Ref. [142]. Explicit expressions for the operator $S_j^z S_{j+1}^z$ were obtained in Ref. [143]. In the following we will first consider the XXZ case with anisotropy parameter $\Delta = \cos\gamma$ and only later specialize to the isotropic limit $\Delta = 1$. Generalising the derivation of Ref. [143] we obtain

(see 5.C for details)

$$\sum_j \langle \lambda_1, \ldots, \lambda_N | \, S^z_j S^z_{j+2} \, | \mu_1, \ldots, \mu_M \rangle =$$

$$Le^{iP_{\{\lambda\}}+2iP_{\{\mu\}}}\delta_{P_{\{\lambda\}},P_{\{\mu\}}}\delta_{M,N}\left\{-\phi(i\gamma)\frac{\prod_k \phi(\lambda_k+i\gamma/2)^2\phi(\mu_k+i\gamma/2)\phi(\mu_k-i\gamma/2)^{-3}}{\prod_{a>b}\phi(\lambda_b-\lambda_a)\prod_{b>a}\phi(\mu_b-\mu_a)}\right.$$
$$\times\sum_n A_n\left(\det\left(G^{(1)}_n+B^{(1)}_n\right)+\det\left(G^{(2)}_n+B^{(2)}_n\right)-\det\left(G^{(1)}\right)-\det\left(G^{(2)}\right)\right)$$
$$-\frac{1}{2}\frac{\prod_k \phi(\lambda_k+i\gamma/2)^3\phi(\mu_k-i\gamma/2)^{-3}}{\prod_{a>b}\phi(\lambda_b-\lambda_a)\prod_{a<b}\phi(\mu_b-\mu_a)}$$
$$\left.\times\sum_{n=1}\sum_{m\neq n}A_{nm}\left[\det\left(G_{nm}+B_{nm}\right)-\det\left(G_{nm}\right)\right]\right\}. \tag{5.39}$$

Here $P_{\{\lambda\}}$ is the total momentum of the state parametrized by the rapidities $\{\lambda_j\}$

$$P_{\{\lambda\}}=\sum_{j=1}^{N}\left[\pi+\ln\left(\frac{\lambda_j+\frac{i\gamma}{2}}{\lambda_j-\frac{i\gamma}{2}}\right)\right], \tag{5.40}$$

and

$$A_n=\sum_n d(\mu_n)\frac{\phi(\mu_n-\frac{i\gamma}{2})}{\phi(\mu_n+\frac{i\gamma}{2})}\prod_i\phi(\mu_i-\mu_n-i\gamma) \tag{5.41}$$

$$H_{ab}=\frac{\phi(i\gamma)}{\phi(\lambda_a-\mu_b)}\Big(a(\mu_b)\prod_{k\neq a}\phi(\lambda_k-\mu_b+i\gamma)-d(\mu_b)\prod_{k\neq a}\phi(\lambda_k-\mu_b-i\gamma)\Big), \tag{5.42}$$

$$(G^{(1)}_n)_{ab}=\begin{cases}H_{ab} & b\neq n\\ \frac{\phi(i\gamma)\phi(2\lambda_a)}{\phi(\lambda_a-\frac{i\gamma}{2})^2\phi(\lambda_a+\frac{i\gamma}{2})^2} & b=n\end{cases}, \tag{5.43}$$

$$(G^{(2)}_n)_{ab}=\begin{cases}H_{ab} & b\neq n\\ \frac{\partial^2}{\partial x^2}\left(\frac{\phi(i\gamma)}{\phi(\lambda_a-x)\phi(\lambda_a-x+i\gamma)}\right)\Big|_{x=\frac{i\gamma}{2}} & b=n\end{cases}, \tag{5.44}$$

$$(B^{(1)}_n)_{ab}=(1-\delta_{bn})d(\mu_b)\prod_{i\neq n}\phi(\mu_i-\mu_b+i\gamma)\phi(\mu_b+i\gamma/2)$$
$$\times\left(\frac{\phi'(i\gamma)}{\phi(i\gamma)}-\sum_{d\neq n}\frac{\phi(i\gamma)}{\phi(\mu_d-i\gamma/2)\phi(\mu_d+i\gamma/2)}+\sum_{d\neq m,n}\frac{\phi'(\mu_d-i\gamma/2)}{\phi(\mu_d-i\gamma/2)}\right.$$
$$\left.-\sum_b\frac{\phi'(\lambda_b+i\gamma/2)}{\phi(\lambda_b+i\gamma/2)}+\frac{\phi(i\gamma)}{\phi(\mu_m+i\gamma/2)\phi(\mu_m-i\gamma/2)}\right), \tag{5.45}$$

$$(B^{(2)}_n)_{ab}=(1-\delta_{bn})\frac{1}{2}d(\mu_b)\prod_{i\neq n}\frac{\phi(\mu_i-\mu_b-i\gamma)\phi(\mu_b+i\gamma)\phi(i\gamma)}{\phi(\lambda_a+i\gamma/2)\phi(\lambda_a-i\gamma/2)}. \tag{5.46}$$

$$A_{nm} = d(\mu_n)\phi(\mu_n - \frac{i\gamma}{2})^2 \phi(\mu_m - \frac{i\gamma}{2}) \prod_i \phi(\mu_i - \mu_n - i\gamma) \tag{5.47}$$

$$\times \prod_j \phi(\mu_j - \mu_m + i\gamma) \left[\frac{\phi(\mu_m - \frac{3i\gamma}{2})}{\phi(\mu_m - \mu_n - i\gamma)} - \frac{\phi(\mu_m + \frac{i\gamma}{2})}{\phi(\mu_m - \mu_n + i\gamma/2)} \right] \tag{5.48}$$

$$(G_{nm})_{ab} = \begin{cases} H_{ab} & b \neq m, n \\ \frac{\phi(i\gamma)\phi(2\lambda_a)}{\phi(\lambda_a - \frac{i\gamma}{2})^2 \phi(\lambda_a + \frac{i\gamma}{2})^2} & b = m \\ \frac{\partial^2}{\partial x^2} \left(\frac{\phi(i\gamma)}{\phi(\lambda_a - x)\phi(\lambda_a - x + i\gamma)} \right) \Big|_{x=\frac{i\gamma}{2}} & b = n \end{cases} \tag{5.49}$$

$$(B_{nm})_{ab} = (1 - \delta_{bm})(1 - \delta_{bn}) d(\mu_b) \prod_{i \neq m,n} \frac{\phi(\mu_i - \mu_b - i\gamma)\phi(\mu_b + i\gamma/2)^2 \phi(i\gamma)}{\phi(\lambda_a - i\gamma/2)\phi(\lambda_a + i\gamma/2)} . \tag{5.50}$$

Finally, the function $\phi(\lambda)$ is given by

$$\phi(\lambda) = \begin{cases} \lambda & \Delta = 1 \\ \sinh(\lambda) & |\Delta| < 1 \end{cases} . \tag{5.51}$$

In the isotropic case $\Delta = 1$ of interest to us the matrix element in the rescaled rapidity variables (4.46) is obtained by simply setting $\gamma = 1$ in the above expressions.

5.4 Decay rates

We are now in a position to compute the rates of decay of the one-spinon excitation into the various multi-particle excitations considered above. In practice the calculation is carried out in a large, finite volume L. The energy eigenstates are of the form (4.42) and involve N rapidity variables, which constitute a solution to the Bethe Ansatz equations. We will denote the states corresponding to the one-spinon and the two-particle one-hole continuum by

$$|N; J\rangle, \qquad |N; I_1^p, I_2^p, I^h\rangle, \tag{5.52}$$

Our notations for the respective energies (4.19) are

$$E(J), \quad E^{pph}(I_1^p, I_2^p, I^h). \tag{5.53}$$

Here J and $I_{1,2}^p, I^h$ denote the half-odd integers corresponding to the spinon and the particles/hole respectively. Other excitations are labelled analogously. The

decay rate is then given by

$$\Gamma_{\mathrm{sp}\to\mathrm{pph}}(p_J) \equiv \kappa^2 \gamma_{\mathrm{sp}\to\mathrm{pph}}(p_J) = \pi\kappa^2 \sum_{I_1^p, I_2^p, I^h} |\langle N; I_1^p, I_2^p, I^h| \sum_{j=1}^{L} S_j^z S_{j+2}^z |N; J\rangle|^2 \times \delta_{J, I_1^p + I_2^p - I^h}\, \delta(E^{pph}(I_1^p, I_2^p, I^h) - E(J)) \,, \quad (5.54)$$

where we have used (4.19) to simplify the momentum conservation delta function. The momentum p_J of the initial spinon excitation is given by

$$p_J = \begin{cases} \frac{2\pi J}{L} & \text{if } |J| > \frac{N}{2} - 1 \,, \\ -\frac{2\pi J}{L} & \text{if } |J| \leq \frac{N}{2}. \end{cases} \quad (5.55)$$

We regularize the delta function expressing energy conservation by

$$\delta_\eta(x) = \frac{1}{\sqrt{\pi}\eta} e^{-\left(\frac{x}{\eta}\right)^2}, \quad (5.56)$$

where $\lim_{\eta\to 0} \delta_\eta(x) = \delta(x)$. For very small η, but still with a sufficient number of final states in the regime where $\delta_\eta(x)$ is large, we expect the result to be close to the answer in the thermodynamic limit. For (5.54) to be finite in the thermodynamic limit, the matrix elements should scale as L^{-1}. As shown in Fig. 5.7, the decay in L is very slightly faster than L^{-2} and is compatible with the functional form

$$\left(\mathcal{M}_{pph}^2 L^2\right) = \frac{a + b/L}{L^c} \,, \quad (5.57)$$

where c is a very small exponent. In the range of lattice lengths accessible to us, equally good fits can be obtained by replacing L^c by $(\ln L)^c$ in (5.57). The situation is analogous to that for the dynamical structure factor [144–151]. For the latter it was shown that in order to obtain finite results in the thermodynamic limit, an infinite summation over states that contain additional particle-hole pairs located at the "Fermi points" $\pm B$ was required. On the other hand, the result obtained by working at a fixed value of $L \approx 1000$ and not carrying out this summation was found to give an excellent approximation to the thermodynamic limit. We expect the decay rate to behave in an analogous way. In the following we determine the contributions of the 3-particle excitations described in Section 5.2.3 to the decay rate for finite system sizes in the range $L \sim 500 - 1000$. We have verified that taking

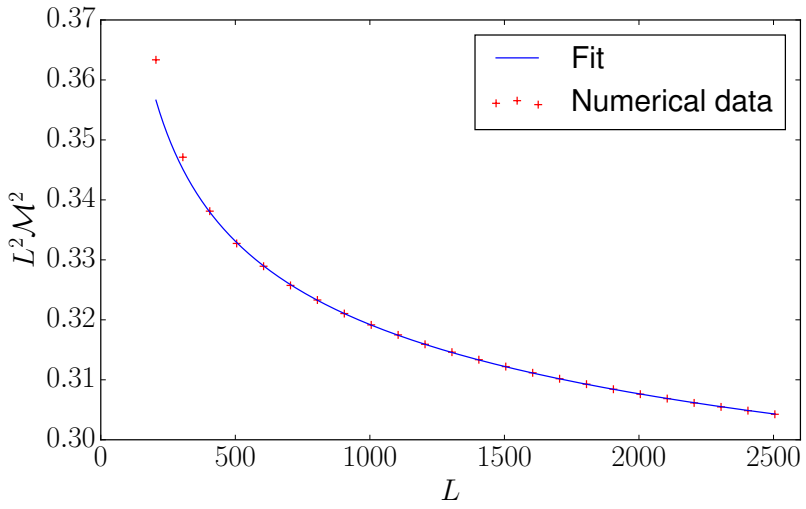

Figure 5.7: Scaling of matrix elements with system size L. The initial state contains one spinon with momentum $p = 5.5$, while the final state contains three high-energy excitations with momenta $p_p = 4.5, p_p = 4.65, p_h = 3.65$. The fit is to the functional form (5.57) with $a = 0.42$, $b = 5.6$, $c = 0.044$. We have also considered additional excitations around the Fermi points in the final state as well as different momenta and found similar behaviour.

into account states with one additional particle-hole excitation gives only small corrections.

We now fix L and then compute (5.54) for several values of the broadening η. The decay rates into the excitations considered in Section 5.2.3 are shown in Figs 5.8a, 5.8b, 5.8c and 5.8d.

We see that the dominant decay channel for a one spinon excitation is decay into a 3-spinon excitation of pph type. We have argued above excitations involving higher numbers of particles should give smaller contributions to the decay rate. In order to check this assumption we have calculated the decay rate into a 5-spinon excitation of type ppphh, which we expect to provide the largest contribution among the 5-spinon excitations. The result is shown in Fig. 5.9b. As expected the contribution is small. Moreover, it is mostly due to umklapp-type terms in the pph-channel, meaning particle-hole type excitations around the "Fermi sea" on top of the pph-type excitations (*cf.* Fig. 5.9a).

It is clear from Fig. 5.8 that all other 3-spinon decay channels can be neglected

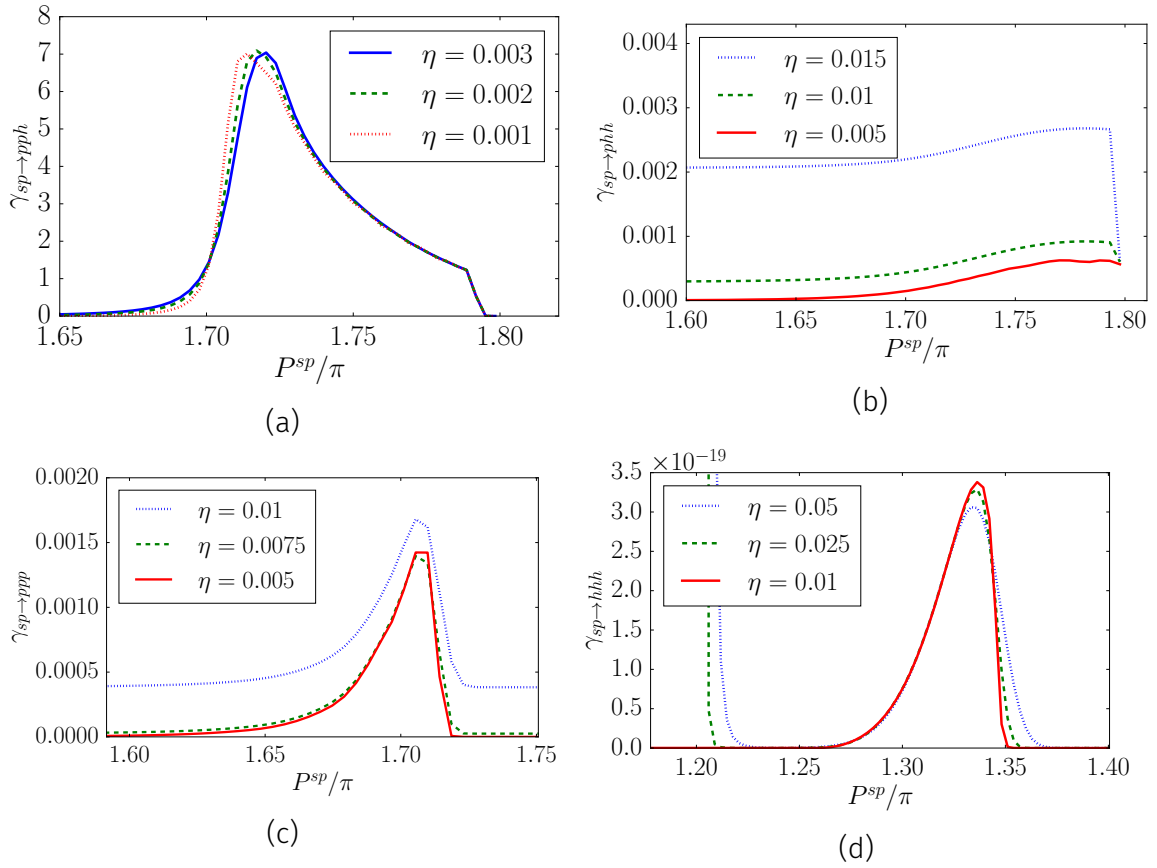

Figure 5.8: Coefficients of the decay rate for magnetization $m = 3/10$ and several values of the broadening η for (a) pph-type processes for $L = 615$, (b) phh-type processes for $L = 435$, (c) ppp-type processes for $L = 455$, (d) hhh-type processes for $L = 675$.

compared to the pph one. Moreover, the decay rate coefficient is of order unity, which means that the decay rate itself is small and proportional to the square of the strength of the integrability breaking perturbation.

5.4.1 Extrapolation to $\eta = 0$

The results of the previous section are for finite values of the system size and require a small, finite regularization parameter η. We will consider the extrapolation of these results to the thermodynamic limit and $\eta = 0$. As we have seen above, the matrix elements of the perturbing operator scale as L^{-1} up to multiplicative corrections that decay algebraically with very small exponent or logarithmically, *cf.*

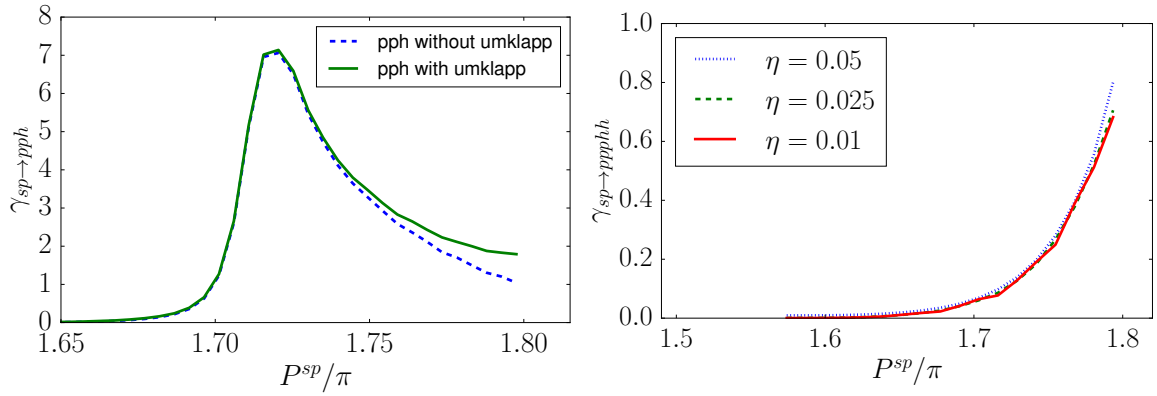

(a) (b)

Figure 5.9: Coefficients of the decay rate for magnetization $m = 3/10$ for (a) pph-type processes with and without umklapp terms for $\eta = 0.002$ at $L = 415$ and (b) ppphh-type processes for $L = 155$ and several values of the broadening η.

Fig. 5.7. We expect that in order to take the thermodynamic limit, one would have to sum over an infinite number of particle-hole excitations at the Fermi points, in analogy with available results for the spin-spin correlation function [147–150, 152]. Our situation is more complicated as we need to consider excited states with several elementary excitations at finite energies and summing over an infinite number of particle-hole excitations on top of these is beyond the scope of our work. However, we note that the main source of finite-size effects in our calculation is the necessity to have a sufficiently large value of the broadening η. This is required in order to obtain a good approximation to density of final states $\rho_f(E_i)$. This imposes a restriction $\eta > \eta_0(L) = \mathrm{const}/L$. Importantly, $\eta_0(L)$ tends to zero much faster than $\mathcal{M}^2 L^2$. This allows us to extrapolate our results to $\eta = 0$ as follows. We construct a smooth interpolation function $\mathcal{M}^{\mathrm{cont}}_{pph}(p, z_1^p, z_2^p)$ for the matrix element multiplied by L, and then turn the sums over Bethe Ansatz (half-odd) integers into integrals using the Euler-Maclaurin sum formula. Taking the limit $\eta \to 0$ results in

$$\gamma^{\mathrm{extra}}_{\mathrm{sp}\to\mathrm{pph}}(p) = \frac{1}{4\pi}\int_D \mathrm{d}z_1^p \int_D \mathrm{d}z_2^p\, \delta(\epsilon_s(z_1^p) + \epsilon_s(z_2^p) + \epsilon_s(z_1^p + z_2^p - p) - \varepsilon_1(p)) \times \left|\mathcal{M}^{\mathrm{cont}}_{pph}(p, z_1^p, z_2^p)\right|^2 , \tag{5.58}$$

where D is the domain where the one-spinon excitation exists (the interval $[\pi/5, 2\pi - \pi/5]$ for magnetization $m = 3/10$). We stress again that we do not claim that this

integral is the exact form one would get after summing all particle-hole pairs in the thermodynamic limit, but that the result of such a calculation is expected to be numerically very close to what is obtained here. One of the integrals can be carried out using the delta-function, which gives

$$\gamma^{\text{extra}}_{\text{sp}\to\text{pph}}(p) = \frac{1}{4\pi}\int_D \mathrm{d}z_1^p \, \frac{\left|\mathcal{M}^{\text{cont}}_{pph}(p, z_1^p, z)\right|^2}{|\epsilon_s'(z) + \epsilon_s'(z_1^p + z - p)|} \,, \tag{5.59}$$

where z is the solution of the equation $\epsilon_s(z_1^p) + \epsilon_s(z) + \epsilon_s(z_1^p + z - p) - \varepsilon_1(p) = 0$. Carrying out the remaining integral numerically leads to the result shown in Fig. 5.10

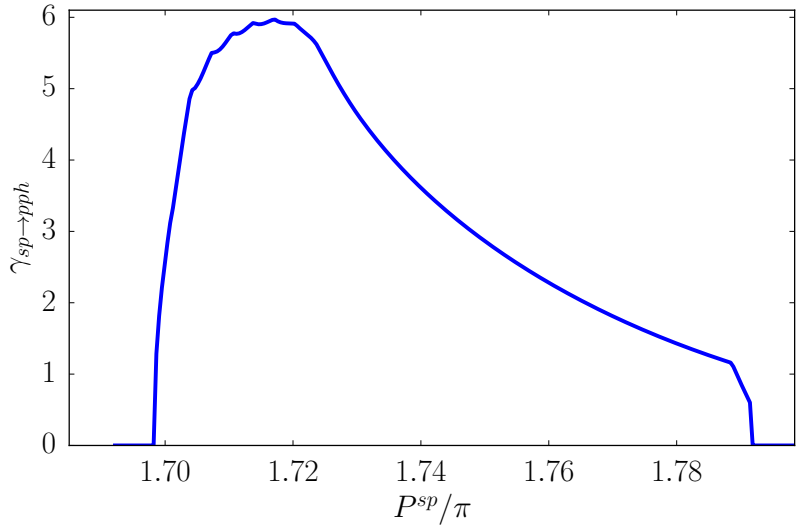

Figure 5.10: Decay rate to the pph-channel for $\eta \to 0$ at magnetization $m = 3/10$. The wiggles are due to the finite size effects of the interpolated matrix element at $L = 615$.

5.4.2 Density of kinematically allowed states and finiteness in the thermodynamic limit

A simpler quantity of interest is the density of final states to which transitions from the 1-spinon excitation are kinematically allowed. For free fermions this density of states exhibits a van Hove singularity that leads to logarithmic divergence at

the threshold [153]. In the thermodynamic limit the pph channel density of kinematically relevant states is given by

$$\rho_{\text{pph}}(p) = \frac{1}{4\pi}\int_D \mathrm{d}z_1^p \, \frac{1}{|\epsilon_s'(\tilde{z}) + \epsilon_s'(z_1^p + z - p)|} \tag{5.60}$$

where z is the same as in (5.59). Analogous expressions hold in the other channels. Results for the various possible types of 3-spinon final states are shown in Fig. 5.11. We see that densities of states are finite and do not display the kind of singularity encountered for free fermions.

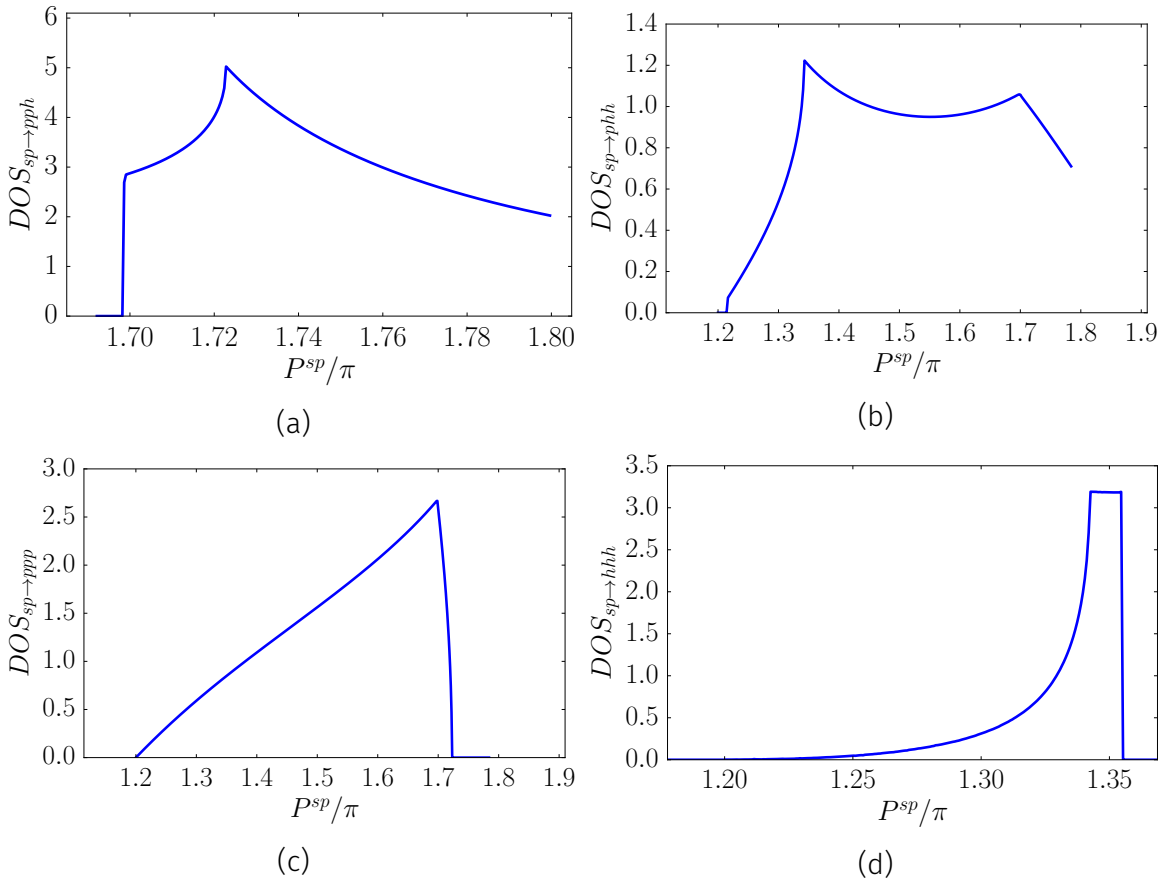

Figure 5.11: Density of states for the (a) pph-channel (b) phh-channel, (c) ppp-channel and (d) hhh-channel in the thermodynamic limit at magnetization $m = 3/10$.

5.A Calculation of dressed energy and momenta for low energy excitations

In this appendix we briefly discuss how to obtain energies and momenta for the elementary excitations in the thermodynamic limit [18, 19, 112].

5.A.1 Length-1 strings

Let us first consider excitations over the Fermi-sea like state, which are themselves length-1 strings. The rapidities of the excitations are then described by the Bethe Ansatz equations

$$L\theta(\lambda_\alpha^{(1)}) = 2\pi I_\alpha^{(1)} + \sum_{\beta=1}^{M} \theta(\lambda_\alpha^{(1)} - \lambda_\beta^{(1)}). \tag{5.61}$$

The Fermi-sea like state in terms of the quantum numbers $I_\alpha^{(1)}$ is described by a region of occupied quantum numbers

We are interested in the situation where there are n particle and m hole excitations on top of the Fermi-sea like state

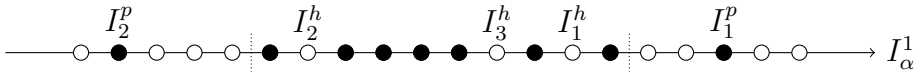

In the thermodynamic limit the solutions of the Bethe Ansatz equations with quantum numbers of this form will be dense in an interval $[-B, B]$, where B is given by the number of down-spins or respectively the magnetic field. The additional particle and hole excitations are parametrized by their rapidities λ_i^p and λ_i^h with $|\lambda_i^p| > B$ and $|\lambda_j^h| < B$ (cf. Fig. 5.12). Let the $\lambda_\alpha^{(1)}$ be the rapidities of the particles in the sea, we then have

$$L\theta(\lambda_\alpha^{(1)}) = 2\pi I_\alpha^{(1)} + \sum_{\beta=1}^{M} \theta\left(\frac{\lambda_\alpha^{(1)} - \lambda_\beta^{(1)}}{2}\right) + \sum_{i=1}^{n} \theta\left(\frac{\lambda_\alpha^{(1)} - \lambda_i^p}{2}\right) \tag{5.62}$$

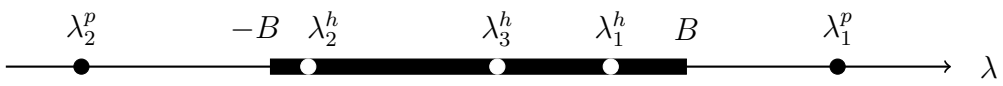

Figure 5.12: As seen in Chapter 4.3.3 and 5.2.3, in the thermodynamic limit the solutions for rapidities of the Bethe equations lie dense on the real line from $-B$ to B, where B depends on the magnetic field. The low energy states correspond to excitations over some fermi-sea like state. One particular class of low energy excitations are given by removing and adding length-1 string excitations.

for these rapidities. We can now go to the thermodynamic limit as outlined in 4.3.3 and we obtain

$$a_1(\lambda) = \int_{-B}^{B} \mathrm{d}\eta\ \rho_{1,p}(\eta) a_2(\lambda-\eta) - \frac{1}{L}\sum_{i=1}^{n} a_2(\lambda-\lambda_i^p) = \rho_{1,p}(\lambda) + \rho_{1,h}(\lambda). \tag{5.63}$$

The hole density is given from the holes within the sea as [18, 112]

$$\rho_{1,h}(\lambda) = \frac{1}{L}\sum_{j=1}^{m} \delta(\lambda-\lambda_j^h). \tag{5.64}$$

We are interested in the $\mathcal{O}(1)$ correction to the $\mathcal{O}(L)$ energy of the sea like state. Let us therefore write the particle density as an $\mathcal{O}(1)$ and $\mathcal{O}(\frac{1}{L})$ part

$$\rho_{1,p} = \rho_{1,p}^{(1)} + \frac{1}{L}\rho_{1,p}^{(2)}. \tag{5.65}$$

The $\mathcal{O}(1)$ part is easily seen to obey

$$\rho_{1,p}^{(1)}(\lambda) = a_1(\lambda) - \int_{-B}^{B} \mathrm{d}\eta\ \rho_{1,p}^{(1)}(\eta) a_2(\lambda-\eta). \tag{5.66}$$

This determines the $\mathcal{O}(L)$ piece of the energy

$$E = L\int_{-B}^{B} d\lambda\ \rho_{1,p}^{(1)}(\lambda)\ \varepsilon_{1,0}(\lambda), \tag{5.67}$$

where $\varepsilon_{1,0}(\lambda)$ is the bare energy of the particles as defined in 4.3.3.

For the $\mathcal{O}(\frac{1}{L})$ corrections of the density of particles we get the integral equation

$$-\sum_{j=1}^{m}\delta(\lambda-\lambda_j^h) - \sum_{i=1}^{n} a_2(\lambda-\lambda_i^p) - \int_{-B}^{B}\mathrm{d}\eta\ \rho_{1,p}^{(2)}(\eta)\ a_2(\lambda-\eta) = \rho_{1,p}^{(2)}(\lambda). \tag{5.68}$$

To obtain the $O(1)$ correction to the energy ΔE we then have to add up the bare energy of the particle excitations. But as we are dealing with an interacting system,

we have to add the change of energy the particles and holes exert on the Fermi sea like state:

$$\Delta E = \sum_{i=1}^{n} \varepsilon_{1,0}(\lambda_i^p) + \int_{-B}^{B} \mathrm{d}\eta \;\; \varepsilon_{1,0}(\eta)\rho_{1,p}^{(2)}(\eta) \tag{5.69}$$

Let us now introduce a linear operator $\hat{K}$ with positive kernel $a_2(\lambda - \mu)$ such that

$$\left(\hat{K} \star \rho_{1,p}^{(2)}\right)(\lambda) = \int_{-B}^{B} \mathrm{d}\eta \; a_2(\lambda - \eta)\rho_{1,p}^{(2)}(\eta). \tag{5.70}$$

We can then write Eq. (5.68) as

$$-\sum_{j=1}^{m} \delta(\lambda - \lambda_j^h) - \sum_{i=1}^{n} a_2(\lambda - \lambda_i^p) - \left(\hat{K} \star \rho_{1,p}^{(2)}\right)(\lambda) = \rho_{1,p}^{(2)}(\lambda). \tag{5.71}$$

Solving (5.71) formally for $\rho_{1,p}^{(2)}$ and inserting into the expression for ΔE, we obtain

$$\Delta E = \sum_{i=1}^{n} \varepsilon_{1,0}(\lambda_i^p) - \int_{-B}^{B} \mathrm{d}\eta \; \varepsilon_{1,0}(\eta) \left((1 + \hat{K})^{-1} \star a_{ph}\right)(\eta) \tag{5.72}$$

where

$$a_{ph}(\mu) = \left(\sum_{i=1}^{n} a_2(\mu - \lambda_i^p) + \sum_{j=1}^{m} \delta(\mu - \lambda_j^h)\right). \tag{5.73}$$

Defining the dressed energy as

$$\varepsilon_1(\lambda) = \left(\varepsilon_{1,0} \star (1 + \hat{K})^{-1}\right)(\lambda) \tag{5.74}$$

and therefore as the solution to the integral equation

$$\varepsilon_1(\lambda) = \varepsilon_{1,0}(\lambda) - \int_{-B}^{B} \mathrm{d}\mu \;\; \varepsilon_1(\mu)a_2(\mu - \lambda), \tag{5.75}$$

ΔE can be written as

$$\Delta E = \sum_{i=1}^{n} \varepsilon_1(\lambda_i^p) - \sum_{j=1}^{m} \varepsilon_1(\lambda_j^h). \tag{5.76}$$

We see that in the thermodynamic limit the energies of the excitations over a fermi sea like state are additive. The momenta are simply given as the sum over the quantum numbers. Every one of those quantum numbers and specifically the quantum number of the particle and hole excitations are given in the thermodynamic limit up to $\mathcal{O}(\frac{1}{L})$ corrections by

$$p(\lambda) = \pi + 2\pi \mathrm{sgn}(|\lambda| - B) \int_{0}^{\lambda} \mathrm{d}\mu \;\; \rho_1(\mu). \tag{5.77}$$

5.A.2 Higher length string excitations

Let us now look at higher string excitations over the fermi-sea like state made up out of length-1 strings. As we are considering the large system size limit, we can assume zero string deviations $\delta^j_{\alpha a}$. Let us specifically look at a length-2 string excitation over a sea of M length-1 strings. Under the string hypothesis the string centers of the excitations are then described by the Bethe Ansatz equations

$$L\theta\left(\frac{\lambda^s}{2}\right) = 2\pi I^s + \sum_{\beta=1}^{M}\left[\theta\left(\frac{\lambda^s-\lambda^{(1)}_\beta}{3}\right)+\theta\left(\lambda^s-\lambda^{(1)}_\beta\right)\right] \tag{5.78}$$

$$L\theta(\lambda^{(1)}_\alpha) = 2\pi I^{(1)}_\alpha + \sum_{\beta=1}^{M}\theta\left(\frac{\lambda^{(1)}_\alpha-\lambda^{(1)}_\beta}{2}\right) - \theta(\lambda^{(1)}_\alpha-\lambda^s) - \theta\left(\frac{\lambda^{(1)}_\alpha-\lambda^s}{3}\right) \tag{5.79}$$

Going to the thermodynamic limit and splitting the density into $\mathcal{O}(1)$ and $\mathcal{O}(\frac{1}{L})$ piece as before, the density of length-1 strings in the sea can be written as

$$\rho^{(2)}_{1,p}(\lambda) = -\int_{-B}^{B}\mathrm{d}\eta\ \ \rho^{(2)}_{1,p}\, a_2(\lambda-\eta) - a_1(\lambda-\lambda^s) - a_3(\lambda-\lambda^s). \tag{5.80}$$

The $\mathcal{O}(1)$ piece of the energy ΔE can then again be written as bare energy of the length-2 string plus the reaction on the length-1 string sea

$$\Delta E = \varepsilon_{2,0}(\lambda^s) + \int_{-B}^{B}\mathrm{d}\eta\ \ \rho^{(2)}_{1,p}(\eta)\varepsilon_{1,0}(\eta). \tag{5.81}$$

Again formally inverting the equation for the density $\rho^{(2)}_{1,p}$ and substituting into the equation for ΔE one gets

$$\Delta E = \varepsilon_2(\lambda^s) \tag{5.82}$$

with

$$\varepsilon_2(\lambda^s) = \varepsilon_{2,0}(\lambda^s) - \int_{-B}^{B}\mathrm{d}\mu\ \varepsilon_1(\mu)\left(a_1(\mu-\lambda^{(s)}) + a_3(\mu-\lambda^s)\right). \tag{5.83}$$

The momentum in the thermodynamic limit up to $\mathcal{O}(\frac{1}{L})$ corrections can be obtained from the first equation of (5.79) by going to the thermodynamic limit:

$$p_s(\lambda) = \theta\left(\frac{\lambda}{2}\right) - \int_{-B}^{B}\mathrm{d}\mu\ \theta_{21}(\lambda-\mu)\rho_{1,p}(\mu) \tag{5.84}$$

Again also higher string excitations in the thermodynamic limit are additive.

5.B Matrix elements and suppression for non-highest weight states

We want to consider the normalised matrix element of δH between a highest weight state and a non-highest weight state

$$\frac{\langle\{\lambda\}|\,(S^+)^k \sum_j S^z_j S^z_{j+2}\,|\{\mu\}\rangle}{\sqrt{\langle\{\lambda\}|\,(S^+S^-)^k\,|\{\lambda\}\rangle}\sqrt{\langle\{\mu\}\mid\{\mu\}\rangle}} \tag{5.85}$$

where $\langle\{\lambda\}|$ and $|\{\mu\}\rangle$ are non-normalised highest weight Bethe ansatz states. We see immediately from the commutation relation

$$[S^+, S^z_j] = -S^+_j \tag{5.86}$$

and from the relation for highest weight states $S^+\,|\{\mu\}\rangle = 0$ that for $k \geq 3$ the matrix element is exactly 0. Furthermore inserting the cyclic shift operator (*cf.* [126]) $\exp(i\hat{P})$ and using

$$e^{-i\hat{P}} S^a_j e^{i\hat{P}} = S^a_{j+1} \quad a = z, +, - \tag{5.87}$$

and the fact that the highest weight states are eigenstates of the shift operator with eigenvalue $\exp\left(iP_{\{\lambda\}}\right)$, where $P_{\{\lambda\}}$ is the momentum of the highest weight state, we obtain

$$\begin{aligned}\langle\{\lambda\}|\,e^{-i\hat{P}} e^{i\hat{P}} (S^+)^k \sum_j S^z_j S^z_{j+2}\,|\{\mu\}\rangle& \\ = e^{i(P_{\{\lambda\}} - P_{\{\mu\}})}\,\langle\{\lambda\}|\,(S^+)^k \sum_j S^z_j S^z_{j+2}\,|\{\mu\}\rangle&\end{aligned} \tag{5.88}$$

and therefore we see that the momenta have to coincide for the matrix element to be non-zero. Using the commutation relation (5.86) we obtain for the normalised

matrix element for $k = 1$ and $k = 2$:

$$\frac{\langle\{\lambda\}|\, S^+ \sum_j S^z_j S^z_{j+2}\, |\{\mu\}\rangle}{\sqrt{\langle\{\mu\}\mid\{\mu\}\rangle\, \langle\{\lambda\}|\, S^+S^+S^-S^-\, |\{\lambda\}\rangle}} = \frac{1}{\sqrt{L-2(N-1)}} \frac{-\langle\{\lambda\}|\sum_j S^+_j S^z_{j+2} + S^z_j S^+_{j+2}\,|\{\mu\}\rangle}{\sqrt{\langle\{\mu\}\mid\{\mu\}\rangle\, \langle\{\lambda\}\mid\{\lambda\}\rangle}}, \tag{5.89}$$

$$\frac{\langle\{\lambda\}|\, (S^+)^2 \sum_j S^z_j S^z_{j+2}\, |\{\mu\}\rangle}{\sqrt{\langle\{\mu\}\mid\{\mu\}\rangle\, \langle\{\lambda\}|\, S^+S^+S^-S^-\, |\{\lambda\}\rangle}} = \frac{1}{\sqrt{L-2(N-1)}\sqrt{L-2(N-2)}} \frac{2\,\langle\{\lambda\}|\sum_j S^+_j S^+_{j+2}\,|\{\mu\}\rangle}{\sqrt{\langle\{\mu\}\mid\{\mu\}\rangle\, \langle\{\lambda\}\mid\{\lambda\}\rangle}} \tag{5.90}$$

We can now check numerically for solutions of the Bethe equation with same momenta using similar determinant expression as in (*cf.* 5.C) for these matrix elements, that due to the normalization factor the matrix element is suppressed for large L at finite magnetic field.

5.C Calculation of the next-nearest neighbour spin operator matrix element

We want to calculate the matrix element

$$\langle\{\lambda\}|\, \sigma^z_j \sigma^z_{j+2}\, |\{\mu\}\rangle \tag{5.91}$$

with $|\{\lambda\}\rangle, |\{\mu\}\rangle$ Bethe states and $\{\mu\}, \{\lambda\}$ satisfying the Bethe equations (4.13). We do the calculation for all Δ. To obtain the formula for $\Delta = 1$ the general functions a and d have to be replaced by the ones mentioned above and γ has to be set to 1 corresponding to the rescaling of $\{\lambda\}$ with γ and then taking the limit $\gamma \to 0$.

The σ operators are given in terms of the elements of the monodromy matrix A, B, C, D, as obtained in [128]:

$$\sigma^z_j = -2 \prod_{i=1}^{j-1} (A+D)(\xi_i) D(\xi_j) \prod_{k=j+1}^{L} (A+D)(\xi_k) + 1, \tag{5.92}$$

where ξ_i is an inhomogeneity parameter, introduced at every site in the chain for technical reasons. We will set $\xi_i \to i\gamma/2$ in the end, but will keep them at

intermediary steps of the calculation. We note that now $d(\lambda)$ is defined as:

$$d(\lambda) = \prod_{l=1}^{L} b(\lambda - \xi_l) \tag{5.93}$$

where $b(\lambda)$ was defined in Eq. (4.37). We then can write the matrix element as:

$$\begin{aligned}\langle\{\lambda\}|\,\sigma_j^z\sigma_{j+2}^z\,|\{\mu\}\rangle &= \langle\{\lambda\}|\,\sigma_j^z\,|\{\mu\}\rangle + \langle\{\lambda\}|\,\sigma_{j+2}^z\,|\{\mu\}\rangle - \langle\{\lambda\}|\{\mu\}\rangle \\ &+ 4\,\langle\{\lambda\}|\prod_{i=1}^{j-1}(A+D)(\xi_i)D(\xi_j)(A+D)(\xi_{j+1})D(\xi_{j+2})\prod_{k=j+3}^{L}(A+D)(\xi_k)\,|\{\mu\}\rangle\,.\end{aligned} \tag{5.94}$$

The matrix elements and the overlap in the first line are known [128, 129]. However as we are interested in $\sum_j \sigma_j^z\sigma_{j+2}^z$ and as $|\{\lambda\}\rangle$ and $|\{\mu\}\rangle$ are orthogonal and eigenstates of σ^z, we only need to calculate the expression in the second line. From the Yang-Baxter algebra one can derive the commutation relations between the operators A, B, C, D and from this one gets ([19]):

$$\begin{aligned}A(\mu)\prod_{j=1}^{N}B(\lambda_j)\,|0\rangle &= a(\mu)\prod_{j=1}^{N}b^{-1}(\lambda_j-\mu)\prod_{j=1}^{N}B(\lambda_j)\,|0\rangle \\ &- \sum_{n=1}^{N}a(\lambda_n)\frac{c(\lambda_n-\mu)}{b(\lambda_n-\mu)}\prod_{j\neq n}^{N}b^{-1}(\lambda_j-\lambda_n)B(\mu)\prod_{j\neq n}^{N}B(\lambda_j)\,|0\rangle\,,\end{aligned} \tag{5.95}$$

$$\begin{aligned}D(\mu)\prod_{j=1}^{N}B(\lambda_j)\,|0\rangle &= d(\mu)\prod_{j=1}^{N}b^{-1}(\mu-\lambda_j)\prod_{j=1}^{N}B(\lambda_j)\,|0\rangle \\ &- \sum_{n=1}^{N}d(\lambda_n)\frac{c(\mu-\lambda_n)}{b(\mu-\lambda_n)}\prod_{j\neq n}^{N}b^{-1}(\lambda_n-\lambda_j)B(\mu)\prod_{j\neq n}^{N}B(\lambda_j)\,|0\rangle\,.\end{aligned} \tag{5.96}$$

We furthermore know that

$$\prod_{i=1}^{j}(A+D)(\xi_i)\,|\{\lambda\}\rangle = \exp\left(-ijP_{\{\lambda\}}\right)|\{\lambda\}\rangle\,, \tag{5.97}$$

where $|\{\lambda\}\rangle$ is a Bethe state and $P_{\{\lambda\}}$ is the total momentum of $|\{\lambda\}\rangle$ and

$$\prod_{i=1}^{L}(A+D)(\xi_i)\,|\{\lambda\}\rangle = 1. \tag{5.98}$$

We now need to calculate the matrix element:

$$\mathcal{D} = \langle\{\lambda\}|\,D(\xi_j)(A+D)(\xi_{j+1})D(\xi_{j+2})\,|\{\mu\}\rangle\,. \tag{5.99}$$

Using the commutation relations for A, B, C, D (cf. [19]) we obtain:

$$\mathcal{D} = \mathrm{I} + \mathrm{II} \tag{5.100}$$

where I is dependent on simple matrix elements where two rapidities are replaced with inhomogeneities and II is dependent on a matrix element with three insertions of inhomogeneities:

$$\begin{aligned}
\mathrm{I} = &\sum_{a=1}^{N} \frac{d(\mu_a)c(\xi_{j+2}-\mu_a)}{b(\xi_{j+2}-\mu_a)} \prod_{i\neq a}^{N} \frac{1}{b(\mu_a-\mu_i)} \Bigg\{ \frac{1}{b(\xi_{j+2}-\xi_{j+1})} \prod_{i\neq a}^{N} \frac{1}{b(\mu_i-\xi_{j+1})} \\
&\times \sum_{b\neq a}^{N} \frac{d(\mu_b)c(\xi_j-\mu_b)}{b(\xi_j-\mu_b)b(\mu_b-\xi_{j+2})} \prod_{i\neq a,b}^{N} \frac{1}{b(\mu_b-\mu_i)} \langle\{\lambda\}| B(\xi_j)B(\xi_{j+2}) \prod_{j\neq a,b}^{N} B(\mu_j) |0\rangle \\
&+ \frac{c(\xi_{j+1}-\xi_{j+2})}{b(\xi_{j+1}-\xi_{j+2})} \prod_{i\neq a}^{N} \frac{1}{b(\mu_i-\xi_{j+2})} \sum_{b\neq a}^{N} \frac{d(\mu_b)c(\xi_j-\mu_b)}{b(\xi_j-\mu_b)} \frac{1}{b(\mu_b-\xi_{j+1})} \\
&\times \prod_{i\neq a,b}^{N} \frac{1}{b(\mu_b-\mu_i)} \langle\{\lambda\}| B(\xi_j)B(\xi_{j+1}) \prod_{j\neq a,b}^{N} B(\mu_j) |0\rangle \Bigg\}, \\
\mathrm{II} = &\sum_{a=1}^{N} \frac{d(\mu_a)c(\xi_{j+2}-\mu_a)}{b(\xi_{j+2}-\mu_a)} \prod_{i\neq a}^{N} \frac{1}{b(\mu_a-\mu_i)} \\
&\Bigg\{ \sum_{b\neq a}^{N} \Bigg[\frac{c(\mu_b-\xi_{j+1})}{b(\mu_b-\xi_{j+1})} \prod_{i\neq a,b}^{N} \frac{1}{b(\mu_i-\mu_b)} \frac{1}{b(\xi_{j+2}-\mu_b)} \\
&\qquad + d(\mu_b) \frac{c(\xi_{j+1}-\mu_b)}{b(\xi_{j+1}-\mu_b)b(\mu_b-\xi_{j+2})} \prod_{i\neq a,b}^{N} \frac{1}{b(\mu_b-\mu_i)} \Bigg] \\
&\sum_{c\neq a,b}^{N} \frac{d(\mu_c)c(\xi_j-\mu_c)}{b(\xi_j-\mu_c)b(\mu_c-\xi_{j+1})b(\mu_c-\xi_{j+2})} \prod_{i\neq a,b,c}^{N} \frac{1}{b(\mu_c-\mu_i)} \\
&\langle\{\lambda\}| B(\xi_j)B(\xi_{j+1})B(\xi_{j+2}) \prod_{i\neq a,b,c}^{N} B(\mu_i) |0\rangle \Bigg\}.
\end{aligned} \tag{5.101}$$

Now we can use Slavnov's formula [129] for the overlap of two states. One of the states has to be a Bethe state, the other state can be parametrized by an arbitrary set of rapidities. Let $\{\lambda\}$ be solutions of the Bethe equations (4.13) and $\{\mu\}$ arbitrary, then one gets:

$$\langle\{\lambda\}|\{\mu\}\rangle = \frac{\det\left(H(\{\lambda\},\{\mu\})\right)}{\prod_{j>k}\phi(\lambda_k-\lambda_j)\prod_{j<k}\phi(\mu_k-\mu_j)}, \tag{5.102}$$

where H is a matrix defined as

$$H_{ab} = \frac{\phi(i\gamma)}{\phi(\lambda_a - \mu_b)} \left(a(\mu_b) \prod_{k \neq a} \phi(\lambda_k - \mu_b + i\gamma) - d(\mu_b) \prod_{k \neq a} \phi(\lambda_k - \mu_b - i\gamma) \right), \quad (5.103)$$

with $\phi(x) = x$ and γ set to 1 in the $\Delta = 1$ scaling limit.

We will now treat I and II separately.

Part II

For this part, the limit of the ξ_j, ξ_{j+1} and ξ_{j+2} can be taken separately for the matrix element and the prefactor. Taking the limit $\xi_i \to i\gamma/2$ for the prefactor amounts to replacing the ξ_i with $i\gamma/2$. For the matrix element we obtain using Slavnov's determinant formula:

$$\langle \{\lambda\}| B(\xi_j)B(\xi_{j+1})B(\xi_{j+2}) \prod_{i \neq k,m,n} B(\mu_i) |0\rangle = \frac{\det\left(H(\{\lambda\}, \{\mu_{i\neq k,m,n}, \xi_j, \xi_{j+1}, \xi_{j+2}\})\right)}{\left(\prod_{a>b} \phi(\lambda_a - \lambda_b) \prod_{a<b} \phi(\mu_b - \mu_a)\right)\big|_{\mu_k \to \xi_j, \mu_m \to \xi_{j+1}, \mu_n \to \xi_{j+2}}}, \quad (5.104)$$

where

$$\prod_{a<b} \phi(\mu_b - \mu_a)\big|_{\mu_k \to \xi_j, \mu_m \to \xi_{j+1}, \mu_n \to \xi_{j+2}} = \frac{\phi(\xi_j - \xi_{j+1})\phi(\xi_j - \xi_{j+2})\phi(\xi_{j+1} - \xi_{j+2})}{\phi(\mu_k - \mu_m)\phi(\mu_k - \mu_n)\phi(\mu_m - \mu_n)} \times \prod_{c \neq k,m,n} \frac{\phi(\xi_j - \mu_c)\phi(\xi_{j+1} - \mu_c)\phi(\xi_{j+2} - \mu_c)}{\phi(\mu_k - \mu_c)\phi(\mu_m - \mu_c)\phi(\mu_n - \mu_c)} \prod_{a<b} \phi(\mu_b - \mu_a), \quad (5.105)$$

and in the determinant we have to replace $\mu_k \to \xi_j, \mu_m \to \xi_{j+1}$ and $\mu_n \to \xi_{j+2}$. Therefore the important part when taking the limits is:

$$\lim_{\xi_j, \xi_{j+2} \to i\gamma/2} \frac{\det\left(H(\{\lambda\}, \{\mu_{i\neq k,m,n}, \xi_j, i\gamma/2, \xi_{j+2}\})\right)}{\phi(\xi_j - i\gamma/2)\phi(\xi_j - \xi_{j+2})\phi(i\gamma/2 - \xi_{j+2})} \quad (5.106)$$

where the limit $\xi_{j+1} \to i\gamma/2$ is already taken. Let us now take the limit $\xi_{j+2} \to i\gamma/2$. We see that both numerator and denominator go to zero here. Therefore using the rule of l'Hospital we obtain:

$$\lim_{\xi_j, \xi_{j+2} \to i\gamma/2} \frac{\det\left(H(\{\lambda\}, \{\mu_{i\neq k,m,n}, \xi_j, i\gamma/2, \xi_{j+2}\})\right)}{\phi(\xi_j - i\gamma/2)\phi(\xi_j - \xi_{j+2})\phi(i\gamma/2 - \xi_{j+2})} = \lim_{\xi_j \to i\gamma/2} \frac{1}{\phi(\xi_j - i\gamma/2)\phi(\xi_j - i\gamma/2)} \lim_{x \to i\gamma/2} \frac{\mathrm{d}}{\mathrm{d}x} \det\left(H(\{\lambda\}, \{\mu_{i\neq k,m,n}, \xi_j, i\gamma/2, x\})\right) \quad (5.107)$$

Analogous to [154] we can now use a Laplace expansion of the determinant for the column that is dependent on x and evaluate the derivative and limit:

$$\begin{aligned}
&\lim_{x\to i\gamma/2}\frac{\mathrm{d}}{\mathrm{d}x}\det\left(H(\{\lambda\},\{\mu_{i\neq k,m,n},\xi_j,i\gamma/2,x\})\right)= \\
&\quad=\lim_{x\to i\gamma/2}\frac{\mathrm{d}}{\mathrm{d}x}\sum_i(-1)^{(n+i)}C_i(x)\ \mathrm{minor}_{ni}(H(\{\lambda\},\{\mu_{i\neq k,m,n},\xi_j,i\gamma/2,x\})) \\
&\quad=\lim_{x\to i\gamma/2}\sum_i(-1)^{(n+i)}\left(\frac{\mathrm{d}}{\mathrm{d}x}C_i(x)\right)\ \mathrm{minor}_{ni}(H(\{\lambda\},\{\mu_{i\neq k,m,n},\xi_j,i\gamma/2,x\}))
\end{aligned} \tag{5.108}$$

where the minor is not dependent on x and $C_i(x)$ is the ith element of the column n of the matrix $H(\{\lambda\},\{\mu_{i\neq k,m,n},\xi_j,i\gamma/2,x\})$. Therefore we get:

$$\lim_{x\to i\gamma/2}\frac{\mathrm{d}}{\mathrm{d}x}\det\left(H(\{\lambda\},\{\mu_{i\neq k,m,n},\xi_j,i\gamma/2,x\})\right)=\det\left(H_1(\{\lambda\},\{\mu\};m,n)\big|_{\mu_k\to\xi_j}\right) \tag{5.109}$$

with

$$(H_1)_{ab}(\{\lambda\},\{\mu\};m,n)=\begin{cases}H_{ab} & b\neq m,n\\ \frac{\phi(i\gamma)}{\phi(\lambda_a-\frac{i\gamma}{2})\phi(\lambda_a+\frac{i\gamma}{2})} & b=m\\ \frac{\phi(i\gamma)\phi(2\lambda_a)}{\phi(\lambda_a-\frac{i\gamma}{2})^2\phi(\lambda_a+\frac{i\gamma}{2})^2} & b=n\end{cases} \tag{5.110}$$

Repeating this step for the limit $\xi_j\to i\gamma/2$ using the rule of l'Hospital twice we finally obtain:

$$\begin{aligned}
M^{(2)}_{ijk}&\equiv\lim_{\xi_j,\xi_{j+1},\xi_{j+2}\to i\gamma/2}\langle\{\lambda\}|\,B(\xi_j)B(\xi_{j+1})B(\xi_{j+2})\prod_{i\neq k,m,n}B(\mu_i)\,|0\rangle \\
&=\frac{1}{2}\prod_i\phi\left(\lambda_i+\frac{i\gamma}{2}\right)^3\phi(\mu_m-\mu_n)\phi(\mu_k-\mu_m)\phi(\mu_k-\mu_n) \\
&\quad\times\prod_{c\neq k,m,n}\frac{\phi(\mu_c-\mu_k)\phi(\mu_c-\mu_m)\phi(\mu_c-\mu_n)}{\phi(\mu_c-\frac{i\gamma}{2})^3} \\
&\quad\times\frac{\det(H_2)}{\prod_{a>b}\phi(\lambda_b-\lambda_a)\prod_{a<b}\phi(\mu_b-\mu_a)}
\end{aligned} \tag{5.111}$$

where

$$(H_2)_{ab}(\{\lambda\},\{\mu\};k,m,n)=\begin{cases}H_{ab} & b\neq m,n,k\\ \frac{\phi(i\gamma)}{\phi(\lambda_a-\frac{i\gamma}{2})\phi(\lambda_a+\frac{i\gamma}{2})} & b=m\\ \frac{\phi(i\gamma)\phi(2\lambda_a)}{\phi(\lambda_a-\frac{i\gamma}{2})^2\phi(\lambda_a+\frac{i\gamma}{2})^2} & b=n\\ \frac{\partial^2}{\partial x^2}\left(\frac{\phi(i\gamma)}{\phi(\lambda_a-x)\phi(\lambda_a-x+i\gamma)}\right)\big|_{x=\frac{i\gamma}{2}} & b=k\end{cases} \tag{5.112}$$

With this we obtain after some algebra:

$$\begin{aligned}\mathrm{II} = -\frac{1}{2}\frac{\prod_k \phi(\lambda_k + i\gamma/2)^3 \phi(\mu_k - i\gamma/2)^{-3}}{\prod_{a>b}\phi(\lambda_b-\lambda_a)\prod_{a<b}\phi(\mu_b-\mu_a)} \sum_{n=1}^{N} d(\mu_n)\phi(\mu_n - i\gamma/2)\prod_i \phi(\mu_i-\mu_n-i\gamma) \\ \sum_{m\neq n}\prod_i \phi(\mu_i-\mu_m+i\gamma)\phi(\mu_m-i\gamma/2)\left[\frac{\phi(\mu_m-3i\gamma/2)}{\phi(\mu_m-\mu_n-i\gamma)} - \frac{\phi(\mu_m+i\gamma/2)}{\phi(\mu_m-\mu_m+i\gamma)}\right] \\ \sum_{k\neq m,n} d(\mu_k)\prod_i \phi(\mu_i-\mu_k-i\gamma)\frac{\phi(\mu_k+i\gamma/2)^2}{\phi(\mu_m-\mu_k-i\gamma)\phi(\mu_n-\mu_k-i\gamma)} \\ \times \det\left(H_2(\{\lambda\},\{\mu\};k,m,n)\right) \end{aligned} \tag{5.113}$$

Using a Lemma from Laplace's determinant formula ([143]) we finally obtain:

$$\begin{aligned}\mathrm{II} = -\frac{1}{2}\frac{\prod_k \phi(\lambda_k + i\gamma/2)^3 \phi(\mu_k - i\gamma/2)^{-3}}{\prod_{a>b}\phi(\lambda_b-\lambda_a)\prod_{a<b}\phi(\mu_b-\mu_a)} \\ \times \sum_{n=1}^{N}\sum_{m\neq n} A_{nm}\left[\det\left(G_{nm}+B_{nm}\right) - \det\left(G_{nm}\right)\right] \end{aligned} \tag{5.114}$$

with

$$A_{nm} = d(\mu_n)\phi(\mu_n - \frac{i\gamma}{2})^2\phi(\mu_m-\frac{i\gamma}{2})\prod_i \phi(\mu_i-\mu_n-i\gamma) \tag{5.115}$$

$$\times \prod_j \phi(\mu_j-\mu_m+i\gamma)\left[\frac{\phi(\mu_m-\frac{3i\gamma}{2})}{\phi(\mu_m-\mu_n-i\gamma)} - \frac{\phi(\mu_m+\frac{i\gamma}{2})}{\phi(\mu_m-\mu_n+i\gamma/2)}\right] \tag{5.116}$$

$$(G_{nm})_{ab} = \begin{cases} H_{ab} & b\neq m,n \\ \frac{\phi(i\gamma)\phi(2\lambda_a)}{\phi(\lambda_a-\frac{i\gamma}{2})^2\phi(\lambda_a+\frac{i\gamma}{2})^2} & b=m \\ \frac{\partial^2}{\partial x^2}\left(\frac{\phi(i\gamma)}{\phi(\lambda_a-x)\phi(\lambda_a-x+i\gamma)}\right)\Big|_{x=\frac{i\gamma}{2}} & b=n \end{cases} \tag{5.117}$$

$$\begin{aligned}(B_{nm})_{ab} = (1-\delta_{bm})(1-\delta_{bn})d(\mu_b) \\ \prod_{i\neq m,n}\phi(\mu_i-\mu_b-i\gamma)\phi(\mu_b+i\gamma/2)^2\frac{\phi(i\gamma)}{\phi(\lambda_a-i\gamma/2)\phi(\lambda_a+i\gamma/2)}\end{aligned} \tag{5.118}$$

Part I

First we can take the limit $\xi_j, \xi_{j+2} \to i\gamma/2$. This again just amounts to replacing the ξ_j and ξ_{j+2} with $i\gamma/2$ in the prefactors and doing a similar analysis for the matrix element depending on both ξ_j and ξ_{j+2} as for the part II. However performing the limit $\xi_{j+1} \to i\gamma/2$ is a bit more involved, as the limit can not be taken independently

for prefactor and matrix elements. This is due to terms $\propto \frac{1}{\xi_{j+1}-i\gamma/2}$ appearing in the prefactors. Doing a consistent series expansion in $\xi_{j+1} - i\gamma/2$ again utilizing the Laplace determinant expansion and then taking the limit $\xi_{j+1} \to i\gamma/2$ we obtain after some calculation:

$$\begin{aligned}
\mathrm{I} = &-\phi(i\gamma)\frac{\prod_k \phi(\lambda_k + i\gamma/2)^2\phi(\mu_k + i\gamma/2)\phi(\mu_k - i\gamma/2)^{-3}}{\prod_{a>b}\phi(\lambda_b - \lambda_a)\prod_{b>a}\phi(\mu_b - \mu_a)} \\
&\Bigg\{\sum_{n=1}^{N} d(\mu_n)\prod_i \phi(\mu_i - \mu_n - i\gamma)\frac{\phi(\mu_n - i\gamma/2)^2}{\phi(\mu_n + i\gamma/2)} \\
&\times\Bigg[\sum_{m\neq n} d(\mu_m)\prod_{i\neq n}\phi(\mu_i - \mu_m - i\gamma)\phi(\mu_m + i\gamma/2) \\
&\Bigg(\frac{\phi'(i\gamma)}{\phi(i\gamma)} - \sum_{d\neq n}\frac{\phi(i\gamma)}{\phi(\mu_d - i\gamma/2)\phi(\mu_d + i\gamma/2)} + \sum_{d\neq m,n}\frac{\phi'(\mu_d - i\gamma/2)}{\phi(\mu_d - i\gamma/2)} \\
&- \sum_b \frac{\phi'(\lambda_b + i\gamma/2)}{\phi(\lambda_b + i\gamma/2)} + \frac{\phi(i\gamma)}{\phi(\mu_m + i\gamma/2)\phi(\mu_m - i\gamma/2)}\Bigg)\det\left(H_3(\{\lambda\},\{\mu\};m,n)\right) + \\
&\sum_{m\neq n} d(\mu_m)\phi(\mu_m + i\gamma/2)\prod_{i\neq n}\phi(\mu_i - \mu_m - i\gamma)\frac{1}{2}\det\left(H_4(\{\lambda\},\{\mu\};m,n)\right)\Bigg]\Bigg\} \qquad (5.119)
\end{aligned}$$

with

$$(H_3)_{ab} = \begin{cases} H_{ab} & b \neq m,n \\ \frac{\phi(i\gamma)}{\phi(\lambda_a + i\gamma/2)\phi(\lambda_a - i\gamma/2)} & b = m \\ \frac{\phi(i\gamma)\phi(2\lambda_a)}{\phi(\lambda_a - \frac{i\gamma}{2})^2\phi(\lambda_a + \frac{i\gamma}{2})^2} & b = n \end{cases} \qquad (5.120)$$

$$(H_4)_{ab} = \begin{cases} H_{ab} & b \neq m,n \\ \frac{\phi(i\gamma)}{\phi(\lambda_a + i\gamma/2)\phi(\lambda_a - i\gamma/2)} & b = m \\ \frac{\partial^2}{\partial x^2}\left(\frac{\phi(i\gamma)}{\phi(\lambda_a - x)\phi(\lambda_a - x + i\gamma)}\right)\Big|_{x=\frac{i\gamma}{2}} & b = n \end{cases} \qquad (5.121)$$

using the Lemma from Laplace's determinant formula again, we finally obtain:

$$\begin{aligned}
\mathrm{I} = &-\phi(i\gamma)\frac{\prod_k \phi(\lambda_k + i\gamma/2)^2\phi(\mu_k + i\gamma/2)\phi(\mu_k - i\gamma/2)^{-3}}{\prod_{a>b}\phi(\lambda_b - \lambda_a)\prod_{b>a}\phi(\mu_b - \mu_a)} \\
&\times\sum_n A_n\Big(\det\left(G_n^{(1)} + B_n^{(1)}\right) + \det\left(G_n^{(2)} + B_n^{(2)}\right) \\
&\qquad - \det\left(G^{(1)}\right) - \det\left(G^{(2)}\right)\Big) \qquad (5.122)
\end{aligned}$$

where

$$A_n = \sum_n d(\mu_n) \frac{\phi(\mu_n - \frac{i\gamma}{2})}{\phi(\mu_n + \frac{i\gamma}{2})} \prod_i \phi(\mu_i - \mu_n - i\gamma) \tag{5.123}$$

$$(G_n^{(1)})_{ab} = \begin{cases} H_{ab} & b \neq n \\ \frac{\phi(i\gamma)\phi(2\lambda_a)}{\phi(\lambda_a - \frac{i\gamma}{2})^2 \phi(\lambda_a + \frac{i\gamma}{2})^2} & b = n \end{cases} \tag{5.124}$$

$$(G_n^{(2)})_{ab} = \begin{cases} H_{ab} & b \neq n \\ \frac{\partial^2}{\partial x^2} \left(\frac{\phi(i\gamma)}{\phi(\lambda_a - x)\phi(\lambda_a - x + i\gamma)} \right) \Big|_{x=\frac{i\gamma}{2}} & b = n \end{cases} \tag{5.125}$$

$$\begin{aligned} (B_n^{(1)})_{ab} = (1 - \delta_{bn}) d(\mu_b) \prod_{i \neq n} \phi(\mu_i - \mu_b + i\gamma)\phi(\mu_b + i\gamma/2) \\ \left(\frac{\phi'(i\gamma)}{\phi(i\gamma)} - \sum_{d \neq n} \frac{\phi(i\gamma)}{\phi(\mu_d - i\gamma/2)\phi(\mu_d + i\gamma/2)} + \sum_{d \neq m,n} \frac{\phi'(\mu_d - i\gamma/2)}{\phi(\mu_d - i\gamma/2)} \right. \\ \left. - \sum_b \frac{\phi'(\lambda_b + i\gamma/2)}{\phi(\lambda_b + i\gamma/2)} + \frac{\phi(i\gamma)}{\phi(\mu_m + i\gamma/2)\phi(\mu_m - i\gamma/2)} \right) \end{aligned} \tag{5.126}$$

$$\begin{aligned} (B_n^{(2)})_{ab} = (1 - \delta_{bn}) \frac{1}{2} d_{\mu_b} \\ \times \prod_{i \neq n} \phi(\mu_i - \mu_b - i\gamma)\phi(\mu_b + i\gamma) \frac{\phi(i\gamma)}{\phi(\lambda_a + i\gamma/2)\phi(\lambda_a - i\gamma/2)} \end{aligned} \tag{5.127}$$

Full matrix element

We can now put together the full matrix element. We obtain

$$\sum_j \langle \{\lambda\} | \, S_j^z S_{j+2}^z \, | \{\mu\} \rangle = e^{iP_{\{\lambda\}} + 2iP_{\{\mu\}}} \sum_j e^{-ij(P_{\{\lambda\}} - P_{\{\mu\}})} \mathcal{D} \tag{5.128}$$

$$= L e^{iP_{\{\lambda\}} + 2iP_{\{\mu\}}} \delta_{P_{\{\lambda\}}, P_{\{\mu\}}} \mathcal{D} \tag{5.129}$$

where $\mathcal{D} = \mathrm{I} + \mathrm{II}$.

III

Conclusions and Outlook

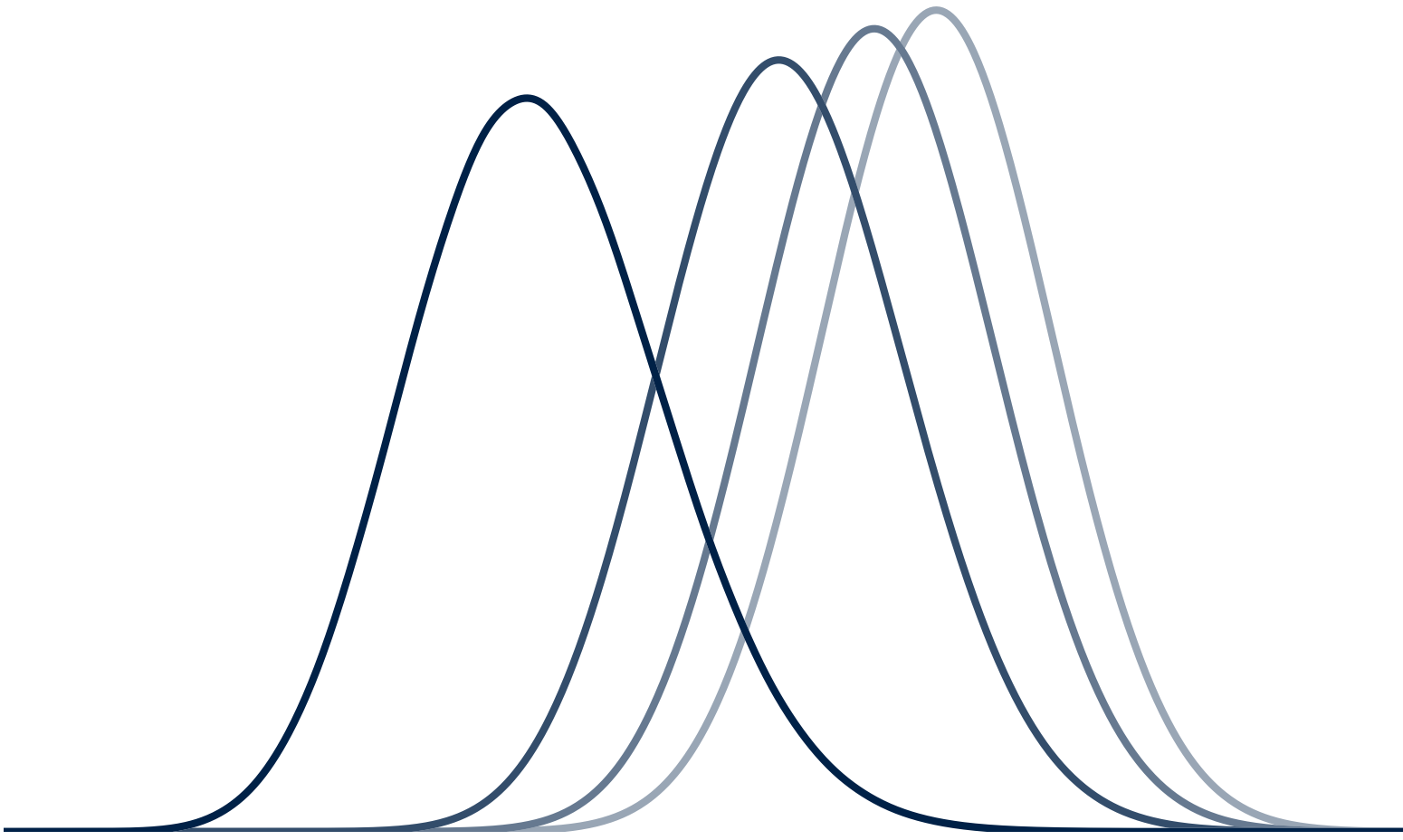

6
Concluding remarks

In this thesis we have investigated two interesting problems in one dimensional many-body quantum systems.

In the first part we have analysed the full counting statistics of the transverse (staggered) magnetization of a subsystem in the thermodynamic limit of the transverse field Ising chain. We derived a convenient determinant representation for the corresponding generating functions $\chi^{(u,s)}(\lambda,\ell,t)$. We first considered the FCS in equilibrium states and showed that the probability distributions are always non-Gaussian except in the limit of infinite subsystem size at finite temperature. We then analysed the FCS after quantum quenches, focussing on transverse field quenches and evolution starting from a classical Néel state. We first determined the FCS in the stationary states reached at late times. The probability distributions are again non Gaussian, except in the limit of infinite subsystem size. We then presented results for the time evolution of the probability distributions $P^{(u,s)}(m,t)$ for a variety of quenches. For transverse field quenches originating in the paramagnetic phase $P^{(u,s)}(m,t)$ showed interesting smoothing and broadening behaviour in time. In contrast, $P^{(u,s)}(m,t)$ displayed a simpler behaviour for quenches originating in the ferromagnetic phase. In the case of a Néel quench $P^{(s)}(m,t)$ encoded detailed information on the restoration of translational invariance. The main result of our work is analytic expression for the FCS after transverse field quenches in the *space-time scaling limit* $t,\ell\to\infty$, t/ℓ fixed. This was obtained by a generalization of the multi-dimensional stationary phase approximation method of Refs [75, 86]. Our final result (3.117) represents the main analytic finding of this work. We note that the resulting generating function exhibits an interesting multiple light-cone structure that has no analogue in either correlation functions of

local observables [82] or in the entanglement entropy [86]. We performed a careful comparison of the asymptotic expansion with numerical results (that have negligible errors) and found excellent agreement on the level of the probability distributions for all cases considered.

Our work provides the first analytic results for FCS after quantum quenches and hopefully will pave the way for further studies. Here we have focussed on the FCS for the transverse magnetization. It would be very interesting to determine the FCS for the longitudinal magnetization, which is the order parameter characterizing the Ising quantum phase transition. A more straightforward but interesting extension would be to study certain observables in free fermion models with long-range hopping and/or pairing [155–157]. Similarly, the probability distribution of the (smooth) subsystem magnetization in the spin-1/2 Heisenberg XXZ chain should be calculable both at finite temperatures [158] and in the stationary states after certain quantum quenches [159–167]. For quantum quenches in the regime where bosonisation provides a good approximation [168] the full time evolution of the probability distribution for certain observables can be obtained in a straightforward way. Finally, the case of integrable chains of higher spin could be studied both in equilibrium [169, 170] and after a quench [166, 171].

In the second part we have considered decay rates of the elementary spinon excitation in the spin-1/2 Heisenberg XXX model in a magnetic field perturbed by a weak integrability breaking interaction $\kappa \sum_j S^z_j S^z_{j+2}$. We have argued that the leading contribution arises from three spinon decay and have determined the corresponding rate. The latter is found to be small, indicating that spinons remain long-lived excitations in the non-integrable theory. Decay of elementary string excitations can be analysed in an analogous fashion. This would be particularly interesting to do in the attractive regime $\Delta < 0$ of the XXZ chain in a field, where they play an important role in the dynamics.

Bibliography

[1] Groha, S. & Essler, F. H. Spinon decay in the spin-1/2 Heisenberg chain with weak next nearest neighbour exchange. *Journal of Physics A: Mathematical and Theoretical* **50,** 334002 (2017).

[2] Groha, S., Essler, F. H. L. & Calabrese, P. Full Counting Statistics in the Transverse Field Ising Chain. arXiv: 1803.09755 (2018).

[3] Giamarchi, T. Quantum Physics in One Dimension (Oxford University Press, 2003).

[4] Jordan, P. & Wigner, E. Über das Paulische Äquivalenzverbot. *Zeitschrift für Physik* **47,** 631–651 (1928).

[5] Lieb, E., Schultz, T. & Mattis, D. Two soluble models of an antiferromagnetic chain. *Annals of Physics* **16,** 407–466 (1961).

[6] Bethe, H. Zur Theorie der Metalle - I. Eigenwerte und Eigenfunktionen der linearen Atomkette. *Zeitschrift für Physik* **71,** 205–226 (1931).

[7] Sklyanin, E. K., Takhtadzhyan, L. A. & Faddeev, L. D. Quantum inverse problem method. I. *Theoretical and Mathematical Physics* **40,** 688–706 (1979).

[8] Born, M. Zur Quantenmechanik der Stossvorgänge. *Zeitschrift für Physik* **37,** 863–867 (1926).

[9] Deutsch, J. M. Quantum statistical mechanics in a closed system. *Physical Review A* **43,** 2046–2049 (1991).

[10] Srednicki, M. Chaos and quantum thermalization. *Physical Review E* **50,** 888–901 (1994).

[11] Rigol, M., Dunjko, V., Yurovsky, V. & Olshanii, M. Relaxation in a completely integrable many-body Quantum system: An Ab initio study of the dynamics of the highly excited states of 1D lattice hard-core bosons. *Physical Review Letters* **98,** 050405 (2007).

[12] Barthel, T. & Schollwöck, U. Dephasing and the steady state in quantum many-particle systems. *Physical Review Letters* **100,** 100601 (2008).

[13] Bertini, B., Essler, F. H., Groha, S. & Robinson, N. J. Prethermalization and Thermalization in Models with Weak Integrability Breaking. *Physical Review Letters* **115,** 180601 (2015).

[14] Bertini, B., Essler, F. H., Groha, S. & Robinson, N. J. Thermalization and light cones in a model with weak integrability breaking. *Physical Review B* **94,** 245117 (2016).

[15] Affleck, I., Kennedy, T., Lieb, E. H. & Tasaki, H. Rigorous results on valence-bond ground states in antiferromagnets. *Physical Review Letters* **59,** 799–802 (1987).

[16] Schollwöck, U. The density-matrix renormalization group in the age of matrix product states. *Annals of Physics* **326,** 96–192 (2011).

[17] Verstraete, F., Murg, V. & Cirac, J. Matrix product states, projected entangled pair states, and variational renormalization group methods for quantum spin systems. *Advances in Physics* **57,** 143–224 (2008).

[18] Essler, F. H. L., Frahm, H., Göhmann, F., Klümper, A. & Korepin, V. E. The One-Dimensional Hubbard Model, 1–674 (Cambridge University Press, Cambridge, 2005).

[19] Korepin, V. E., Bogoliubov, N. M. & Izergin, A. G. Quantum Inverse Scattering Method and Correlation Functions (Cambridge University Press, Cambridge, 1993).

[20] Hofheinz, M., Wang, H., Ansmann, M., Bialczak, R. C., Lucero, E., Neeley, M., O'Connell, A. D., Sank, D., Wenner, J., Martinis, J. M. & Cleland, A. N. Synthesizing arbitrary quantum states in a superconducting resonator. *Nature* **459,** 546–549 (2009).

[21] Lundeen, J. S., Sutherland, B., Patel, A., Stewart, C. & Bamber, C. Direct measurement of the quantum wavefunction. *Nature* **474,** 188–191 (2011).

[22] Mirhosseini, M., Magaña-Loaiza, O. S., Hashemi Rafsanjani, S. M. & Boyd, R. W. Compressive direct measurement of the quantum wave function. *Physical Review Letters* **113,** 090402 (2014).

[23] Mahan, G. D. Many-Particle Physics (Springer US, Boston, MA, 1990).

[24] Collura, M., Essler, F. H. & Groha, S. Full counting statistics in the spin-1/2 Heisenberg XXZ chain. *Journal of Physics A: Mathematical and Theoretical* **50,** 414002 (2017).

[25] Nazarov, Y. Quantum Noise in Mesoscopic Physics (ed Nazarov, Y. V.) (Springer Netherlands, Dordrecht, 2003).

[26] Blanter, Y. M. & Buttiker, M. Shot Noise in Mesoscopic Conductors. *Physics Reports* **336,** 1–166 (1999).

[27] Hofferberth, S., Lesanovsky, I., Schumm, T., Imambekov, A., Gritsev, V., Demler, E. & Schmiedmayer, J. Probing quantum and thermal noise in an interacting many-body system. *Nature Physics* **4,** 489–495 (2008).

[28] Kitagawa, T., Pielawa, S., Imambekov, A., Schmiedmayer, J., Gritsev, V. & Demler, E. Ramsey interference in one-dimensional systems: The full distribution function of fringe contrast as a probe of many-body dynamics. *Physical Review Letters* **104,** 255302 (2010).

[29] Kitagawa, T., Imambekov, A., Schmiedmayer, J. & Demler, E. The dynamics and prethermalization of one-dimensional quantum systems probed through the full distributions of quantum noise. *New Journal of Physics* **13,** 073018 (2011).

[30] Gring, M., Kuhnert, M., Langen, T., Kitagawa, T., Rauer, B., Schreitl, M., Mazets, I., Adu Smith, D., Demler, E. & Schmiedmayer, J. Relaxation and prethermalization in an isolated quantum system. *Science* **337,** 1318–1322 (2012).

[31] Armijo, J., Jacqmin, T., Kheruntsyan, K. V. & Bouchoule, I. Probing three-body correlations in a quantum gas using the measurement of the third moment of density fluctuations. *Physical Review Letters* **105,** 230402 (2010).

[32] Jacqmin, T., Armijo, J., Berrada, T., Kheruntsyan, K. V. & Bouchoule, I. Sub-poissonian fluctuations in a 1D bose gas: From the quantum quasicondensate to the strongly interacting regime. *Physical Review Letters* **106,** 230405 (2011).

[33] Cherng, R. W. & Demler, E. Quantum noise analysis of spin systems realized with cold atoms. *New Journal of Physics* **9,** 7–7 (2007).

[34] Lamacraft, A. & Fendley, P. Order parameter statistics in the critical quantum ising chain. *Physical Review Letters* **100,** 165706 (2008).

[35] Ivanov, D. A. & Abanov, A. G. Characterizing correlations with full counting statistics: Classical Ising and quantum XY spin chains. *Physical Review E - Statistical, Nonlinear, and Soft Matter Physics* **87,** 022114 (2013).

[36] Shi, Y. & Klich, I. Full counting statistics and the Edgeworth series for matrix product states. *Journal of Statistical Mechanics: Theory and Experiment* **2013,** P05001 (2013).

[37] Eisler, V. Universality in the full counting statistics of trapped fermions. *Physical Review Letters* **111,** 080402 (2013).

[38] Klich, I. A note on the full counting statistics of paired fermions. *Journal of Statistical Mechanics: Theory and Experiment* **2014,** P11006 (2014).

[39] Stéphan, J. M. & Pollmann, F. Full counting statistics in the Haldane-Shastry chain. *Physical Review B* **95,** 035119 (2017).

[40] Najafi, K. & Rajabpour, M. A. Full counting statistics of the subsystem energy for free fermions and quantum spin chains. *Physical Review B* **96,** 235109 (2017).

[41] Humeniuk, S. & Büchler, H. P. Full Counting Statistics for Interacting Fermions with Determinantal Quantum Monte Carlo Simulations. *Physical Review Letters* **119,** 236401 (2017).

[42] Bastianello, A., Piroli, L. & Calabrese, P. Exact local correlations and full counting statistics for arbitrary states of the one-dimensional interacting Bose gas. arXiv: 1802.02115 (2018).

[43] Gritsev, V., Altman, E., Demler, E. & Polkovnikov, A. Full quantum distribution of contrast in interference experiments between interacting one-dimensional Bose liquids. *Nature Physics* **2,** 705–709 (2006).

[44] Imambekov, A., Gritsev, V. & Demler, E. Fundamental noise in matter interferometers. arXiv: 0703766 [cond-mat] (2007).

[45] Eisler, V. & Rácz, Z. Full counting statistics in a propagating quantum front and random matrix spectra. *Physical Review Letters* **110,** 060602 (2013).

[46] Lovas, I., Dóra, B., Demler, E. & Zaránd, G. Full counting statistics of time-of-flight images. *Physical Review A* **95,** 053621 (2017).

[47] Klich, I. & Levitov, L. Quantum noise as an entanglement meter. *Physical Review Letters* **102,** 100502 (2009).

[48] Klich, I. & Levitov, L. Many-body entanglement: A new application of the full counting statistics. in *AIP Conference Proceedings* **1134** (AIP, 2009), 36–45. arXiv: 0901.3391.

[49] Hsu, B., Grosfeld, E. & Fradkin, E. Quantum noise and entanglement generated by a local quantum quench. *Physical Review B - Condensed Matter and Materials Physics* **80,** 235412 (2009).

[50] Song, H. F., Flindt, C., Rachel, S., Klich, I. & Le Hur, K. Entanglement entropy from charge statistics: Exact relations for noninteracting many-body systems. *Physical Review B - Condensed Matter and Materials Physics* **83,** 161408 (2011).

[51] Song, H. F., Rachel, S., Flindt, C., Klich, I., Laflorencie, N. & Le Hur, K. Bipartite fluctuations as a probe of many-body entanglement. *Physical Review B - Condensed Matter and Materials Physics* **85,** 035409 (2012).

[52] Calabrese, P., Mintchev, M. & Vicari, E. Exact relations between particle fluctuations and entanglement in Fermi gases. *EPL (Europhysics Letters)l* **98,** 20003 (2012).

[53] Levine, G. C., Bantegui, M. J. & Burg, J. A. Full counting statistics in a disordered free fermion system. *Physical Review B - Condensed Matter and Materials Physics* **86,** 174202 (2012).

[54] Süsstrunk, R. & Ivanov, D. A. Free fermions on a line: Asymptotics of the entanglement entropy and entanglement spectrum from full counting statistics. *EPL (Europhysics Letters)* **100,** 60009 (2012).

[55] Calabrese, P., Le Doussal, P. & Majumdar, S. N. Random matrices and entanglement entropy of trapped Fermi gases. *Physical Review A - Atomic, Molecular, and Optical Physics* **91,** 012303 (2015).

[56] Herviou, L., Mora, C. & Le Hur, K. Bipartite charge fluctuations in one-dimensional Z2 superconductors and insulators. *Physical Review B* **96,** 121113 (2017).

[57] Saminadayar, L., Glattli, D. C., Jin, Y. & Etienne, B. Observation of the e/3 fractionally charged laughlin quasiparticle. *Physical Review Letters* **79,** 2526–2529 (1997).

[58] De-Picciotto, R., Reznikov, M., Heiblum, M., Umansky, V., Bunin, G. & Mahalu, D. Direct observation of a fractional charge. *Nature* **389,** 162–164 (1997).

[59] Scully, M. O. & Zubairy, M. S. Quantum optics (Cambridge University Press, Cambridge, 1997).

[60] Anderson, M. H., Ensher, J. R., Matthews, M. R., Wieman, C. E. & Cornell, E. A. Observation of Bose-Einstein Condensation in a Dilute Atomic Vapor. *Science* **269,** 198–201 (1995).

[61] Davis, K. B., Mewes, M. O., Andrews, M. R., Van Druten, N. J., Durfee, D. S., Kurn, D. M. & Ketterle, W. Bose-Einstein condensation in a gas of sodium atoms. *Physical Review Letters* **75,** 3969–3973 (1995).

[62] Bradley, C. C., Sackett, C. A., Tollett, J. J. & Hulet, R. G. Evidence of Bose-Einstein condensation in an atomic gas with attractive interactions. *Physical Review Letters* **75,** 1687–1690 (1995).

[63] Andrews, M. R., Townsend, C. G., Miesner, H. J., Durfee, D. S., Kurn, D. M. & Ketterle, W. Observation of interference between two bose condensates. *Science* **275,** 637–641 (1997).

[64] Mewes, M. O., Andrews, M. R., Kurn, D. M., Durfee, D. S. & Townsend, C. G. Output coupler for bose-einstein condensed atoms. *Physical Review Letters* **78,** 582–585 (1997).

[65] Duine, R. A. & Stoof, H. T. Atom-molecule coherence in Bose gases. *Physics Reports* **396,** 115–195 (2004).

[66] Köhler, T., Góral, K. & Julienne, P. S. Production of cold molecules via magnetically tunable Feshbach resonances. *Reviews of Modern Physics* **78,** 1311–1361 (2006).

[67] Greiner, M., Mandel, O., Esslinger, T., Hänsch, T. W. & Bloch, I. Quantum phase transition from a superfluid to a mott insulator in a gas of ultracold atoms. *Nature* **415,** 39–44 (2002).

[68] Stamper-Kurn, D. M. & Ketterle, W. in *Coherent atomic matter waves* 139–217 (Springer, Berlin, Heidelberg, 2000). arXiv: `0005001 [cond-mat]`.

[69] Nelson, K. D., Li, X. & Weiss, D. S. Imaging single atoms in a three-dimensional array. *Nature Physics* **3,** 556–560 (2007).

[70] Greif, D., Parsons, M. F., Mazurenko, A., Chiu, C. S., Blatt, S., Huber, F., Ji, G. & Greiner, M. Site-resolved imaging of a fermionic Mott insulator. *Science* **351,** 953–957 (2016).

[71] Mazurenko, A., Chiu, C. S., Ji, G., Parsons, M. F., Kanász-Nagy, M., Schmidt, R., Grusdt, F., Demler, E., Greif, D. & Greiner, M. A cold-atom Fermi-Hubbard antiferromagnet. *Nature* **545,** 462–466 (2017).

[72] Adu Smith, D., Gring, M., Langen, T., Kuhnert, M., Rauer, B., Geiger, R., Kitagawa, T., Mazets, I., Demler, E. & Schmiedmayer, J. Prethermalization revealed by the relaxation dynamics of full distribution functions. *New Journal of Physics* **15,** 075011 (2013).

[73] Polkovnikov, A., Altman, E. & Demler, E. Interference between independent fluctuating condensates. *Proceedings of the National Academy of Sciences* **103,** 6125–6129 (2006).

[74] Sachdev, S. Quantum Phase Transitions (Cambridge University Press, Cambridge, 2011).

[75] Calabrese, P., Essler, F. H. & Fagotti, M. Quantum quench in the transverse field Ising chain: I. Time evolution of order parameter correlators. *Journal of Statistical Mechanics: Theory and Experiment* **2012,** P07016 (2012).

[76] Essler, F. H. & Fagotti, M. Quench dynamics and relaxation in isolated integrable quantum spin chains. *Journal of Statistical Mechanics: Theory and Experiment* **2016,** 064002 (2016).

[77] Barouch, E. & McCoy, B. M. Statistical mechanics of the XY model. II. Spin-correlation functions. *Physical Review A* **3,** 786–804 (1971).

[78] Barouch, E. & McCoy, B. M. Statistical mechanics of the XY model. III. *Physical Review A* **3,** 2137–2140 (1971).

[79] Barouch, E., McCoy, B. M. & Dresden, M. Statistical mechanics of the XY model. I. *Physical Review A* **2,** 1075–1092 (1970).

[80] Iglói, F. & Rieger, H. Long-range correlations in the nonequilibrium quantum relaxation of a spin chain. *Physical Review Letters* **85,** 3233–3236 (2000).

[81] Sengupta, K., Powell, S. & Sachdev, S. Quench dynamics across quantum critical points. *Physical Review A - Atomic, Molecular, and Optical Physics* **69,** 053616 (2004).

[82] Calabrese, P., Essler, F. H. & Fagotti, M. Quantum quench in the transverse-field ising chain. *Physical Review Letters* **106,** 227203 (2011).

[83] Calabrese, P., Essler, F. H. & Fagotti, M. Quantum quenches in the transverse field Ising chain: II. Stationary state properties. *Journal of Statistical Mechanics: Theory and Experiment* **2012,** P07022 (2012).

[84] Essler, F. H. L., Evangelisti, S. & Fagotti, M. Dynamical correlations after a quantum quench. *Physical Review Letters* **109,** 247206 (2012).

[85] Calabrese, P. & Cardy, J. Evolution of entanglement entropy in one-dimensional systems. *Journal of Statistical Mechanics: Theory and Experiment* **2005,** P04010 (2005).

[86] Fagotti, M. & Calabrese, P. Evolution of entanglement entropy following a quantum quench: Analytic results for the XY chain in a transverse magnetic field. *Physical Review A - Atomic, Molecular, and Optical Physics* **78,** 010306 (2008).

[87] Fagotti, M. & Essler, F. H. L. Reduced density matrix after a quantum quench. *Physical Review B - Condensed Matter and Materials Physics* **87,** 245107 (2013).

[88] Calabrese, P., Essler, F. H. & Mussardo, G. Introduction to 'Quantum Integrability in out of Equilibrium Systems'. *Journal of Statistical Mechanics: Theory and Experiment* **2016,** 064001 (2016).

[89] Peschel, I. Calculation of reduced density matrices from correlation functions. *Journal of Physics A: Mathematical and General* **36,** L205–L208 (2003).

[90] Latorre, J. I., Rico, E. & Vidal, G. Ground state entanglement in quantum spin chains. *Quantum Info. Comput.* **4,** 48–92 (2003).

[91] Peschel, I. & Eisler, V. Reduced density matrices and entanglement entropy in free lattice models. *Journal of Physics A: Mathematical and Theoretical* **42,** 504003 (2009).

[92] Fagotti, M. & Calabrese, P. Entanglement entropy of two disjoint blocks in XY chains. *Journal of Statistical Mechanics: Theory and Experiment* **2010,** P04016 (2010).

[93] Rossini, D., Silva, A., Mussardo, G. & Santoro, G. E. Effective thermal dynamics following a quantum quench in a spin chain. *Physical Review Letters* **102,** 127204 (2009).

[94] Rossini, D., Suzuki, S., Mussardo, G., Santoro, G. E. & Silva, A. Long time dynamics following a quench in an integrable quantum spin chain: Local versus nonlocal operators and effective thermal behavior. *Physical Review B - Condensed Matter and Materials Physics* **82,** 144302 (2010).

[95] Foini, L., Cugliandolo, L. F. & Gambassi, A. Fluctuation-dissipation relations and critical quenches in the transverse field Ising chain. *Physical Review B - Condensed Matter and Materials Physics* **84,** 212404 (2011).

[96] Rieger, H. & Iglói, F. Semiclassical theory for quantum quenches in finite transverse Ising chains. *Physical Review B - Condensed Matter and Materials Physics* **84,** 165117 (2011).

[97] Schuricht, D. & Essler, F. H. Dynamics in the Ising field theory after a quantum quench. *Journal of Statistical Mechanics: Theory and Experiment* **2012,** P04017 (2012).

[98] Foini, L., Cugliandolo, L. F. & Gambassi, A. Dynamic correlations, fluctuation-dissipation relations, and effective temperatures after a quantum quench of the transverse field Ising chain. *Journal of Statistical Mechanics: Theory and Experiment* **2012,** P09011 (2012).

[99] Heyl, M., Polkovnikov, A. & Kehrein, S. Dynamical quantum phase transitions in the transverse-field ising model. *Physical Review Letters* **110,** 135704 (2013).

[100] Kormos, M., Bucciantini, L. & Calabrese, P. Stationary entropies after a quench from excited states in the Ising chain. *EPL (Europhysics Letters)* **107,** 40002 (2014).

[101] Bucciantini, L., Kormos, M. & Calabrese, P. Quantum quenches from excited states in the Ising chain. *Journal of Physics A: Mathematical and Theoretical* **47,** 175002 (2014).

[102] Abeling, N. O. & Kehrein, S. Quantum quench dynamics in the transverse field Ising model at nonzero temperatures. *Physical Review B* **93,** 104302 (2016).

[103] Calabrese, P. & Cardy, J. Time dependence of correlation functions following a quantum quench. *Physical Review Letters* **96,** 136801 (2006).

[104] Calabrese, P. & Cardy, J. Quantum quenches in extended systems. *Journal of Statistical Mechanics: Theory and Experiment* **2007,** P06008–P06008 (2007).

[105] Bonnes, L., Essler, F. H. L. & Läuchli, A. M. "Light-Cone" Dynamics After Quantum Quenches in Spin Chains. *Physical Review Letters* **113,** 187203 (2014).

[106] Alba, V. & Calabrese, P. Entanglement and thermodynamics after a quantum quench in integrable systems. *Proceedings of the National Academy of Sciences* **114,** 7947–7951 (2017).

[107] Alba, V. & Calabrese, P. Entanglement dynamics after quantum quenches in generic integrable systems. *SciPost Physics* **4.** arXiv: 1712.07529 (2018).

[108] Widom, H. Asymptotic behavior of block Toeplitz matrices and determinants. II. *Advances in Mathematics* **21,** 1–29 (1976).

[109] Böttcher, A. & Widom, H. Szegö via Jacobi. *Linear Algebra and Its Applications* **419,** 656–667 (2006).

[110] Ilievski, E., De Nardis, J., Wouters, B., Caux, J. S., Essler, F. H. L. & Prosen, T. Complete Generalized Gibbs Ensembles in an Interacting Theory. *Physical Review Letters* **115,** 157201 (2015).

[111] Ilievski, E., Medenjak, M., Prosen, T. & Zadnik, L. Quasilocal charges in integrable lattice systems. *Journal of Statistical Mechanics: Theory and Experiment* **2016,** 064008 (2016).

[112] Takahashi, M. Thermodynamics of One-Dimensional Solvable Models, 268 (Cambridge University Press, Cambridge, 1999).

[113] Hohenberg, P. C. Existence of long-range order in one and two dimensions. *Physical Review* **158,** 383–386 (1967).

[114] Mermin, N. D. & Wagner, H. Absence of ferromagnetism or antiferromagnetism in one- or two-dimensional isotropic Heisenberg models. *Physical Review Letters* **17,** 1133–1136 (1966).

[115] Essler, F. H. L. Applications of Integrable Models in Condensed Matter and Cold Atom Physics. in *Les Houches Summer School on Integrability: From Statistical Systems to Gauge Theory* (2016).

[116] Gogolin, A. O., Nersesyan, A. A. & Tsvelik, A. M. Bosonization and Strongly Correlated Systems, 448. arXiv: 9909069 [cond-mat] (Cambridge University Press, 2004).

[117] Kenzelmann, M., Coldea, R., Tennant, D. A., Visser, D., Hofmann, M., Smeibidl, P. & Tylczynski, Z. Order-to-disorder transition in the XY-like quantum magnet Cs2CoCl4 induced by noncommuting applied fields. *Physical Review B* **65,** 144432 (2002).

[118] Zaliznyak, I. A., Woo, H., Perring, T. G., Broholm, C. L., Frost, C. D. & Takagi, H. Spinons in the strongly correlated copper oxide chains in SrCuO2. *Physical Review Letters* **93,** 087202 (2004).

[119] Stone, M. B., Reich, D. H., Broholm, C., Lefmann, K., Rischel, C., Landee, C. P. & Turnbull, M. M. Extended Quantum Critical Phase in a Magnetized Spin-1/2 Antiferromagnetic Chain. *Physical Review Letters* **91,** 037205 (2003).

[120] Mourigal, M., Enderle, M., Klöpperpieper, A., Caux, J. S., Stunault, A. & Rønnow, H. M. Fractional spinon excitations in the quantum heisenberg antiferromagnetic chain. *Nature Physics* **9,** 435–441 (2013).

[121] Orbach, R. Linear antiferromagnetic chain with anisotropic coupling. *Physical Review* **112,** 309–316 (1958).

[122] Gaudin, M. & Caux, J.-S. The Bethe Wavefunction (Cambridge University Press, Cambridge, 2014).

[123] Vladimirov, A. A. Non-string two-magnon configurations in the isotropic Heisenberg magnet. *Physics Letters A* **105,** 418–420 (1984).

[124] Essler, F. H., Korepin, V. E. & Schoutens, K. Fine structure of the Bethe ansatz for the spin-1/2 Heisenberg XXX model. *Journal of Physics A: General Physics* **25,** 4115–4126 (1992).

[125] Hagemans, R. & Caux, J.-S. Deformed strings in the Heisenberg model. *Journal of Physics A: Mathematical and Theoretical* **40,** 14605–14647 (2007).

[126] Faddeev, L. D. & Takhtadzhyan, L. A. Spectrum and scattering of excitations in the one-dimensional isotropic Heisenberg model. *Journal of Soviet Mathematics* **24,** 241–267 (1984).

[127] Yang, C. N. & Yang, C. P. Thermodynamics of a one-dimensional system of bosons with repulsive delta-function interaction. *Journal of Mathematical Physics* **10,** 1115–1122 (1969).

[128] Kitanine, N., Maillet, J. M. & Terras, V. Form factors of the XXZ Heisenberg finite chain. *Nuclear Physics B* **554,** 647–678 (1999).

[129] Slavnov, N. a. Calculation of scalar product of wave function and Form Factor in the framework of algebraic Bethe Ansatz. *Theoretical and Mathematical Physics* **79,** 502–508 (1989).

[130] Faddeev, L. & Takhtajan, L. A. What is the spin of a spin-wave. *Physics Letters A* **85,** 375–377 (1981).

[131] Delfino, G., Mussardo, G. & Simonetti, P. Non-integrable quantum field theories as perturbations of certain integrable models. *Nuclear Physics B* **473,** 469–508 (1996).

[132] Delfino, G. & Mussardo, G. Non-integrable aspects of the multi-frequency sine-Gordon model. *Nuclear Physics B* **516,** 675–703 (1998).

[133] Delfino, G., Grinza, P. & Mussardo, G. Decay of particles above threshold in the Ising field theory with magnetic field. *Nuclear Physics B* **737,** 291–303 (2006).

[134] Pozsgay, B. & Takács, G. Characterization of resonances using finite size effects. *Nuclear Physics B* **748,** 485–523 (2006).

[135] Imambekov, A., Schmidt, T. L. & Glazman, L. I. One-dimensional quantum liquids: Beyond the Luttinger liquid paradigm. *Reviews of Modern Physics* **84,** 1253–1306 (2012).

[136] Essler, F. H., Pereira, R. G. & Schneider, I. Spin-charge-separated quasiparticles in one-dimensional quantum fluids. *Physical Review B - Condensed Matter and Materials Physics* **91,** 245150 (2015).

[137] Schmidt, T. L., Imambekov, A. & Glazman, L. I. Spin-charge separation in one-dimensional fermion systems beyond Luttinger liquid theory. *Physical Review B - Condensed Matter and Materials Physics* **82,** 245104 (2010).

[138] Peskin, M. E. & Schroeder, D. V. An Introduction to quantum field theory (Addison-Wesley, Reading, USA, 1995).

[139] Mussardo, G. Statistical field theory : an introduction to exactly solved models in statistical physics (Oxford University Press, 2009).

[140] Gaudin, M., McCoy, B. M. & Wu, T. T. Normalization sum for the Bethe's hypothesis wave functions of the Heisenberg-Ising chain. *Physical Review D* **23,** 417–419 (1981).

[141] Korepin, V. E. Calculation of norms of Bethe wave functions. *Communications in Mathematical Physics* **86,** 391–418 (1982).

[142] Kitanine, N., Maillet, J. M. & Terras, V. Correlation functions of the XXZ Heisenberg spin-1/2 chain in a magnetic field. *Nuclear Physics B* **567,** 554–582 (2000).

[143] Klauser, A., Mossel, J. & Caux, J. S. Adjacent spin operator dynamical structure factor of the S = 1/2 Heisenberg chain. *Journal of Statistical Mechanics: Theory and Experiment* **2012,** P03012 (2012).

[144] Caux, J.-S. Correlation functions of integrable models: A description of the ABACUS algorithm. *Journal of Mathematical Physics* **50,** 095214 (2009).

[145] Pereira, R. G., Sirker, J., Caux, J. .-.-S., Hagemans, R., Maillet, J. M., White, S. R. & Affleck, I. Dynamical structure factor at small q for the XXZ spin-1/2 chain. *Journal of Statistical Mechanics: Theory and Experiment* **2007,** P08022–P08022 (2007).

[146] Caux, J. S., Hagemans, R. & Maillet, J. M. Computation of dynamical correlation functions of Heisenberg chains: The gapless anisotropic regime. *Journal of Statistical Mechanics: Theory and Experiment* **2005,** 83–102 (2005).

[147] Shashi, A., Glazman, L. I., Caux, J. S. & Imambekov, A. Nonuniversal prefactors in the correlation functions of one-dimensional quantum liquids. *Physical Review B - Condensed Matter and Materials Physics* **84,** 045408 (2011).

[148] Shashi, A., Panfil, M., Caux, J. S. & Imambekov, A. Exact prefactors in static and dynamic correlation functions of one-dimensional quantum integrable models: Applications to the Calogero-Sutherland, Lieb-Liniger, and XXZ models. *Physical Review B - Condensed Matter and Materials Physics* **85,** 155136 (2012).

[149] Kitanine, N., Kozlowski, K. K., Maillet, J. M., Slavnov, N. A. & Terras, V. On the thermodynamic limit of form factors in the massless XXZ Heisenberg chain. *Journal of Mathematical Physics* **50,** 095209 (2009).

[150] Kitanine, N., Kozlowski, K. K., Maillet, J. M., Slavnov, N. A. & Terras, V. The thermodynamic limit of particle-hole form factors in the massless XXZ Heisenberg chain. *Journal of Statistical Mechanics: Theory and Experiment* **2011,** P05028 (2011).

[151] Kitanine, N., Kozlowski, K. K., Maillet, J. M., Slavnov, N. A. & Terras, V. Form factor approach to dynamical correlation functions in critical models. *Journal of Statistical Mechanics: Theory and Experiment* **2012,** P09001 (2012).

[152] Kitanine, N., Kozlowski, K. K., Maillet, J. M., Slavnov, N. A. & Terras, V. A form factor approach to the asymptotic behavior of correlation functions in critical models. *Journal of Statistical Mechanics: Theory and Experiment* **2011,** P12010 (2011).

[153] Pereira, R. G., White, S. R. & Affleck, I. Spectral function of spinless fermions on a one-dimensional lattice. *Physical Review B - Condensed Matter and Materials Physics* **79,** 165113 (2009).

[154] Hagemans, R. Dynamics of Heisenberg spin chains. PhD thesis (2007).

[155] Van Regemortel, M., Sels, D. & Wouters, M. Information propagation and equilibration in long-range Kitaev chains. *Physical Review A* **93,** 032311 (2016).

[156] Buyskikh, A. S., Fagotti, M., Schachenmayer, J., Essler, F. & Daley, A. J. Entanglement growth and correlation spreading with variable-range interactions in spin and fermionic tunneling models. *Physical Review A* **93,** 053620 (2016).

[157] Lepori, L., Trombettoni, A. & Vodola, D. Singular dynamics and emergence of nonlocality in long-range quantum models. *Journal of Statistical Mechanics: Theory and Experiment* **2017,** 033102 (2017).

[158] Dugave, M., Göhmann, F. & Kozlowski, K. K. Thermal form factors of the XXZ chain and the large-distance asymptotics of its temperature dependent correlation functions. *Journal of Statistical Mechanics: Theory and Experiment* **2013,** P07010 (2013).

[159] Caux, J. S. & Essler, F. H. Time evolution of local observables after quenching to an integrable model. *Physical Review Letters* **110,** 257203 (2013).

[160] Wouters, B., De Nardis, J., Brockmann, M., Fioretto, D., Rigol, M. & Caux, J. S. Quenching the anisotropic Heisenberg chain: Exact solution and generalized gibbs ensemble predictions. *Physical Review Letters* **113,** 117202 (2014).

[161] Brockmann, M., Wouters, B., Fioretto, D., De Nardis, J., Vlijm, R. & Caux, J. S. Quench action approach for releasing the Néel state into the spin-1/2 XXZ chain. *Journal of Statistical Mechanics: Theory and Experiment* **2014,** P12009 (2014).

[162] Pozsgay, B., Mestyán, M., Werner, M. A., Kormos, M., Zaránd, G. & Takács, G. Correlations after quantum quenches in the XXZ Spin Chain: Failure of the generalized Gibbs ensemble. *Physical Review Letters* **113,** 117203 (2014).

[163] Mestyán, M., Pozsgay, B., Takács, G. & Werner, M. A. Quenching the XXZ spin chain: Quench action approach versus generalized Gibbs ensemble. *Journal of Statistical Mechanics: Theory and Experiment* **2015,** P04001 (2015).

[164] Ilievski, E., De Nardis, J., Wouters, B., Caux, J. S., Essler, F. H. L. & Prosen, T. Complete Generalized Gibbs Ensembles in an Interacting Theory. *Physical Review Letters* **115,** 157201 (2015).

[165] Ilievski, E., Quinn, E., De Nardis, J. & Brockmann, M. String-charge duality in integrable lattice models. *Journal of Statistical Mechanics: Theory and Experiment* **2016,** 063101 (2016).

[166] Piroli, L., Vernier, E. & Calabrese, P. Exact steady states for quantum quenches in integrable Heisenberg spin chains. *Physical Review B* **94,** 054313 (2016).

[167] Piroli, L., Vernier, E., Calabrese, P. & Rigol, M. Correlations and diagonal entropy after quantum quenches in XXZ chains. *Physical Review B* **95,** 054308 (2017).

[168] Collura, M., Calabrese, P. & Essler, F. H. Quantum quench within the gapless phase of the spin- 12 Heisenberg XXZ spin chain. *Physical Review B - Condensed Matter and Materials Physics* **92,** 125131 (2015).

[169] Jee, Y. J., Lee, K. J. B. & Schlottmann, P. Critical behavior of the SU(3) ferromagnetic Heisenberg chain. *Physical Review B* **39,** 2815–2818 (1989).

[170] Babujian, H. M. Exact solution of the isotropic Heisenberg chain with arbitrary spins: Thermodynamics of the model. *Nuclear Physics, Section B* **215,** 317–336 (1983).

[171] Mestyán, M., Bertini, B., Piroli, L. & Calabrese, P. Exact solution for the quench dynamics of a nested integrable system. *Journal of Statistical Mechanics: Theory and Experiment* **2017,** 083103 (2017).